NASACR-159,574

CR-159574

3 1176 00156 6489

NASA-CR-159574
19790016847

Internally Coated Air-Cooled Gas Turbine Blading

by L. Hsu, W.G. Stevens, A.R. Stetson

SOLAR TURBINES INTERNATIONAL
An Operating Group of International Harvester

Prepared for

National Aeronautics and Space Administration

LIBRARY COPY
JUL 9 1979
LANGLEY RESEARCH CENTER
LIBRARY, NASA
HAMPTON, VIRGINIA

Lewis Research Center

Contract NAS3-21039

1. Report No.
CR-159574

2. Government Accession No.

3. Recipient's Catalog No.

4. Title and Subtitle
Internally Coated Air-Cooled Gas Turbine Blading

5. Report Date
March, 1979

6. Performing Organization Code

7. Author(s)
L. Hsu, W. G. Stevens, A. R. Stetson

8. Performing Organization Report No.
SR79-R-4655-15

9. Performing Organization Name and Address
SOLAR Turbines International
An Operating Group of International Harvester
2200 Pacific Highway, P.O. Box 80966
San Diego, California 92138

10. Work Unit No.

11. Contract or Grant No.
NAS3-21039

12. Sponsoring Agency Name and Address
National Aeronautics & Space Administration
Lewis Laboratories
21000 Brookpark Road, Cleveland, Ohio 44135

13. Type of Report and Period Covered
Final Technical
August 1977 - December 1978

14. Sponsoring Agency Code

15. Supplementary Notes

16. Abstract

The increasing use of air-cooled blading in advanced, high-temperature engines requires that technology is available for application of protective coatings to internal cooling air passages to minimize oxidation/hot corrosion attack. In this program, ten candidate modified nickel-aluminide coatings were developed for this purpose using the slip pack process. These coatings contain additives such as silicon, chromium and columbium in a nickel-aluminum coating matrix with directionally solidified MAR-M200 + Hf as the substrate alloy. Following a series of screening tests which included strain tolerance, dynamic oxidation and hot corrosion testing, the Ni-19Al-1Cb (nominal composition) coating was selected for application to the internal passages of four first-stage turbine blades.

Process development results indicated that a dry pack process was suitable for internal coating application resulting in 18 percent or less reduction in air flow. Coating uniformity, based on coated air-cooled blades, was within ±20 percent.

Test results show that the presence of additives (silicon, chromium or columbium) appeared to improve significantly the ductility of the NiAl matrix. However, the environmental resistance of these modified nickel-aluminides were generally inferior to the simple aluminides.

17. Key Words (Suggested by Author(s))
Air-cooled, blades, internal coating, nickel aluminide, slip pack, MAR-M200+Hf, directional solidification, superalloy, strain tolerance, burner rig, dynamic oxidation, hot corrosion.

18. Distribution Statement
Unclassified - unlimited

19. Security Classif. (of this report)
Unclassified

20. Security Classif. (of this page)

21. No. of Pages
95

22. Price*

* For sale by the National Technical Information Service, Springfield, Virginia 22161

N79-25018#

FOREWORD

This final technical report covers the work performed under Contract NAS3-21039 from August 1977 to December 1978. It is published for technical information only and does not necessarily represent recommendations, conclusions or approval of NASA.

The program was conducted at Solar Turbines International, an Operating Group of International Harvester, located in San Diego, California. The NASA Program Monitor was Mr. John Merutka and Mr. A. R. Stetson was Solar's Technical director. Ms. Lulu Hsu and Dr. W. G. Stevens were the Principal Investigators.

Table of Contents

Page

INTRODUCTION 1

- Current coating Process Limitations 1
- Program Objective 2

EXPERIMENTAL 7

- Materials 7
- Coating Processes 10
- Evaluation Techniques 14
  - Strain Tolerance/Ductile-Brittle Transition Temperature Testing 14
  - Hot Corrosion Burner Rig Tests 15
  - Oxidation Burner Rig Test 17
  - Cold Flow Check 17
  - Metallography 22

COATING PROCESS DEVELOPMENT 23

COATING EVALUATION 49

- Strain Tolerance/DBTT Testing 49
- Hot Corrosion Testing 51
- Dynamic Oxidation Testing 63

COATING APPLICATION TO ENGINE HARDWARE 77

- Selection of Coating 77
- Coating of Mars Blade 78
  - Processing Steps for Coating Application of Mars First-Stage Blade 79
- Evaluation of Coated Mars Blade 80

CONCLUSIONS 85

- Recommendations 86

APPENDIX A - DETERMINATION OF RIG OPERATING CONDITIONS 87

REFERENCES 93

LIST OF FIGURES

Figure		Page
1	Flow Chart of Activities in Task 1	3
2	As-Cast MAR-M200 + Hf (DS) Round Test Bars	4
3	Multiple Hole Pin Specimen Rig Tests	5
4	Coupons Cut From MAR-M200 + HF (DS) Cast Stock	8
5	Completed Pin Specimens With Six Transverse Holes	9
6	First-Stage MAR-M200 + Hf (DS) Turbine Blades	11
7	Mars First-Stage Blade Castings Showing Grain Etch	12
8	Radiograph of As-Received MAR-M200 + Hf (DS) Blades	12
9	MAR-M200 Test Pins Prepared for Application of External MCrAlY Coating	13
10	Instron Model TT-D Tensile Machine	14
11	Gas Turbine Environmental Simulators	16
12	Control Console for Gas Turbine Environmental Simulators	16
13	Coated Test Specimens Prepared for Burner Rig Testing	17
14	Burner Rig Test Showing Rotating Specimen in Hot Gas Stream	18
15	Schematic of Salt Solution Doped Fuel System	18
16	Salt Particles From Hot Gas Stream in Burner Rig	19
17	Typical Temperature Profile During Thermal Cycling	19
18	Solar's Flow Bench Apparatus	21
19	Flow Check Fixture Used in Monitoring Air Flow Discharge of Pin Specimens	22
20	Microstructure of D300 Coated MAR-M421	24
21	Cross-Section Through Coated 0.7 mm Hole in MAR-M421	25
22	Microstructure of Ni-20Cr on MAR-M421	25
23	Cr-Ni Phase Diagram	26
24	Chromized Internal Coating on MAR-M421 Deposited by Slip Pack Process	27
25	Ni-S Binary Phase Diagram	28

LIST OF FIGURES (Cont)

Figure		Page
26	Silicided MAR-M421 Specimen Surface (F100) Showing Dark Area Containing NaCl	29
27	Silicide Coating Formed on MAR-M421 After Eight Hours at 816°C	29
28	Microstructure of Silicon Coating MAR-M200 + Hf (DS)	29
29	Columbium Coating on MAR-M200 + Hf (DS) (E101)	30
30	Al-Ni Binary Phase System	31
31	Extrapolated Relationship of Aluminum Pickup and Ni-Al Ratio	32
32	Microstructure of Ni-20Al Coating (A107)	32
33	Microstructure of Ni-17Al Coating	33
34	Microstructure of Ni-15Al Coating	33
35	Nickel and Aluminum Concentration Profiles on Ni-20Al Coating on MAR-M421	35
36	Ni-20Al Coating (#1) on MAR-M200 + Hf (DS)	37
37	Ni-19Al-1Cb Coating (#2) on MAR-M200 + Hf (DS)	38
38	Ni-17Al Coating (#2) on MAR-M200 + Hf (DS)	39
39	Ni-16Al-5Si Coating (#4) on MAR-M200 + Hf (DS)	40
40	Ni-14Al-20Cr Coating (#5) on MAR-M200 + Hf (DS)	41
41	Ni-13Al-20Cr-1Cb Coating (#6) on MAR-M200 + Hf (DS)	42
42	Ni-15Al Coating (#7) on MAR-M200 + Hf (DS)	43
43	Ni-14Al-1Cb Coating (#8) on MAR-M200 + Hf (DS)	44
44	Ni-12Al-20Cr Coating (#9) on MAR-M200 + Hf (DS)	45
45	Ni-12Al-20Cr-5Si Coating (#10) on MAR-M200 + Hf (DS)	46
46	Strain Tolerance of Coated MAR-M200 + Hf (DS)	50
47	Cross-Section of Transverse Hole in Specimen P1 After 49 Hours of Hot Corrosion Testing	54
48	Coating No. 1 After Hot Corrosion Testing at 899°C	55
49	Coating No. 3 After Hot Corrosion Testing at 899°C	56
50	Coating No. 7 After Hot Corrosion Testing at 899°C	57
51	Coating No. 2 After Hot Corrosion Testing at 899°C	58
52	Coating No. 8 After Hot Corrosion Testing at 899°C	59
53	Coating No. 6 After Hot Corrosion Testing at 899°C	60
54	Coating No. 4 After Hot Corrosion Testing at 899°C	61

LIST OF FIGURES (Cont)

Figure		Page
55	Coating No. 10 After Hot Corrosion Testing at 899°C	62
56	Coating No. 5 After Hot Corrosion Testing at 899°C	63
57	Coating No. 2 After Hot Corrosion Testing at 899°C	64
58	Coating No. 1 After Dynamic Oxidation Testing at 1050°C	67
59	Coating No. 3 After Dynamic Oxidation Testing at 1050°C	68
60	Coating No. 7 After Dynamic Oxidation Testing at 1050°C	69
61	Coating No. 2 After Dynamic Oxidation Testing at 1050°C	69
62	Coating No. 8 After Dynamic Oxidation Testing at 1050°C	70
63	Coating No. 4 After Dynamic Oxidation Testing at 1050°C	71
64	Coating No. 10 After Dynamic Oxidation Testing at 1050°C	72
65	Coating No. 6 After Dynamic Oxidation Testing at 1050°C	72
66	Coating No. 5 After Dynamic Oxidation Testing at 1050°C	73
67	Coating No. 9 After Dynamic Oxidation Testing at 1050°C	74
68	Schematic Indicating Location of Photomicrographs in Figure 69	80
69	Internally Coated (Ni-19Al-1Cb) Air-Cooled Blade	81
70	Erosion Rig Chart for Calculation of Hot Gas Stream Velocity	91

LIST OF TABLES

Table		Page
1	Coating Compositions	4
2	Certification Analysis for MAR-M200 + Hf (DS) Castings	8
3	Sources of Materials Used	9
4	Certification Analysis of MAR-M200 + Hf (DS) Blades	10
5	Hot Corrosion Rig Parameters	20
6	Synthetic Sea Water	20
7	Dynamic Oxidation Rig Parameters	21
8	Chromium Pack Compositions	23
9	Microprobe Analysis of Three-Zone Nickel Aluminum Coating	36
10	Coating Process Parameters	36
11	Microprobe Analysis of Coating Composition	47
12	Strain Tolerance Test Results	50
13	Cold Flow Check of Coated Burner Rig Test Specimens	52
14	Coating Weight of Burner Rig Test Specimens	53
15	Specimen Parameters After 49 Hours Hot Corrosion Test at 899°C	53
16	Hot Corrosion Test Data	66
17	Dynamic Oxidation Test Results	75
18	Review of Test Results	78
19	Mass Flow Data of Mars Blades	84

SUMMARY

The demands of greater turbine efficiency and power output have led to increasingly high turbine rotor inlet temperatures (T.R.I.T.s) and widespread use of air cooling (film and impingement) in hot section components such as turbine blades and vanes. However, oxidation and corrosion attack at the internal surfaces of such air-cooled components have proven to be a life-limiting problem. The objective of this program was to develop ten candidate nickel-aluminum diffusion coating systems that can be applied uniformly to the internal geometries of air-cooled blades in order to significantly improve environmental resistance without severely compromising surface ductility.

The program alloy was directionally solidified (DS) MAR-M200 + Hf. The coatings were applied by the slip pack process whereby a pack composition was formulated and prepared using elemental powder(s) and the appropriate inert diluent (e.g., Al_2O_3) and halide activator (e.g., NH_4Cl, NaCl). Process parameters such as furnace time and temperature were empirically selected to achieve compositional goals. Program coating compositions are listed in Table 1 with the actual compositions obtained as determined from microprobe analysis of as-coated specimens.

Table 1

Microprobe Analysis of Coating Composition

Coating Number	Program Composition	Actual Composition
1	Ni-20Al	Ni-17Al
2	Ni-19Al-1Cb	Ni-22Al-1Cb
3	Ni-17Al	Ni-18Al
4	Ni-16Al-5Si	Ni-13Al-2Si
5	Ni-14Al-20Cr	Ni-14Al-24Cr
6	Ni-13Al-20Cr-1Cb	Ni-9Al-23Cr-1Cb
7	Ni-15Al	Ni-13Al
8	Ni-14Al-1Cb	Ni-14Al-2Cb
9	Ni-12Al-20Cr	Ni-13Al-23Cr
10	Ni-12Al-20Cr-5Si	Ni-12Al-21Cr-1Si

Screening tests for evaluation of the ten coating systems included ductile-brittle transition temperature (strain tolerance), dynamic oxidation and hot corrosion. All test specimens were subjected to the following heat treatment prior to testing: 1204°C (14 hrs); 1038°C (2 hrs) and 870°C (32 hrs).

The results of the strain tolerance tests are shown graphically in Figure 1. Generally, the simple aluminides, Ni-20Al, Ni-17Al and Ni-15Al (Nos. 1, 3 and 7) were the most brittle with cracking initiating at 500°C and above and at <2 percent strain levels. Upon the inclusion of additives such as chromium, silicon and columbium, ductility was significantly improved as can be observed in the duplex and triplex systems. The Ni-16Al-5Si and Ni-12Al-20Cr coatings (Nos. 4 and 9) appeared to have excellent strain tolerance with cracks occurring only upon specimen rupture. In the case of the Ni-19Al-1Cb coating (No. 2), which differed from the Ni-20Al coating (No. 1) only in the presence of columbium, significant ductility enhancement was observed. The same observation can be made for coatings Nos. 5, 6 and 7, 8; columbium present in Nos. 6 and 8 and not in Nos. 5 and 7. Again, marked improvement in strain tolerance was noted in Nos. 6 and 8.

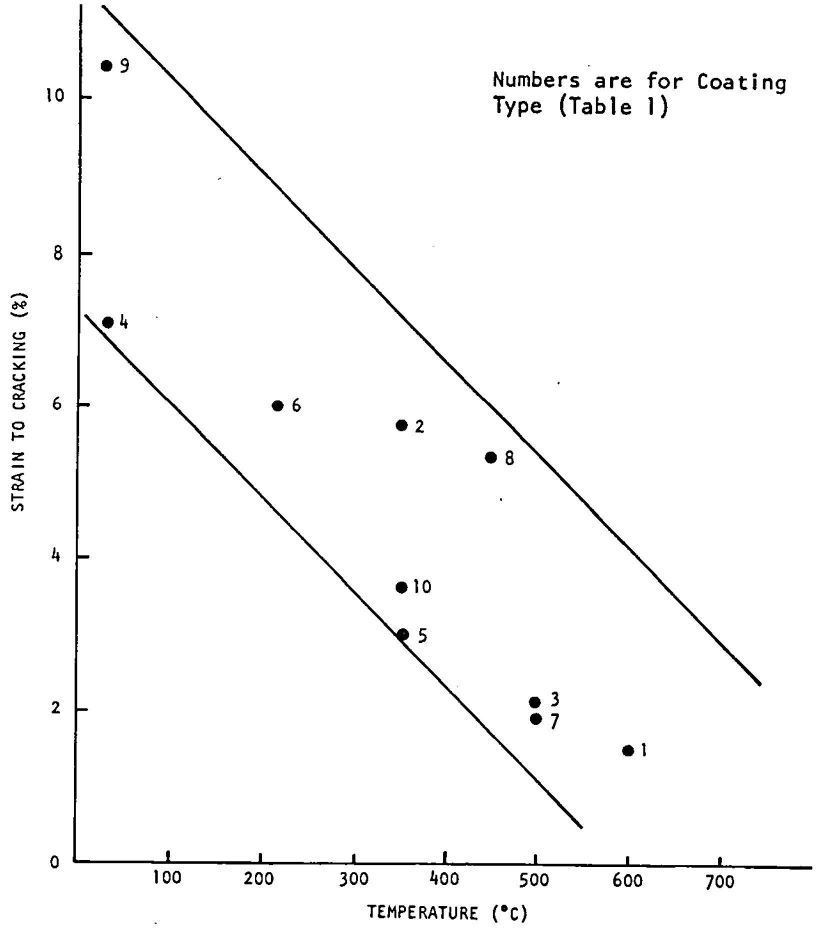

Figure 1. Strain Tolerance of Coated MAR-M200 + Hf (DS)

Therefore, these test data seem to indicate that the presence of additives in the nickel-aluminide matrix can increase strain accommodation in the coating structure, probably by increasing defect mobility in the direction of strain.

Dynamic oxidation and hot corrosion tests were conducted on environmental simulator burner rigs operating on JP-5 fuel. In hot corrosion testing, sea salt solution was injected into the fuel such that upon combustion, the salt content in the air was 4 ppm. The velocity of the hot gases at the nozzle exit was approximately 650 m/sec at 0.85 Mach number. Both tests involved one-hour cycles to test temperatures of 899°C (219 hours total) and 1050°C (235 hours total) for hot corrosion and oxidation tests respectively.

Post-test metallography shows that subsurface voids were detected in the coatings with oxide layer formations on the coating surfaces. Interdiffusion across the coating interface was also noted as both meta-stable systems (coating and substrate alloy) moved towards thermodynamic equilibrium.

The results from both burner rig tests are summarized in Table 2, together with ductility test data. (The coatings are listed in the order of decreasing ductility.) Since three test specimens were damaged towards the end of oxidation testing, the penetration measurements obtained after 72 hours of oxidation exposure are also included in Table 2.

Table 2

Summary of Test Results

Coating	Composition	Ductility	Corrosion* (219 hrs at 899°C, 1 hr Cycles)	Oxidation* (1 hr cycles) (72 hrs at 1050°C)	Oxidation* (1 hr cycles) (235 hrs at 1050°C)
9	Ni-12Al-20Cr	Good	Medium	Medium	Poor
4	Ni-16Al-5Si	Good	Poor	Medium	Medium
6	Ni-13Al-20Cr-1Cb	Medium	Poor	Medium	**
2	Ni-19Al-1Cb	Medium	Medium	Medium	Medium
8	Ni-14Al-1Cb	Medium	Poor	Medium	Poor
10	Ni-12Al-20Cr-5Si	Medium	Medium	Good	**
5	Ni-14Al-20Cr	Medium	Poor	Good	Poor
3	Ni-17Al	Poor	Good	Good	Poor
7	Ni-15Al	Poor	Good-Medium	Good	**
1	Ni-20Al	Poor	Good	Good	Medium

* Zero to 33% coating penetration - good.
33-67% coating penetration - medium.
67-100% coating penetration - poor.

** Specimen broke off during testing.

In general, oxidation/corrosion resistance appeared to bear an inverse relationship with ductility. This inverse correlation is a consequence of the brittle behavior of the protective beta phase (NiAl) typically formed in medium-to-high activity diffusion aluminides. As the aluminum content decreases, the less protective but more ductile gamma prime phase (Ni_3Al) tends to predominate in the matrix. The presence of secondary phase additives such as silicon, chromium and columbium in the duplex and triplex coatings, were found to mitigate the tradeoff in ductility and protectivity of nickel-aluminides. For example, the three least ductile coatings provided the best protection against the hot gas environment. But upon modifying the aluminide matrix (in essence, dilution) with the addition of other element(s) to the coating, substantial improvements in ductility were observed at the expense of some loss in oxidation/corrosion resistance.

Based on the above results, the Ni-19Al-1Cb (No. 2) coating was selected as exhibiting the best overall characteristics. Coating microstructure is shown in Figure 2. Application of this coating to the internal surfaces of first-stage turbine blades (Mars engine) showed uniform coverage with coating thickness averaging 60μm and standard deviation of ±10μm. Mass flow data of coated blades revealed flow reduction of ≤18 percent. The coating process used in blade applications utilized a dry pack process which was similar to the slurry pack process except for the exclusion of solvent/binder. This dry method was found to be more readily removed from the core cavity and is recommended for future work for such applications.

Magnification: 500X

Etchant: 2% Chromic

As Coated

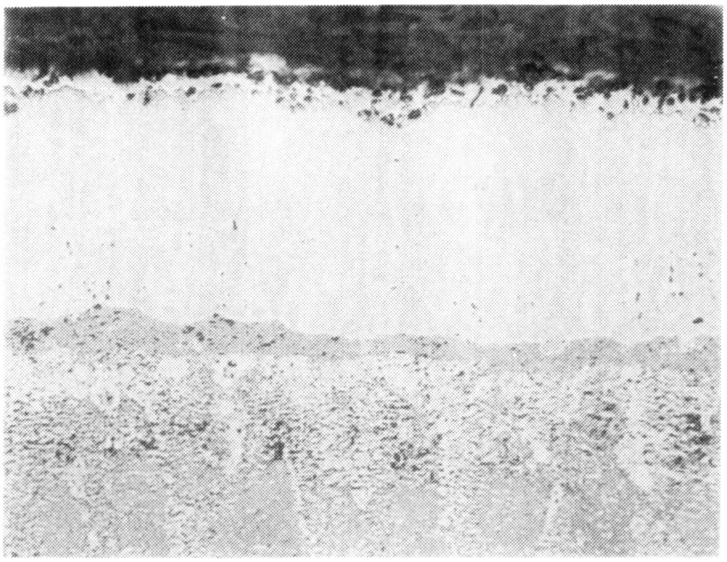

Magnification: 500X

Etchant: 2% Chromic

Heat Treated

Figure 2. Ni-19Al-1Cb Coating (#2) on MAR-M200 + Hf (DS)

1

INTRODUCTION

The quest for greater turbine efficiency and increased power output has led to the development of increasingly high-temperature materials that can withstand the high turbine rotor inlet temperature (TRIT) that are characteristic of advanced aircraft engines. The stringent demands placed on turbine blades require that high-temperature nickel-base alloys be the material of choice. The development of directionally solidified (DS) superalloys, such as MAR-M200, signified a notable achievement as these gamma prime strengthened alloys have excellent high-temperature creep capability and increased resistance to thermal fatigue cracking. This is largely the result of elimination of grain boundaries oriented at right angles to the main stress axis and in part due to a lower Young's modulus parallel to growth axis when compared to equiaxed alloys.

Another approach to operating at high TRIT is to utilize impingement and film cooling within the airfoil to maintain metal temperature within a reasonable range and to retain adequate alloy stress-rupture properties. However, heat flux and surface temperature determinations have shown that these internal passageways can approach 900 to 950°C where oxidation/hot corrosion is the life-limiting problem. The viable solution to this is to apply a protective coating on these internal surfaces to reduce the rate of degradation. Furthermore, the protective coating must be diffusionally stable and have good adherence to the substrate alloy and spallation of protective oxide scales must be minimized. Passageway plugging and even partial coolant flow restriction can lead to a ratcheting scenario: increased temperatures, more plugging, etc., with eventual local airfoil failure caused by burnout or melting. Thus, these internal airfoil coatings must resist the hot gas environment as well as remain in place during the life of the airfoil.

CURRENT COATING PROCESS LIMITATIONS

Because of the nature of the internal passages, most current coating processes are not capable of applying a uniform protective coating of the desired composition due to the line-of-sight limitation associated with processes such as spraying and physical vapor deposition. On the other hand, pack processes are not line-of-sight limited and may be used for such applications.

In principle, there are three types of pack processes - powder packs, slurry packs and vapor only packs. These differ in the means by which vapors of the alloying coating element are transported to and deposited on the substrate surface. In the powder pack process, the component to be coated is embedded in a pack of the appropriate composition (coating element, activator and inert filler material) and during the firing cycle, the metal constituent is activated by forming a vapor phase product (usually a halide) which in turn is reduced by and diffuses into the substrate alloy. The slurry or slip pack process is similar to the powder pack process with the difference being that the pack materials are made into a slurry by adding a vehicle/binder system with which the part is subsequently coated and fired. The third pack process is, in actual fact, a vapor only deposition process whereby the source of the metallic vapor or pack is removed from actual contact with the component. Instead, the vapors are borne by a flowing inert fluid (such as argon gas) from the source toward the specimen where reduction and deposition occurs. However, the limitation of this process is the "throwing power" of the process as a result of loss of active metal bearing vapors and a buildup of corrosive by-product vapors.

PROGRAM OBJECTIVE

The objective of this program was to use the slip pack process to develop ten coating compositions that can be applied to the internal surfaces of air-cooled, DS MAR-M200 (2% Hf) airfoils cast in the configuration of the Mars (Solar's 10,000 hp engine) first-stage blade. Screening tests for the coatings include ductility and hot corrosion/oxidation resistance. The coating process itself must be compatible with the blade design in terms of acceptable airflow characterization and must also be compatible with the application of a controlled composition reaction sintered (CCRS) MCrAlY coating to the external surfaces of the blade (Ref. 1).

The scope of this program is described in the following paragraphs and summarized in Figure 1. Initially, ten coating compositions and coating/process sequences were developed utilizing (DS) MAR-M200+Hf coupon specimens. The specified coating compositions are listed in Table 1 and are basically modified nickel-aluminide coatings. All compositions and coating thickness variations were held to the specified ±20 percent limits imposed. Upon confirmation by metallographic and microprobe characterization of the ten coating compositions, application to DS MAR-M200 + Hf test specimens were conducted. These include ten standard round (6.25 mm dia.) test bars and 40 (3.12 mm dia.) hollow pins, as shown in Figures 2 and 3, respectively. The test bars were cast-to-shape while the pins had to be electrodischarge machined.

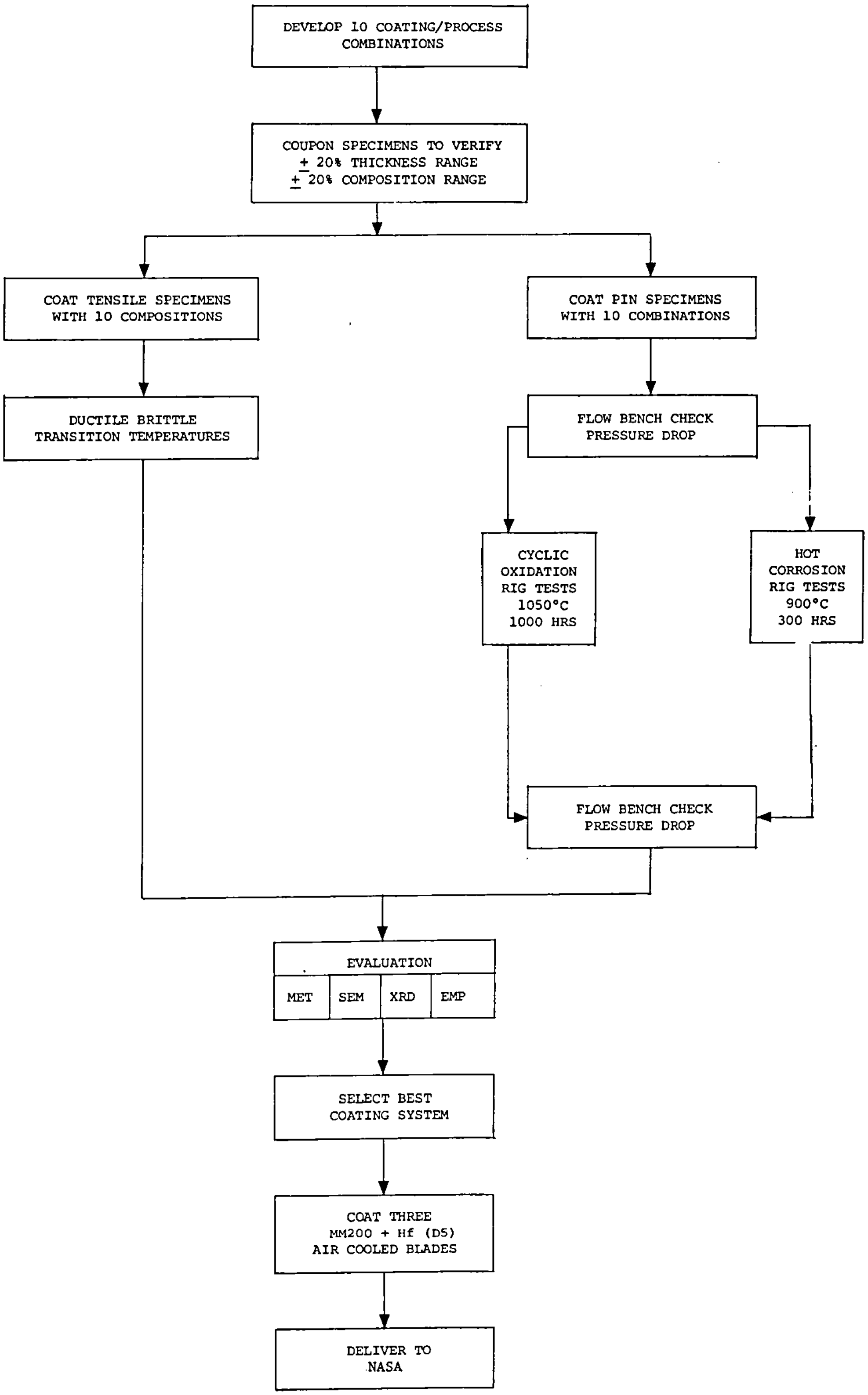

DEVELOP 10 COATING/PROCESS COMBINATIONS
COUPON SPECIMENS TO VERIFY ± 20% THICKNESS RANGE ± 20% COMPOSITION RANGE
COAT TENSILE SPECIMENS WITH 10 COMPOSITIONS
COAT PIN SPECIMENS WITH 10 COMBINATIONS
DUCTILE BRITTLE TRANSITION TEMPERATURES
FLOW BENCH CHECK PRESSURE DROP
CYCLIC OXIDATION RIG TESTS 1050°C 1000 HRS
HOT CORROSION RIG TESTS 900°C 300 HRS
FLOW BENCH CHECK PRESSURE DROP
EVALUATION
MET
SEM
XRD
EMP
SELECT BEST COATING SYSTEM
COAT THREE MM200 + Hf (DS) AIR COOLED BLADES
DELIVER TO NASA

Figure 1. Flow Chart of Activities in Task I

Table 1
Coating Compositions

Precursor Compositions		Final Coating Compositions	Coating Number
First	Second		
		Ni-20Al	1
	Ni-2.5Cb	Ni-19Al-1Cb	2
		Ni-17Al	3
	Ni-8Si	Ni-1-Al-5Si	4
Ni-2.5Cb	Ni-20Cr-1Cb	Ni-13Al-20Cr-1Cb	6
		Ni-15Al	7
	Ni-2.5Cb	Ni-14Al-1Cb	8
	Ni-20Cr	Ni-12Al-20Cr	9
Ni-8Si	Ni-20Cr-5Si	Ni-12Al-20Cr-5Si	10

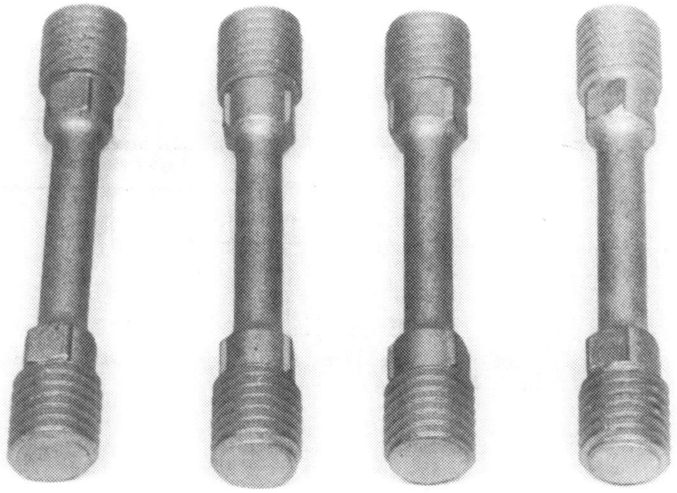

Figure 2. As-Cast Mar-M200 + Hf (DS) Round Test Bars

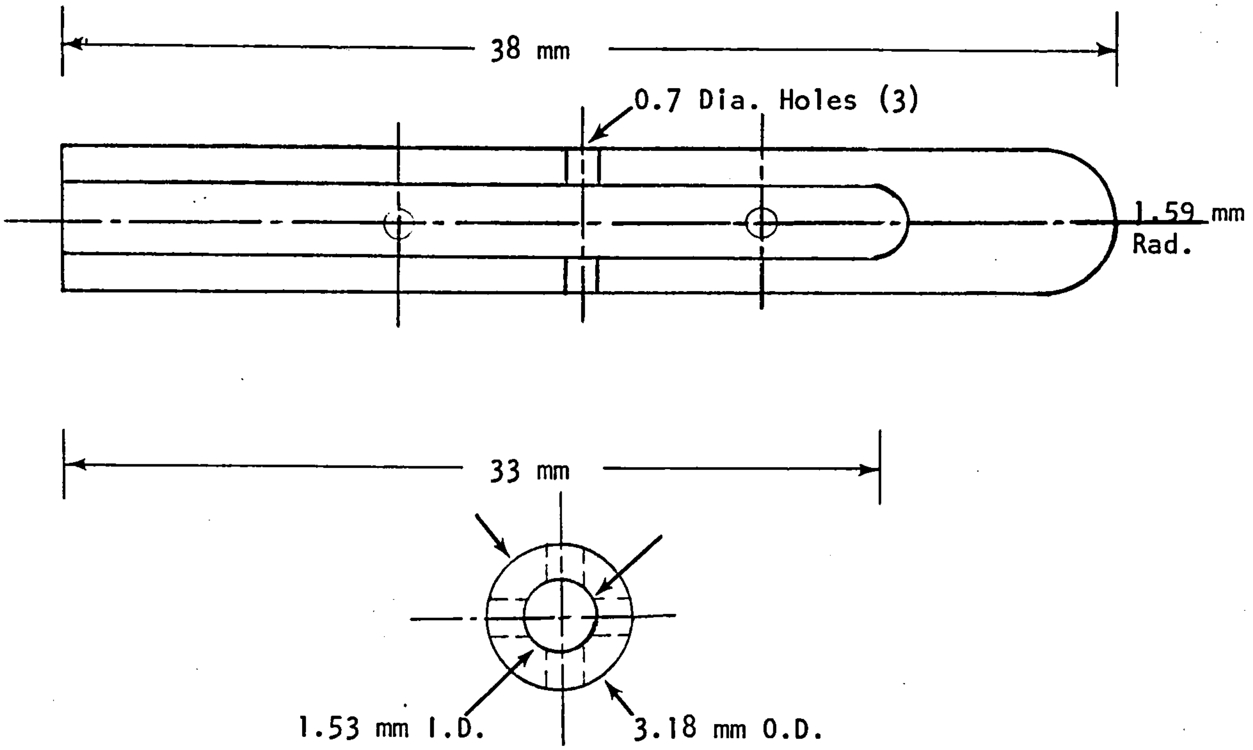

Figure 3. Multiple Hole Pin Specimen

In order to monitor the effectiveness of the pack removal process, the hollow pins were checked for airflow on a cold flow bench before and after processing to measure the loss in mass flow (if any) as a result of coating application.

After completion of the evaluation tests, which include metallography and other qualitative and semi-quantitative analytical techniques, one out of the ten compositions was selected for application to three DS Mars MAR-M200 first-stage blades. The basis for the selection was good ductility and adequate resistance to a hot gas environment.

2

EXPERIMENTAL

The following subsections provide the details of materials and hardware procurement and also describe the diagnostic tests and evaluation techniques employed.

MATERIALS

Procurement of investment cast DS MAR-M200 + Hf test specimens was from Jetshapes, Inc. Certification analysis provided by Systems Chem Lab, Inc. is reported in Table 2. The hafnium content was 1.92 weight percent. Hafnium enhances ductility by the formation of unusually large amounts of interdendritic blocky gamma prime (Refs. 2, 3, and 4). Sprues and gatings from the molds were also supplied by Jetshapes and these were machined to provide coupon specimens for coating development, see Figure 4. Cast round tensile bars (Fig. 2) were used in the as-cast condition after the usual pre-coating preparations such as degreasing and grit blast operations. The 40 (3.12 mm dia.) rods received from Jetshapes were electrodischarge machined to the specifications shown in Figure 3. A typical example of a machined pin is shown in Figure 5. Due to the configurational difficulties encountered in cleanup of the internal cavity of these specimens, they were degreased and acid etched (H_2O_2-HCl) instead of the standard grit blast process.

Table 3 lists the materials used in formulating the various packs. The CoNiCrY powder used in application of the external CCRS coating was purchased from Alloy Metals (Lot 9653) with an analyzed composition of 54.7Co-24.95Cr-19.61Ni-0.64Y. The sieve analysis was -325 with 98.75 percent of the powder at -400 mesh.

In the latter phase of the program, the coating of choice was applied to several Mars first-stage DS MAR-M200 + Hf blades. These components were from a different cast lot than the test specimens and a separate certification analysis is provided in Table 4. A total of 12 blades were received, as shown in Figure 6. Some of the blades have core breaks which show at the trailing edge and wall thickness may be deviant. The grain etch (Fig. 7) shows an irregular DS columnar structure on some of the airfoils, which would not be acceptable for engine applications. However, for the coating studies in this program, the inspection specifications were relaxed and three of the better blades from this lot were selected for final coating. Radiographic documentation was also done and Figure 8 shows clearly the internal passages of the blade design.

Table 2
Certification Analysis for MAR-M200 + Hf (DS) Castings

Element	JE77-10189 PWA 1422 K B-876
Carbon	0.14%
Sulfur	0.006
Manganese	<0.10
Phosphorus	<0.01
Silicon	<0.10
Boron	0.013
Copper	<0.01
Chromium	8.95
Cobalt	9.75
Tungsten	12.25
Columbium	0.85
Titanium	2.00
Hafnium	1.92
Zirconium	0.04
Iron	0.09
Aluminum	4.90
Lead	2.0 ppm
Bismuth	ND <0.3
Selenium	ND <0.5
Tellurium	ND <0.5
Thallium	ND <0.5
Nickel	Remainder

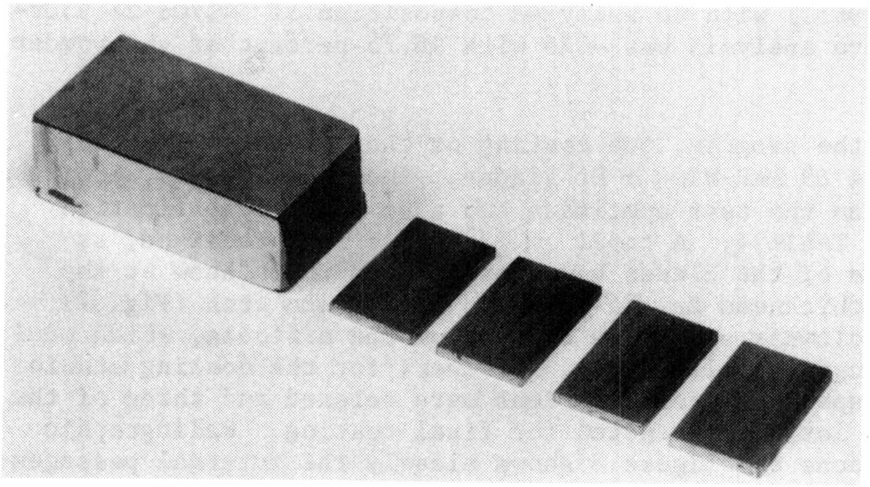

Figure 4.

Coupons Cut From MAR-M200 + Hf (DS) Cast Stock

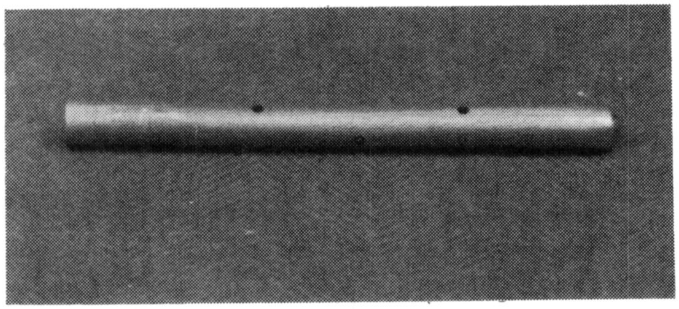

Figure 5.

Completed Pin Specimens With Six Transverse Holes

Table 3

Sources of Materials Used

Material	Supplier	Analysis	Particle Characterization
Cobalt	African Metals	0.32 Ni, 0.08 Fe, 0.08 Ca, 0.06 Si, 0.022 Mn, 0.022C, 0.015 S, 0.01 Cr, Bal. Co	94.7% <37 μm
Nickel	Glidden Metals	0.005 C, 99.59 Ni	96.3% <44 μm
Chromium (MD101)	Alcan	0.23 Fe, 0.04N, 0.03 Al, 0.035-0.01 C, 0.01 Si, 0.006 P	149 μm
Aluminum (201)	Alcoa	--	--
Aluminum Oxide (El)	Norton	--	100 μm, blocky
Ammonium Chloride	J. T. Baker	Analyzed Reagent 5-0660	Granular
Polyvinylchloride (PVC)	B. F. Goodrich	--	--
Columbium	Teledyne Wah Chang	650 ppm O_2, 5 ppm H_2, 39 ppm N_2, 63 ppm Al, 63 ppm Fe, <50 ppm Si, 746 ppm Ta, <50 ppm C, Bal. Cb	-100 +325 mesh
Silicon	Keokuk Electro Metals Co.	0.33 Fe, 0.04 Ca, 0.21 Al, Bal. Si	-200 mesh

Table 4

Certification Analysis of MAR-M200 + Hf (DS) Blades

Element	Concentration (w/o)
Cobalt	10.87
Aluminum	5.09
Chromium	8.15
Tungsten	12.04
Titanium	1.80
Iron	0.09
Columbium	0.88
Tantalum	0.018
Zirconium	<0.1
Copper	<0.05
Magnesium	0.0007
Hafnium	≃1.70
Carbon	0.14
Manganese	<0.1
Silicon	<0.1
Phosphorus	0.004
Sulfur	0.0016
Boron	0.016
Lead	1.0 ppm
Bismuth	<0.3 ppm
Silver	<5.0 ppm
Selerium	0.5 ppm
Nickel	Balance

COATING PROCESSES

In the developmental phase of the program, all coatings were applied by means of the slip (or slurry) pack process. This consisted of suspending the appropriate pack composition in a xylene/ethyl cellulose system with a specific gravity of about two. The specimens (initially MAR-M421 alloy was used until MAR-M200 + Hf (DS) was received) were dipped into the well-stirred slurry and the bisque formed was subsequently dried. Repeated applications were made if a heavier buildup was required as the volume of dried bisque was dependent on the weights of the powder constituents and the specific gravity of the slip. The minimum amount of bisque required per unit area of substrate can be estimated by calculating the weight gain to be attained and correlating it to the weight of pack to be used, assuming total consumption. When the desired bisque thickness was deposited on the specimen, it was allowed to dry thoroughly before being placed in a Hastelloy X retort and weld sealed. The furnace cycle, which was one of the parameters developed for each coating, was varied from 4 to 16 hours at selected temperatures.

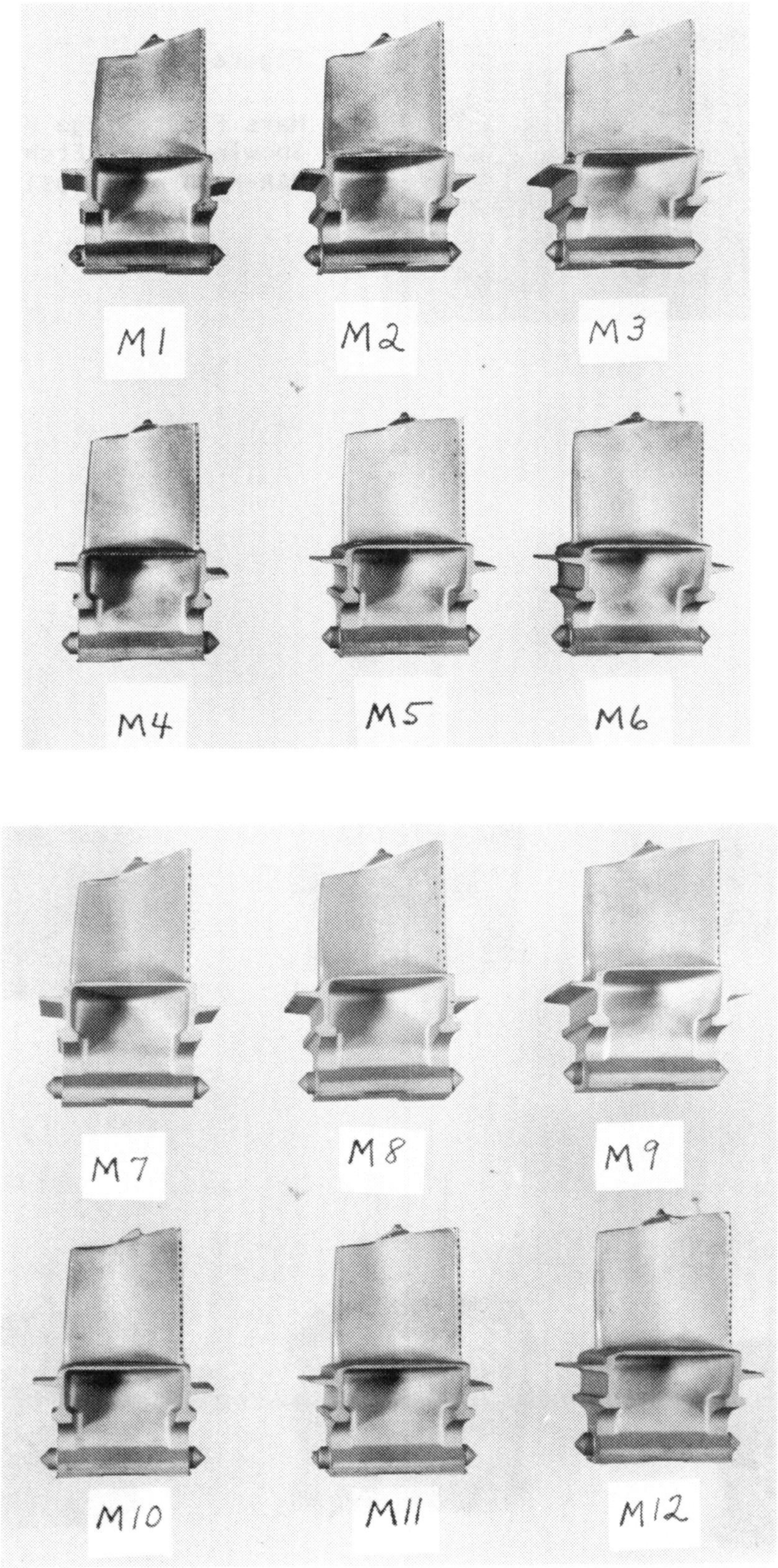
M1
M2
M3
M4
M5
M6
M7
M8
M9
M10
M11
M12

Figure 6. First-Stage MAR-M200 + Hf (DS) Turbine Blades

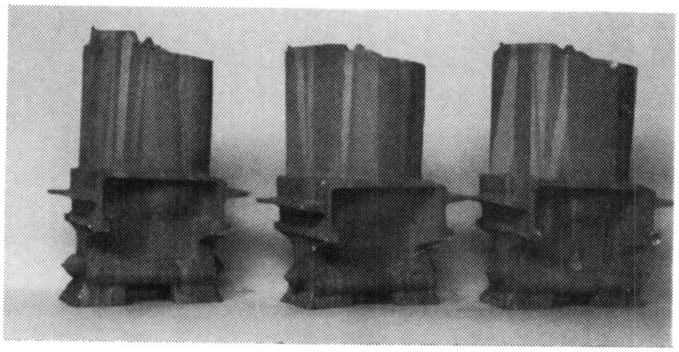

Figure 7.

Mars First-Stage Blade Castings Showing Grain Etch (Alloy MAR-M200 + Hf (DS))

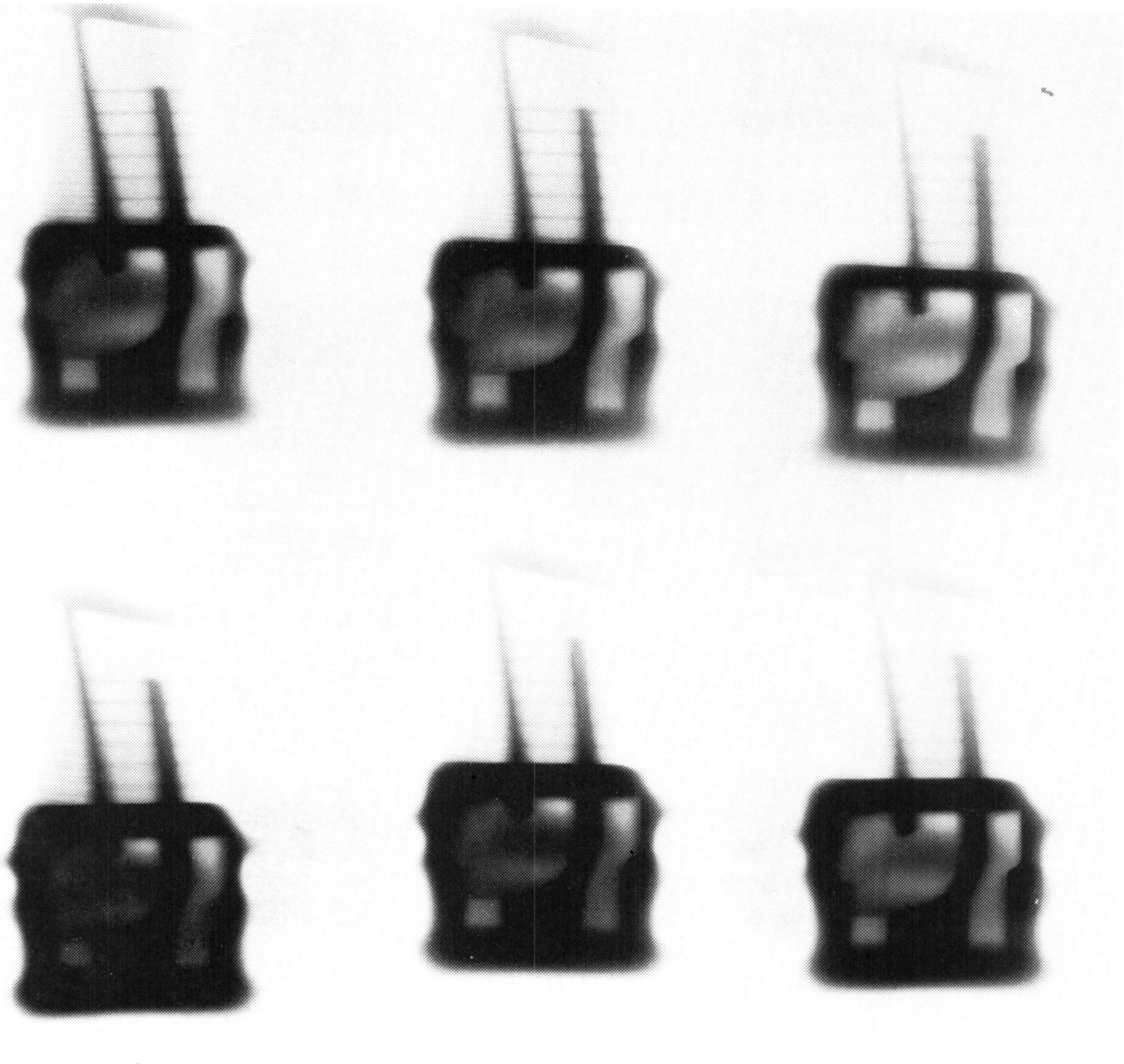

Figure 8. Radiographs of As-Received MAR-M200 + Hf (DS) Blades

In the case of the hollow pin specimens, the slip was injected into the hollow cavity, making sure that no air was trapped within and then allowed to air dry for 24 hours before firing. The external surfaces of these specimens were coated with the CCRS CoNiCrAlY coating which was applied simultaneously with the final internal aluminizing step. The procedure is described as follows.

The aluminum slip pack was injected into the internal bore of the specimen, as mentioned above. Then the overflow out of the transverse holes was carefully cleaned up and sized rods inserted through these transverse holes, as shown in Figure 9. Next, the CoNiCrY slip (xylene/ethyl cellulose) was slurry sprayed, using a DeVilbiss spray gun, onto the external surfaces of the specimen. Upon thorough drying, the pins were removed and the specimen was placed in a controlled composition medium activity aluminizing pack and fired. After cooldown, the retort was cut open and the specimen removed. By gently tapping the sides of the specimen, the near-depleted internal pack was removed and the entire specimen was thoroughly rinsed with pressurized water. In some instances, difficulty was experienced in removing the internal packs in which case, a drill tip was used to loosen up and extract the particles. Cold flow checks before and after processing were used to monitor the effectiveness of the pack removal process.

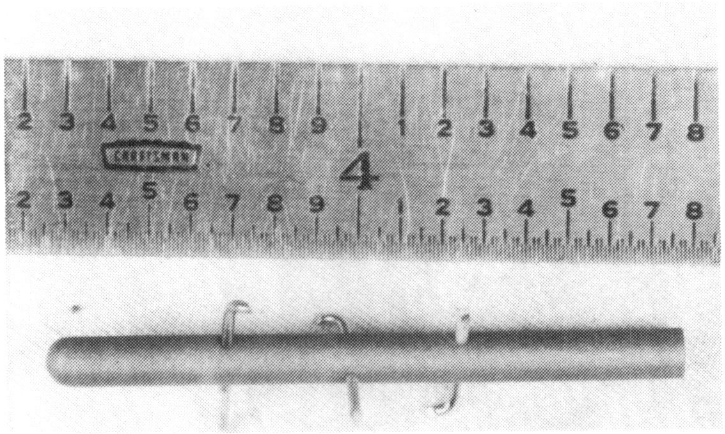

Figure 9.

MAR-M200 Test Pins Prepared For Application Of External MCrAlY Coating

All coated specimens were exposed to the recommended alloy heat treatment (Ref. 3) prior to testing. The heat treatment consisted of four hours solutioning at 1204°C (2200°F) followed by two hours at 1038°C (1900°F) and a 32-hour age at 870°C (1600°F).

EVALUATION TECHNIQUES

After attaining program goals inasfar as coating composition and thickness, each coating was subjected to a series of tests to demonstrate its strain tolerance and resistance to oxidation and hot corrosion. Each test is described in the following sections.

Strain Tolerance/Ductile-Brittle Transition Temperature Testing

An Instron Model TT-D testing machine, as shown in Figure 10, was used to determine and compare the relative strain tolerance of each composition. Initially, the coatings were dye penetrant examined (Zyglo) to identify any coating defects (cracks). Next, each coated specimen was loaded at 750°C and strained to 0.5 percent at a rate of 0.1 mm/mm/min. Upon cooldown, the specimen was unloaded and the coating surface examined for microcracks by the dye penetrant method. If the coating was free of cracks, the specimen was reloaded at a temperature 50°C lower and strained again to an additional 0.5 percent. This process was repeated at 50°C increments until a crack in the coating was initiated.

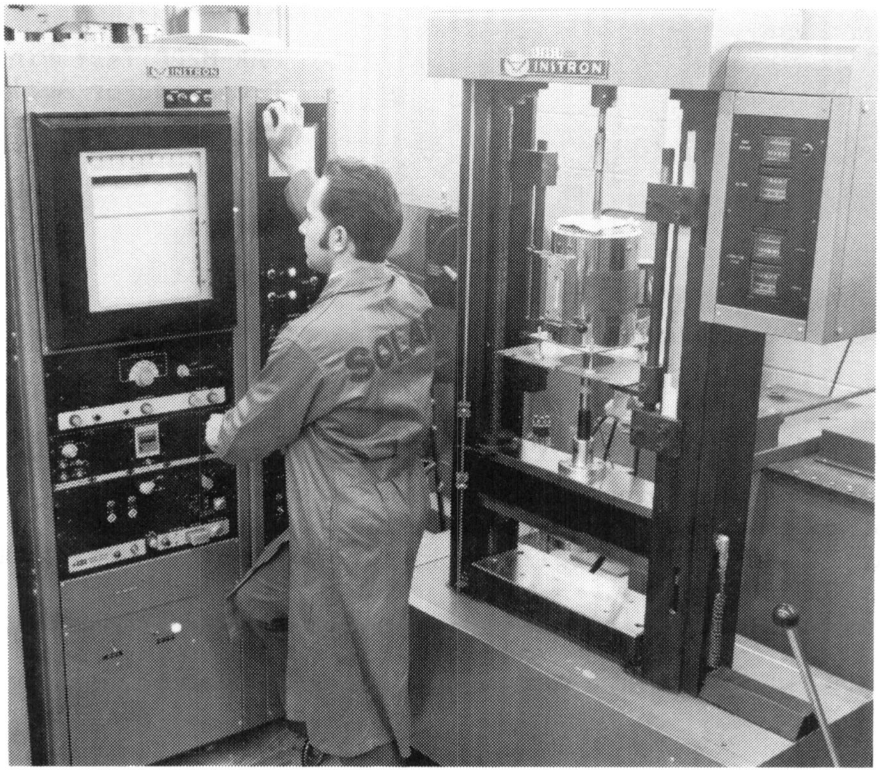

Figure 10. Instron Model TT-D Tensile Machine

Hot Corrosion Burner Rig Tests

Dynamic hot corrosion tests were conducted on Solar's gas turbine environmental simulators (burner rigs) that are similar in features to those of Solar's small modern commercial gas turbine combustors. A straight-through can type combustor is used for long-term trouble-free operation. The simulators are shown in Figure 11 together with the control panels in Figure 12. The combustor is mounted vertically and the hot gas is vented directly upwards into a stainless steel, heavily insulated stack. The specimen holder is connected to a horizontal hydraulic drive shaft that drives the specimens in and out of the hot gas stream, as desired. A slip ring assembly was mounted to the drive shaft of a 1725 rpm specimen drive motor which allowed continuous electrical contact to be maintained, thus permitting round-the-clock monitoring of temperatures.

During testing, the 22 pin specimen holder, shown in Figure 13, was located such that the closest distance to the combustor nozzle was 2.5 cm. A closeup view of the test in progress with the insulated shields removed is provided in Figure 14. Specimen rotation allowed exposure of each specimen in an identical fashion to the combustion gas and homogeneity of test conditions was easily maintained. A well insulated shroud enclosed the region between the combustor nozzle plate and the exhaust stack which helped reduce radiation heat losses to the surroundings.

JP-5 (MIL-J-5634F) fuel was used throughout the burner rig tests. The sulfur content analyzed was 0.047 percent, which is typical of the fuel received at Solar (Ref. 5).

To introduce sea water into the combustor exhaust gas at 4 ppm of the gas flow, the system shown schematically in Figure 15 was used. It consisted of a T-joint into which sea water solution was pumped and allowed to mix through a 1.59 mm (1/16 in.) tube with the oncoming fuel. The fuel-water mixture then entered a homogenizer filter further downstream. This filter was made of stainless steel and contained eight wire screens stacked together. The screen openings were about 250 μm. The distribution of salt particles from this system was measured by passing a metal slide through the gas stream at the point of nearest approach of the test specimens. Figure 16 shows the range of particle size distribution to be typically 10 to 50 μm based on the splat diameter.

Automatic control of temperature was achieved by using an electro-pneumatic controller connected to a pneumatically operated fuel flow control valve. The triggering device leading to the controller was the chromel-alumel thermocouple inserted in a dummy specimen in the holder, which was linked to the slip ring. Any deviation between the specimen temperature and the set point on the controller was automatically adjusted by varying the pneumatic diaphragm on the fuel valve assembly. This, in turn, changed the fuel flow and allowed close, automatic control of specimen temperature. A typical temperature profile is shown in Figure 17. The test parameters are listed in

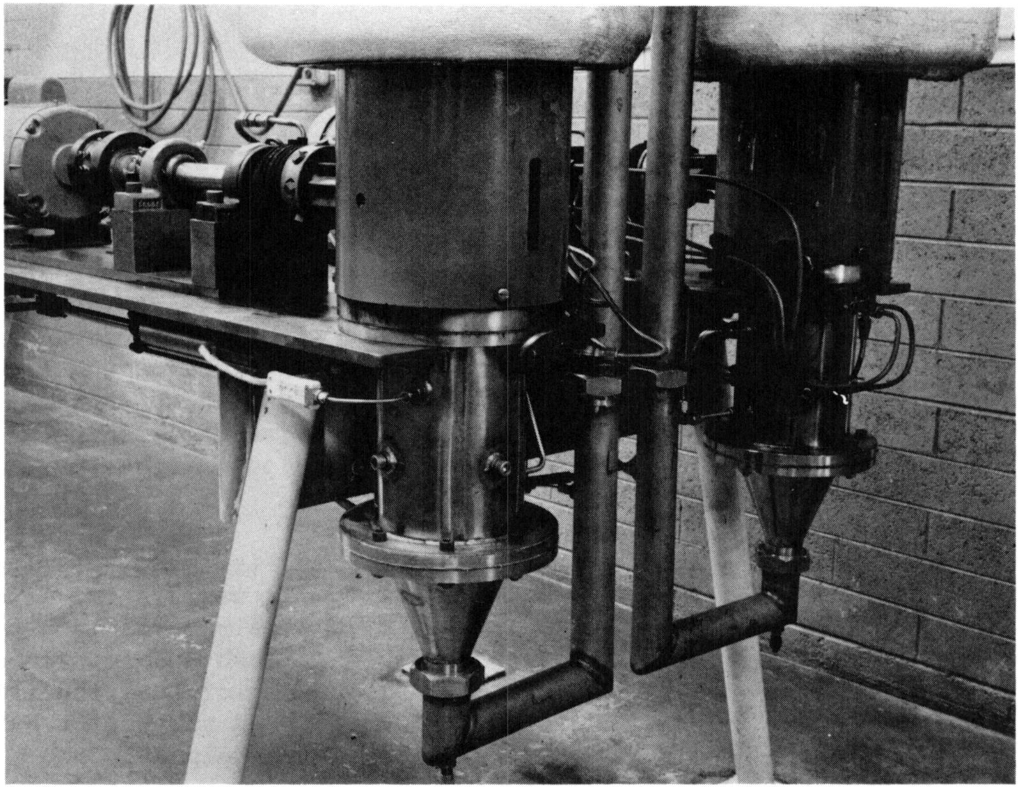

Figure 11. Gas Turbine Environmental Simulators

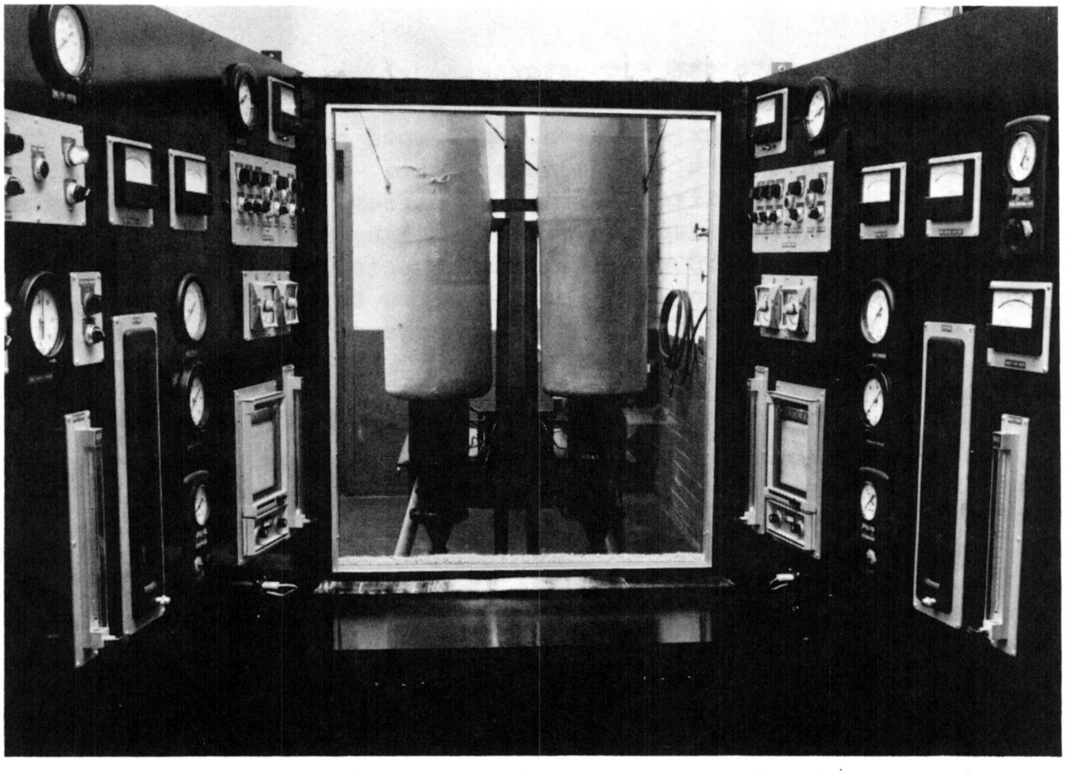

Figure 12. Control Console for Gas Turbine Environmental Simulators

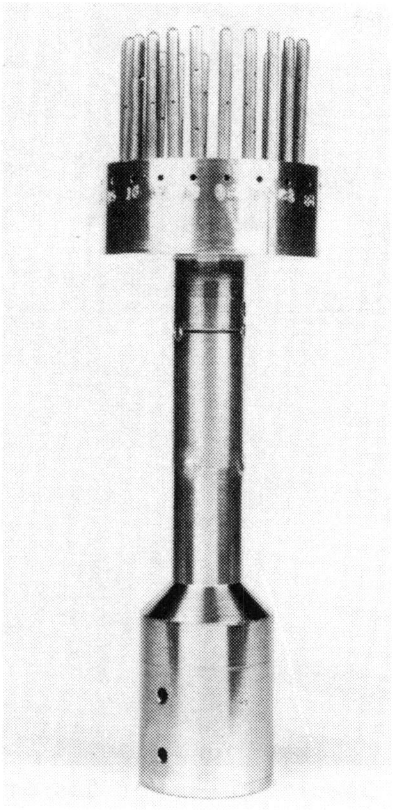

Figure 13.

Coated Test Specimens Prepared for Burner Rig Testing

Table 5. Other details of rig operation and calibration are provided in Appendix A. The synthetic sea water composition is reported in Table 6 in terms of weight percent of the various ions present in the solution.

Oxidation Burner Rig Test

The same burner rig as described above was used to perform the cyclic dynamic oxidation testing. The major modification was the removal of the salt injection line. The test temperature was 1050°C (1922°F) and the test parameters are reported in Table 7.

Cold Flow Check

One of the major considerations in the development phase of the program was to demonstrate the ability to completely remove the pack from the internal cavity. To monitor this, a cold flow check system was established using production flow bench facilities (Fig. 18) which are used to characterize mass flow through air-cooled components prior to engine assembly. A special fixture was designed and fabricated to hold the test pin tightly but without

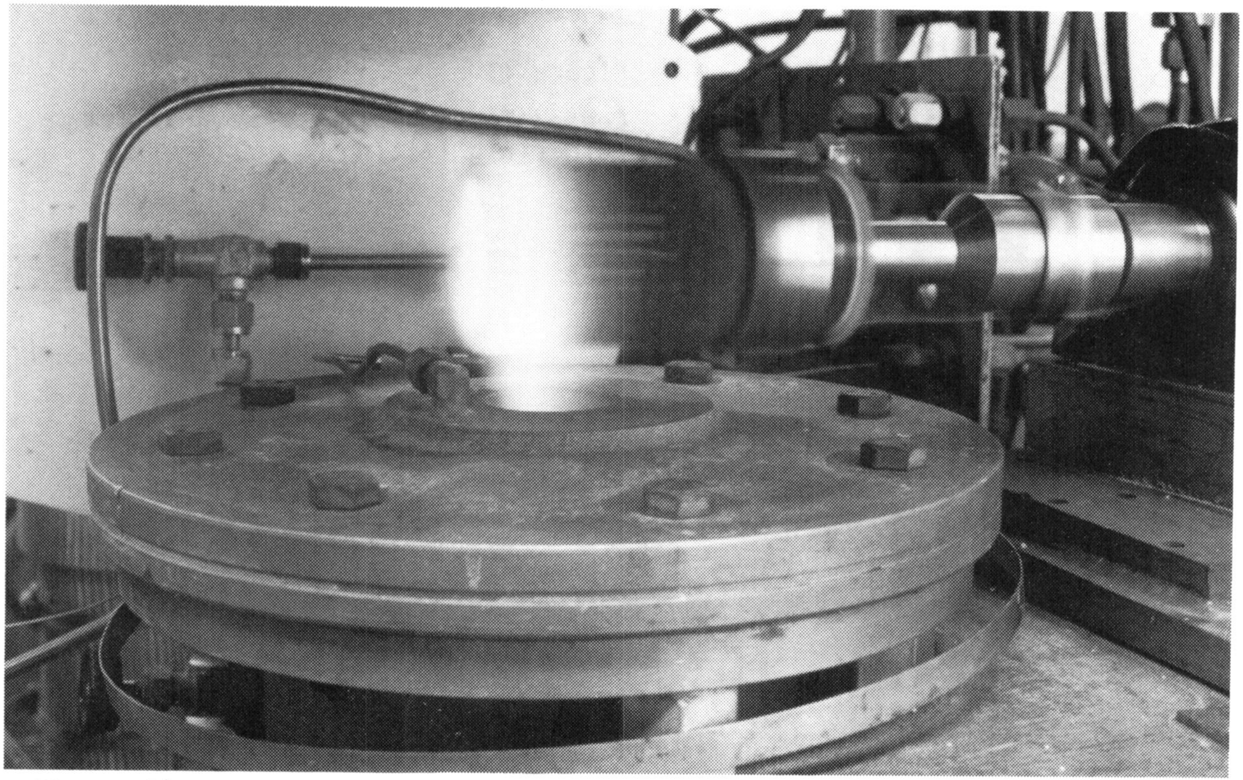

Figure 14. Burner Rig Test Showing Rotating Specimens in Hot Gas Stream

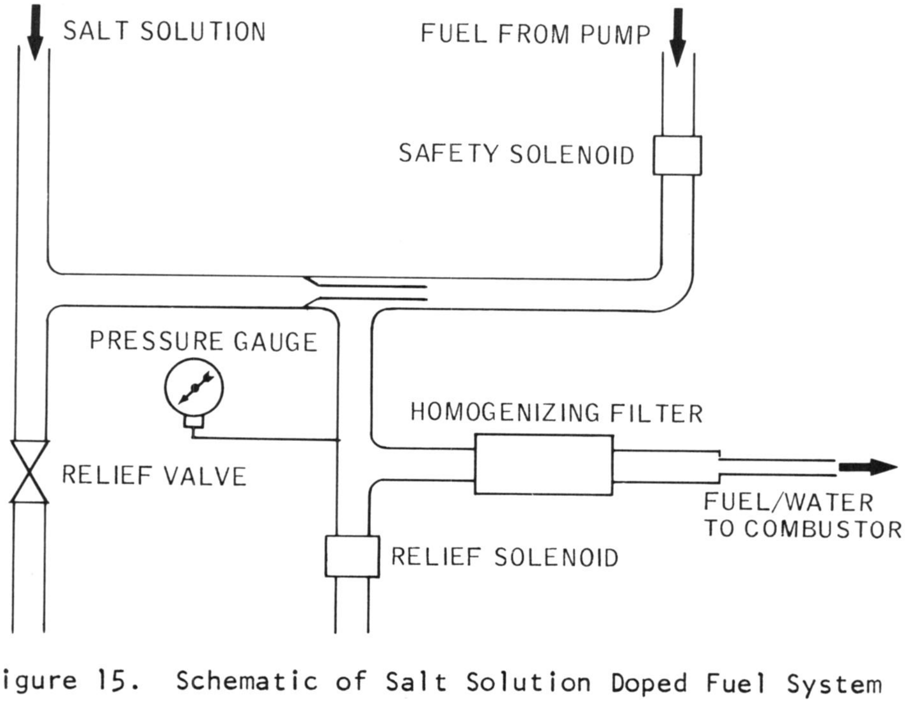
SALT SOLUTION
FUEL FROM PUMP
SAFETY SOLENOID
PRESSURE GAUGE
HOMOGENIZING FILTER
RELIEF VALVE
FUEL/WATER TO COMBUSTOR
RELIEF SOLENOID

Figure 15. Schematic of Salt Solution Doped Fuel System

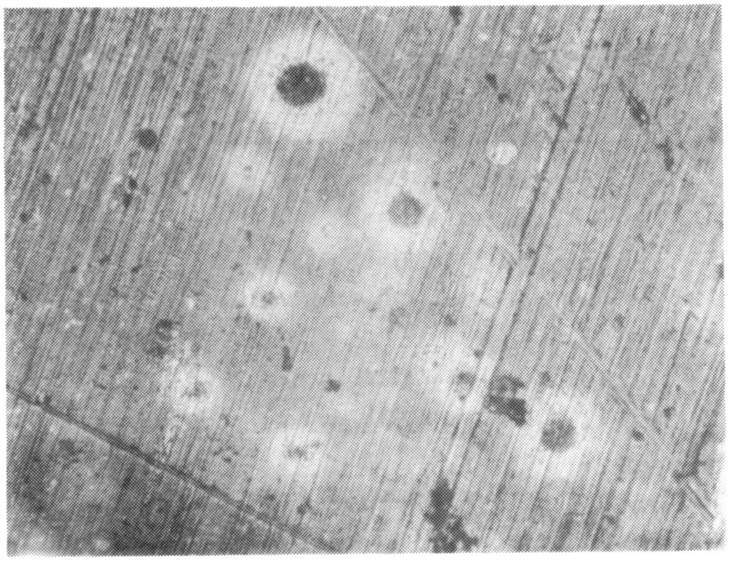

Figure 16.

Salt Particles From Hot Gas Stream in Burner Rig

Magnification: 200X

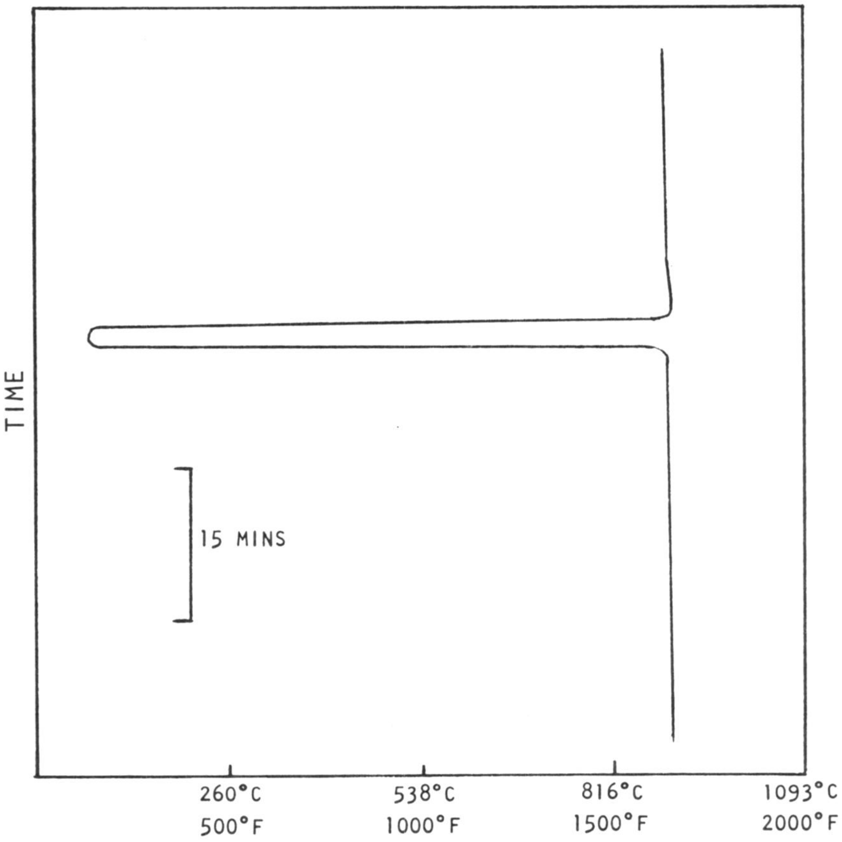

Figure 17. Typical Temperature Profile During Thermal Cycling

Table 5

Hot Corrosion Rig Parameters

Specimen temperature	899°C (1650°F)
Preheated air temperature	∿191°C (375°F)
Inlet air temperature	∿27°C (80°F)
Flame velocity	624 m/sec (2048 ft/sec)
Salt content	∿4 ppm
Combustor pressure	0.158 kPa (22.9 psi)
Air flow	95 g/sec (0.21 lb/sec)
Fuel	JP-5
Fuel flow	3 g/sec (0.416 lb/min)
Air/fuel ratio	41.5
P_{total}/P_{static}	1.58
Mach number	0.85
Cycle	1 cycle/hour
Number of cycles	219

Table 6

Synthetic Sea Water

Ions	Dry Salt (Wt %)
Na^+	28
K^+	1
Mg^{2+}	5
Ca^{2+}	1
Cl^-	56
Br^-	2
SO_4^{2-}	7

Table 7

Dynamic Oxidation Rig Parameters

Specimen temperature	1050°C (1922°F)
Preheated air temperature	∿232°C (450°F)
Inlet air temperature	∿24°C (75°F)
Flame velocity	676 m/sec (2218 ft/sec)
Combustor pressure	0.160 kPa (23.2 psi)
Fuel	JP-5
Fuel flow	3.1 g/sec (0.4316 lb/min)
Air/fuel ratio	25.1
P_{total}/P_{static}	1.58
Mach number	0.85
Cycle	1 cycle/hour
Number of cycles	235

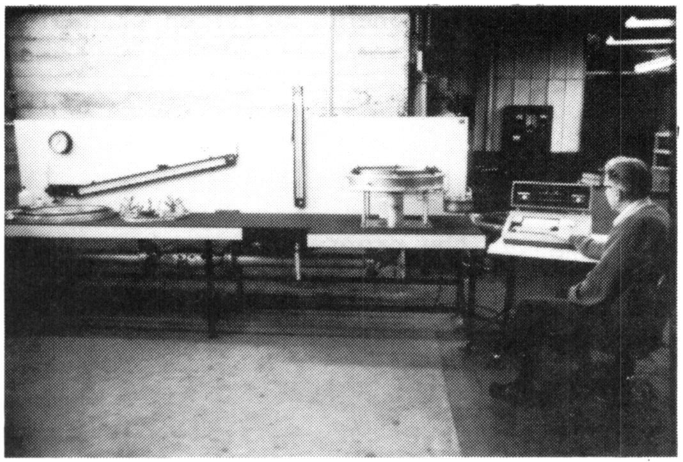

Figure 18.
Solar's Flow Bench Apparatus

flow restriction against a large plenum supplied with oil-free, dirt-free, dry cold air. The fixture itself is shown in Figure 19 and was demonstrated to position the test pin in a reproducible manner. Each part was held at a fixed pressure ratio which then eliminated the need for atmospheric pressure corrections. Air mass flow rate, plenum pressure, and temperature are combined in a flow function equation (using a laminar flow element) which can be calculated in a pre-programmed desk calculator. The flow check process is independent of variation in atmospheric pressure and temperature and upon keying in the plenum temperature, flow function readings were accurately read with standard deviations of less than one percent.

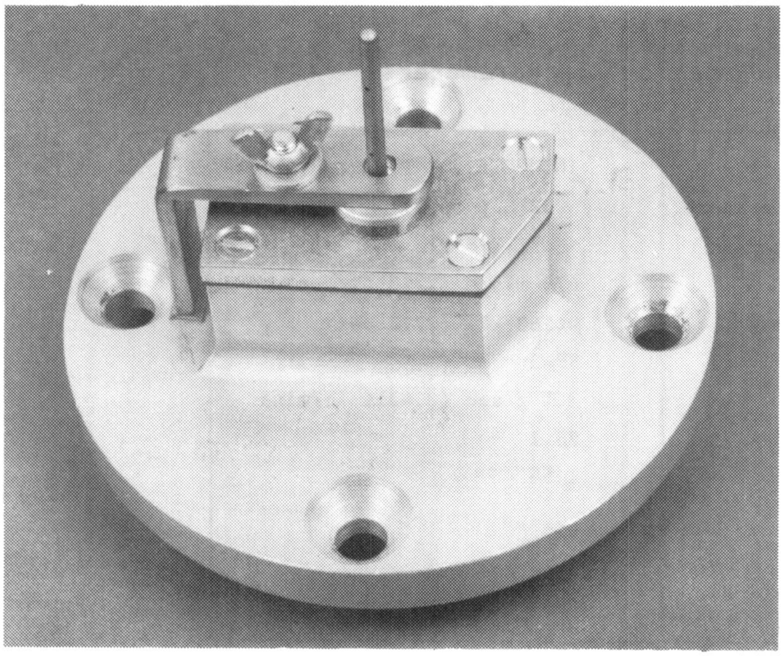

Figure 19.

Flow Check Fixture Used in Monitoring Air Flow Discharge of Pin Specimens

The same system was used to monitor flow values through the Mars 1st-stage blade. In this case, the part, being an engine component, utilized standard production fixtures and procedures.

Metallography

Metallography was employed routinely throughout the program to examine microstructure and bonding of the coatings to the substrate. Other methods of semi-quantitative analyses utilized include X-ray fluorescence, electron microprobe and scanning electron microscopy (energy dispersive X-ray) analyses.

3

COATING PROCESS DEVELOPMENT

The first step toward process development was the selection of a suitable diluent for slip packs. Essentially, all pack processes use some form of inert diluent to prevent the active metallic components in the pack from sintering. The problem of cementation of the metallic constituents of the slip pack during the heat cycle can be severe, especially in chromium containing packs. The approach taken was two-fold - an inert material was selected and the optimum balance struck between inert diluent and active metals in the pack.

Three inert "filler" materials were investigated, CaO, MgO and Al_2O_3. A series of chromium slip packs were prepared, as reported in Table 8. These slip packs were applied to small (1.27 x 1.27 x 0.25 mm) MAR-M421 coupons with 0.7 mm holes drilled through the center of each piece to simulate the small holes typically found in air-cooled blading. After a furnace cycle of four hours at 1100°C the following observations were made.

Table 8

Chromium Pack Compositions

Specimen No.	Pack Composition	Activator	Weight Gain (mg/cm^2)
D100	$80Al_2O_3$-20Cr	0.5w/o NH_4Cl	4.8
D200	80CaO-20Cr	0.5w/o NH_4Cl	2.4
D300	80MGO-20Cr	0.5w/o NH_4Cl	4.5
D400	$79Al_2O_3$-20Cr	1.0w/o NaCl	4.4

With 0.5 weight percent NH_4Cl activator, the CaO and MgO slip packs were more easily removed than the Al_2O_3 pack. However, a scale was formed on the substrate with the D100 and D200 packs. Upon metallurgical examination, it was found that oxidation attack had occurred, resulting in the microstructure shown in Figure 20. This degradation of the substrate can be related to the affinity of alkaline earth oxide for water when exposed to the environment

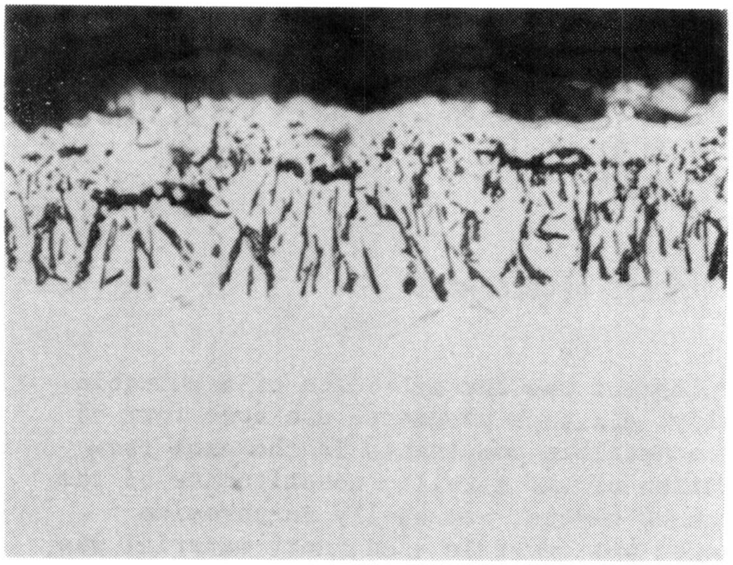

Figure 20.

Microstructure of D300 Coated MAR-M421 (Note Severe Internal Oxidation)

Magnification: 500X

Unetched

even at ambient temperature. In order to avoid this, a moisture-free environment must be maintained during all stages of handling and pack preparation to minimize oxidants such as H_2O.

The Al_2O_3-NH_4Cl pack was difficult to remove by conventional methods of pressure washing and air blasting. By substituting NaCl for NH_4Cl in the D400 test run, the fired bisque appeared to be readily removed by pressure washing. It is well known, especially in relation to high activity aluminide processing, that the choice of activator can critically affect the thermodynamics and kinetics of the diffusion process (Ref. 6). Depending on the type of halide used and the operating conditions, the rate determining phenomenon can be pack activity, gaseous diffusion or solid state diffusion of nickel and aluminum. In this case, by substituting NaCl for NH_4Cl, chromium particle agglomeration and reaction sintering of the chromium particles in the pack with the substrate surface was apparently reduced and pack removal facilitated.

Based on the above investigation, it was decided to use Al_2O_3 as the inert filler for all subsequent packs in order to eliminate the water induced corrosion associated with the alkaline earth oxides.

Metallographic evaluation of the NaCl activated chromium pack specimen, D400, as can be seen in Figure 21, showed excellent coating uniformity. Figure 22 shows that a chromium-rich coating region approximately 55 micrometers (2 mils) thick was formed at the substrate surface which was primarily gamma nickel chromium substitutional solid solution with alpha-chromium in a semi-continuous layer at the outer surface (see Fig. 23 for Cr-Ni binary phase diagram). X-ray fluorescent analysis of this region indicated chromium levels to be 22 to 25 weight percent, which was in good agreement with program goals. At the same time, line profile analysis was performed using the electron microprobe giving the trace shown in Figure 24.

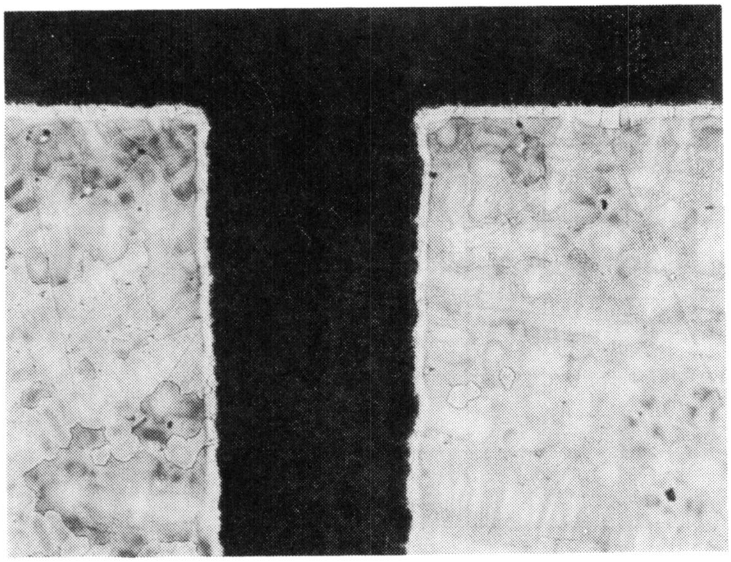

Figure 21.

Cross-Section Through Coated 0.7 mm Hole in MAR-M421 (Specimen D400)

Magnification: 40X

Etchant: Kalling's

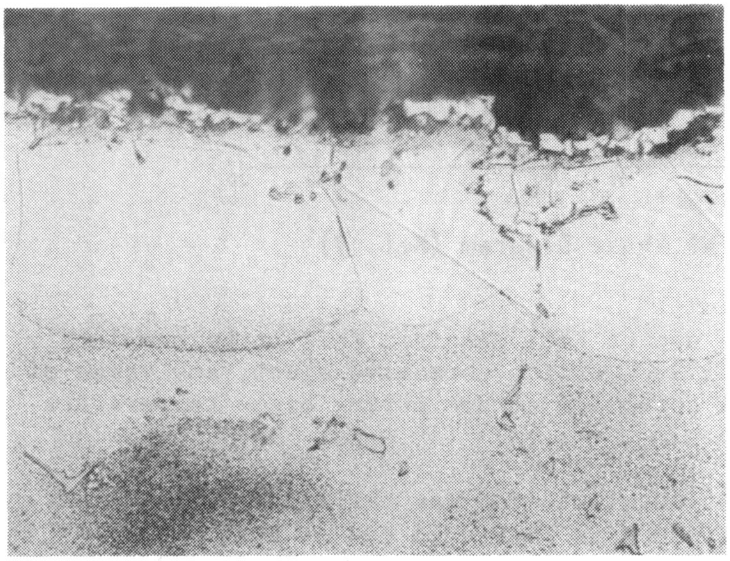

Figure 22.

Microstructure of Ni-20Cr on MAR-M421 (Specimen D400)

Magnification: 500X

Etchant: Kalling's

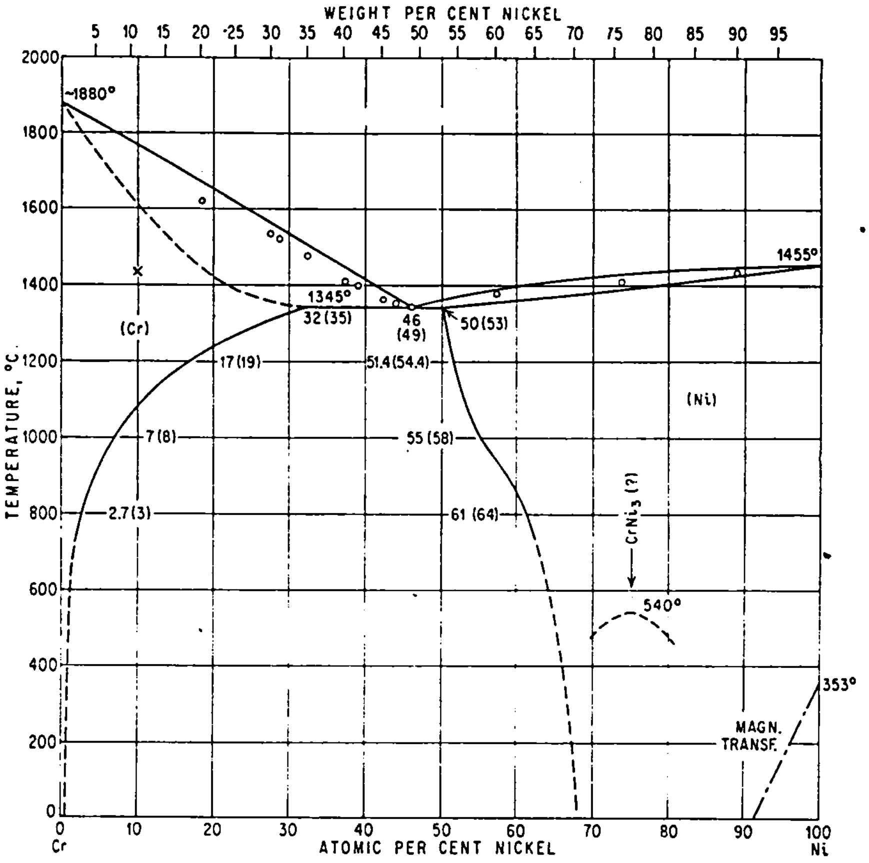

Figure 23. Cr-Ni Phase Diagram (Ref. 7)

It should be pointed out that the use of NaCl requires that it be completely removed after processing. As NaCl is itself a corrosive agent, any trace of salt or chloride will enhance hot corrosion attack during high- temperature operation.

The next single element pack constituent studied was the silicon slip pack. The Ni-Si binary phase diagram is shown in Figure 25 and at near stoichiometric Ni-Si (30 weight percent Si) a low melting eutectic is formed at 960°C. A 100 percent silicon pack activated with 0.5 weight percent NaCl was prepared and fired at 816°C for a period of eight hours. Gravimetric measurements found only 1 to 2 mg/cm^2 weight gain and closer scrutiny revealed the presence of dark globular phases on the substrate surface, as seen in Figure 26. Electron microprobe results indicated the presence of sodium in these dark areas.

Another silicon pack was prepared with 25 percent inert Al_2O_3 diluent and 0.5 weight percent NH_4Cl. Following a furnace cycle of 816°C for eight hours, a 4 mg/cm^2 weight gain was noted. X-ray fluorescent analysis at the substrate surface indicated approximately 20 weight percent silicon. Some particle sintering and entrapment was noted on the substrate surface which probably added to the surface silicon X-ray counts. Upon microstructural examination (Fig. 27) it was found that the silicided layer extended approximately 70 µm into the substrate, which exceeded the program specification of 39 µm.

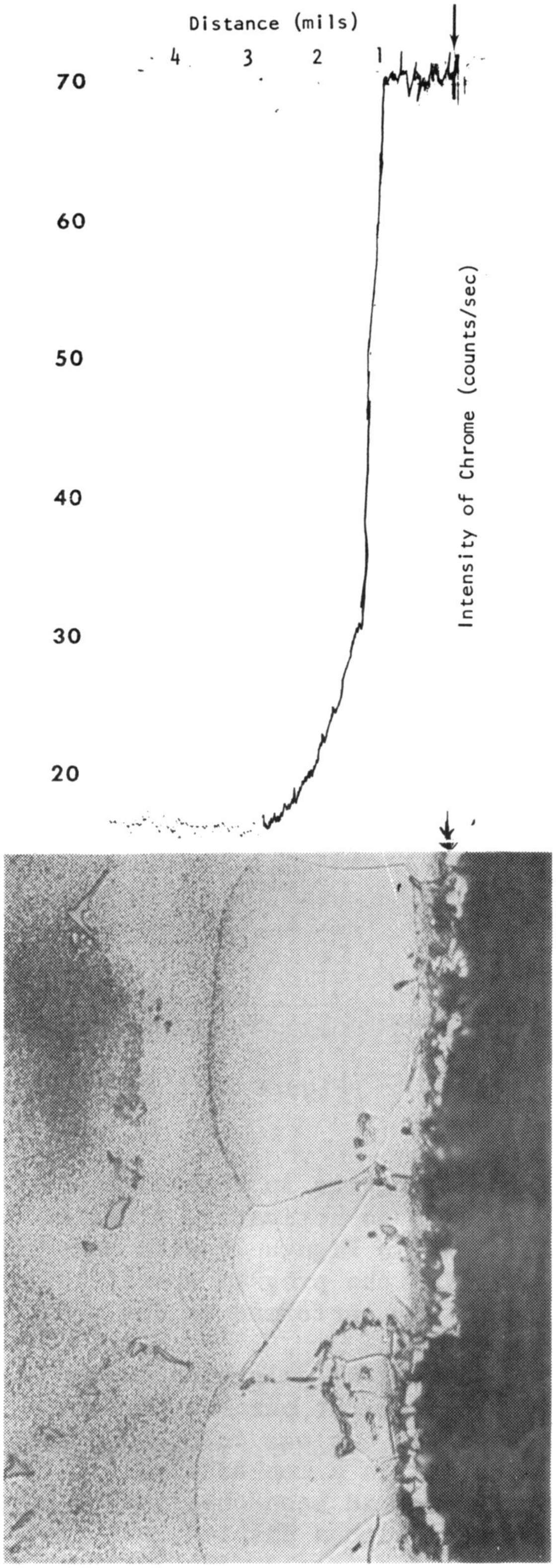
Distance (mils)
4
3
2
1
70
60
50
40
30
20
Intensity of Chrome (counts/sec)

Magnification: 500X
Etchant: Kalling's
Specimen D400

Figure 24. Chromized Internal Coating on MAR-M421 Deposited by Slip Pack Process

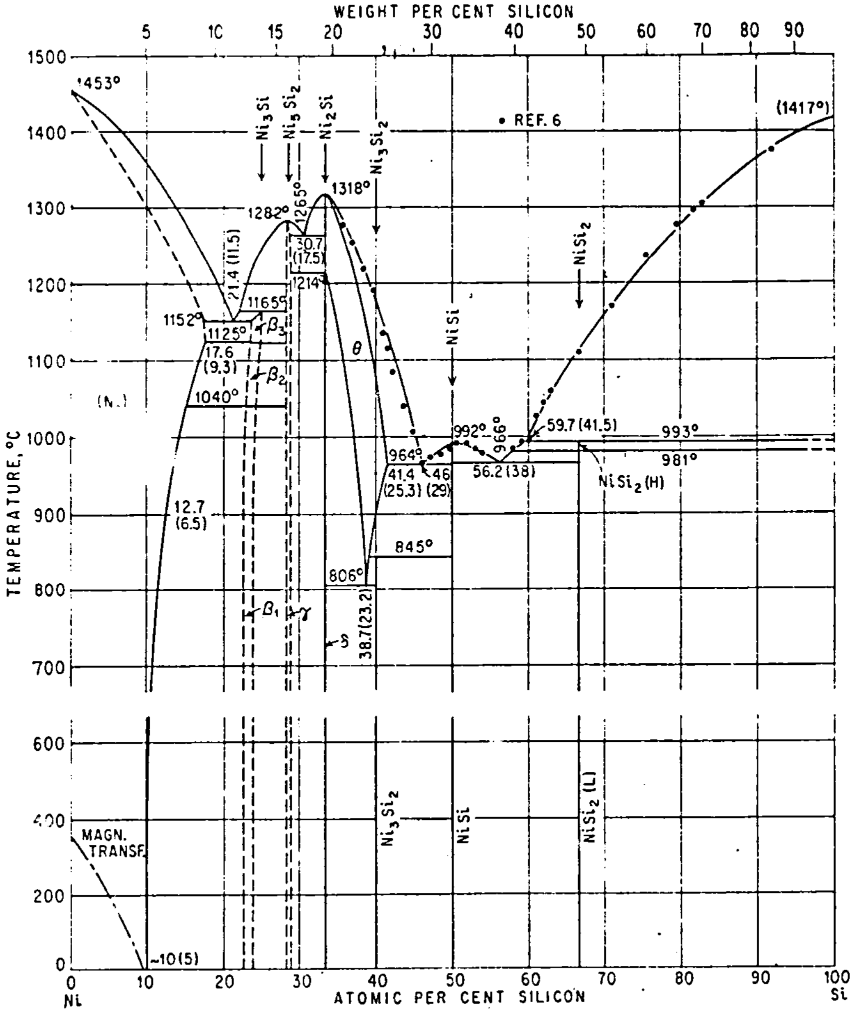

Figure 25. Ni-Si Binary Phase Diagram (Ref. 7)

Further efforts in this direction resulted in formulation of a 75Si-25Al_2O_3-pack with no activator, fired at 871°C for four hours. The coating structure is shown in Figure 28 with MAR-M200 + Hf as the substrate. This coating satisfied the program specification. (The rest of the coating development effort was performed on the program alloy MAR-M200 + Hf.)

Development of columbium coating started with a 100 percent columbium slip with 0.5 weight percent NH_4Cl run at 1100°C for two hours. Under these conditions, it was found that approximately 1 mg/cm^2 of columbium was deposited in a non-adherent flaky film at the substrate . A similar phenomena had been observed by other investigators (Ref. 7). The next run was made with a diluted pack (75Cb-25Al_2O_3-0.5NH_4Cl) at 1138°C for six hours. The coating formed (Fig. 29) was approximately 12 microns thick and microprobe analysis detected approximately one weight percent columbium in the nickel matrix.

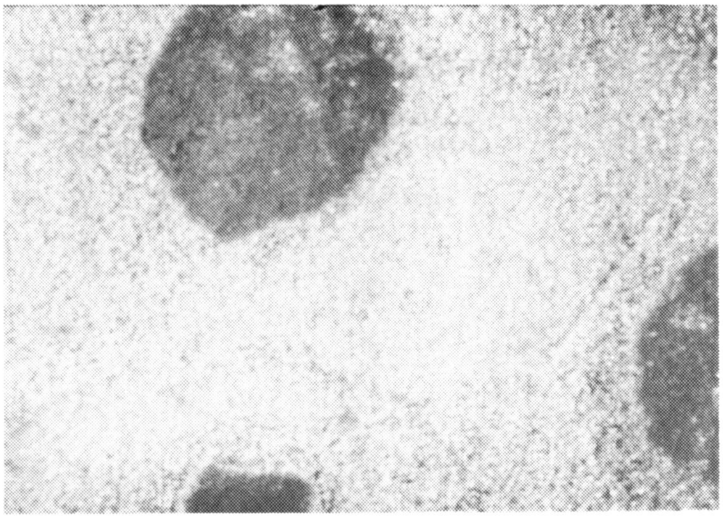

Figure 26.

Silicided MAR-M421 Specimen Surface (F100) Showing Dark Area Containing NaCl

Magnification: 14X

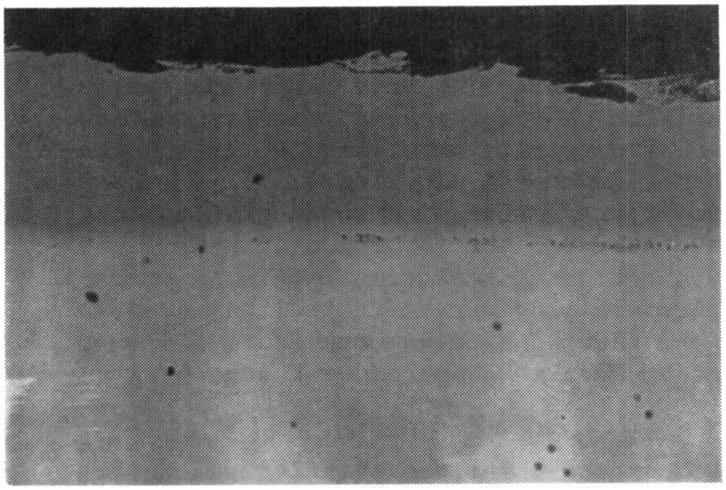

Figure 27.

Silicide Coating Formed on MAR-M421 After Eight Hours at 816°C

Magnification: 250X

Unetched

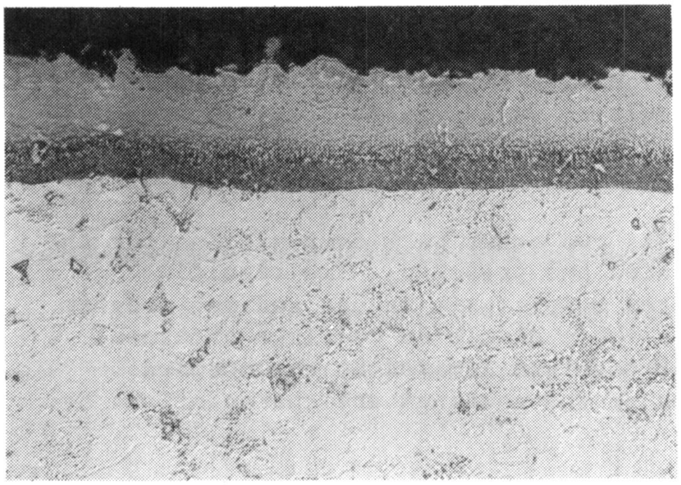

Figure 28.

Microstructure of Silicon Coating on MAR-M200 + Hf (DS)

Magnification: 500X

Etchant: Kallings

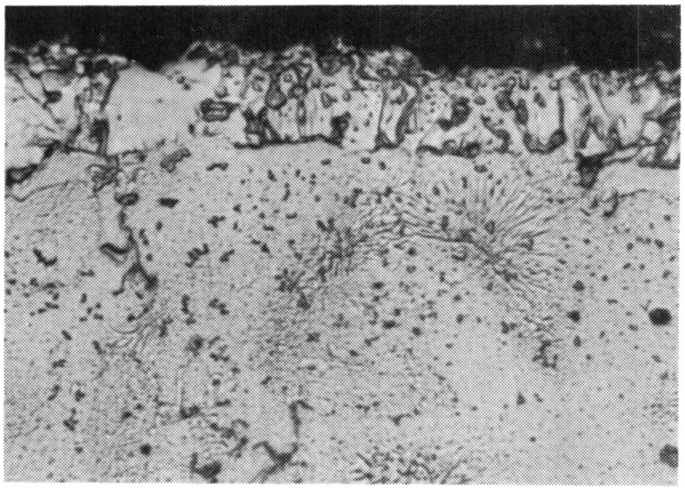

Figure 29.

Columbium Coating on MAR-M200 + Hf (DS) (E101)

Magnification: 500X

Development of the three nickel-aluminum compositions, Ni-20Al, Ni-17Al and Ni-15Al was based on Solar's extensive experience with aluminizing packs. Figure 30 shows the aluminum-nickel binary phase system. At 1079°C (1975°F), which is a commonly used temperature for coating applications, Ni-20Al to Ni-15Al lie in the mixed field region of nickel-rich beta plus gamma prime. In order to form the desired aluminide on the gamma-gamma prime strengthened superalloy, the pack activity has to be carefully controlled to attain the required amount of aluminum diffusion. From past experience, it is known that high activity aluminum packs (mostly aluminum with some chromium) the thermodynamics of the system are favorable for the formation of near stoichiometric beta, even in fairly short periods of time. This is primarily due to the increased diffusion of aluminum as the rate-controlling step. To reduce the pack activity and lower the rate of aluminum transport and diffusion into the alloy, nickel and/or cobalt can be added to the pack as alloying components.

The approximate weight gains for each of the three candidate (62 μm thick) aluminide coatings were calculated to be 8.3 mg/cm^2, 7.4 mg/cm^2 and 6.6 mg/cm^2 for the corresponding Ni-20Al, Ni-17Al and Ni-15Al coatings. These calculated values were based on density values given in Reference 8.

Two aluminum packs were prepared with the following compositions: Ni-60Al and Ni-70Al with 60 percent pack dilution with Al_2O_3. The firing time was held to 16 hours at 1079°C and the resulting weight gains were 8.3 and 5.6 mg/cm^2, respectively. The Ni-60Al pack appeared to be appropriate for the formation of Ni-20Al coating.

By extrapolation, as shown in Figure 31, two other pack compositions for the Ni-17Al and Ni-15Al packs were formulated and prepared. The resulting coatings formed confirmed the calculated weight gain values and met program goals. Figures 32 through 34 show the three aluminide coatings obtained. The coatings are all characteristic of coatings limited by the outward diffusion of nickel. The three layers of the coatings are characterized by:

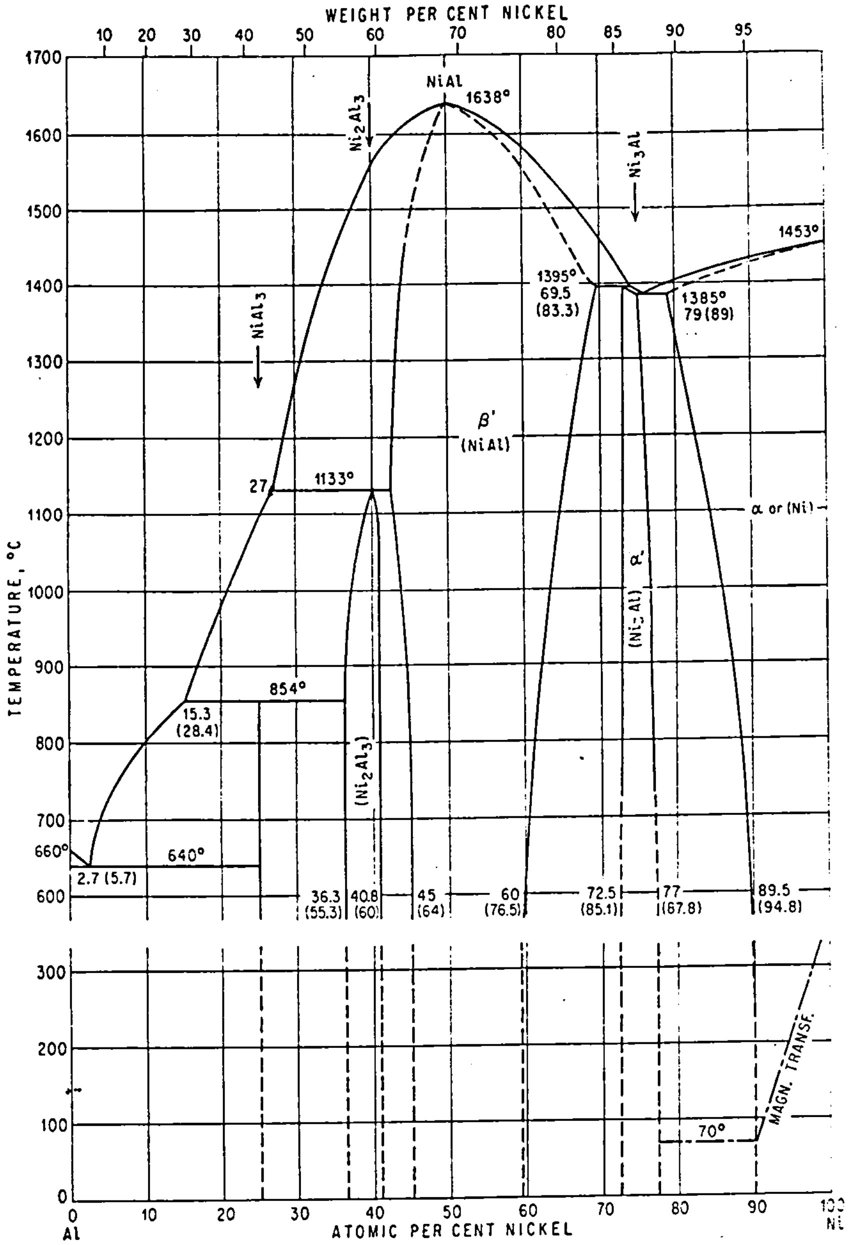

Figure 30. Al-Ni Binary Phase System

A. An outer layer in which some precipitation of chromium is present,

B. A central denuded zone of beta-nickel essentially free of secondary phases; and

C. A multiple phase zone low in nickel and high in chromium and refractory solid solution strengthening elements.

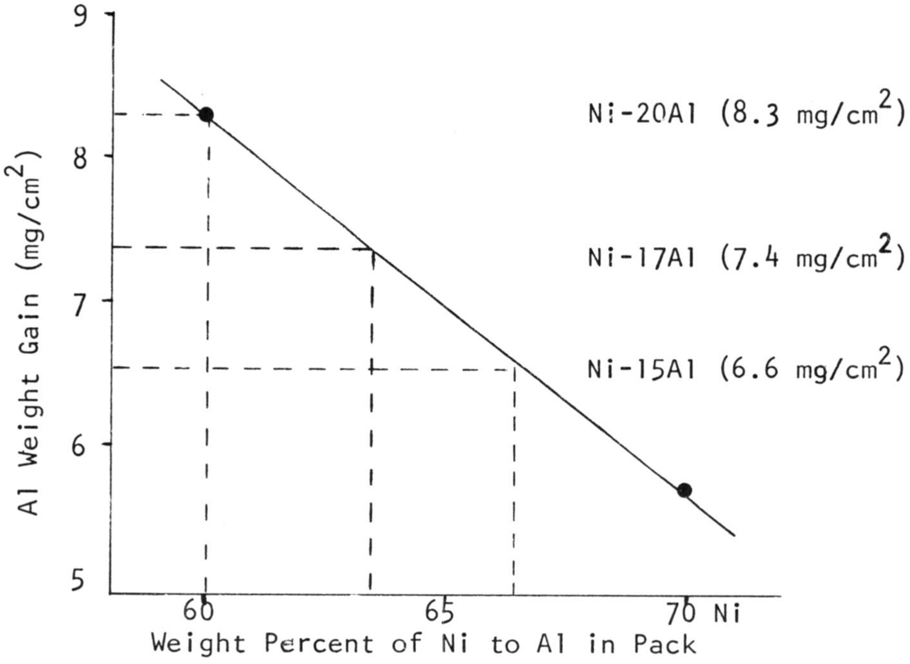

Figure 31. Extrapolated Relationship of Aluminum Pickup and Ni-Al Ratio

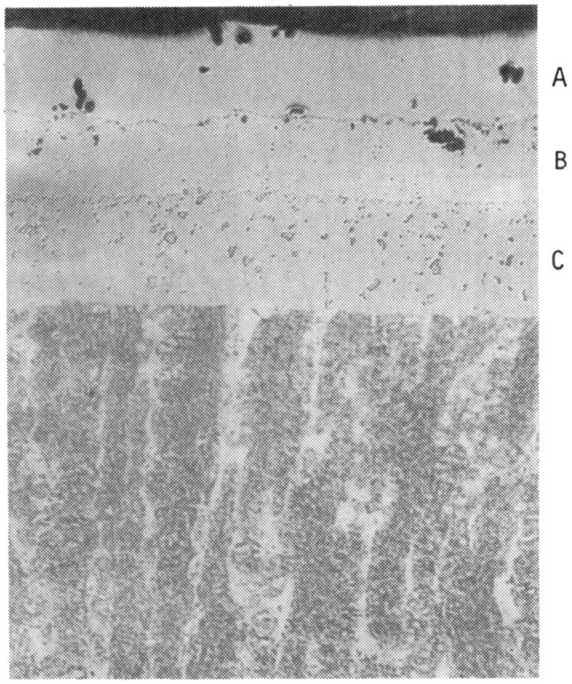

Figure 32.

Microstructure of Ni-20Al Coating (A107)

Magnification: 500X

Etchant: 2% Chromic

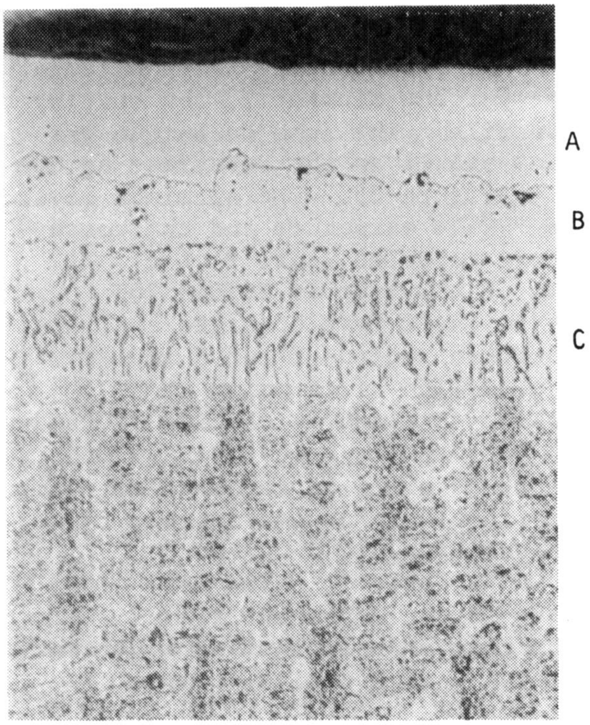

Figure 33.
Microstructure of Ni-17Al Coating

Magnification: 500X
Etchant: 2% Chromic

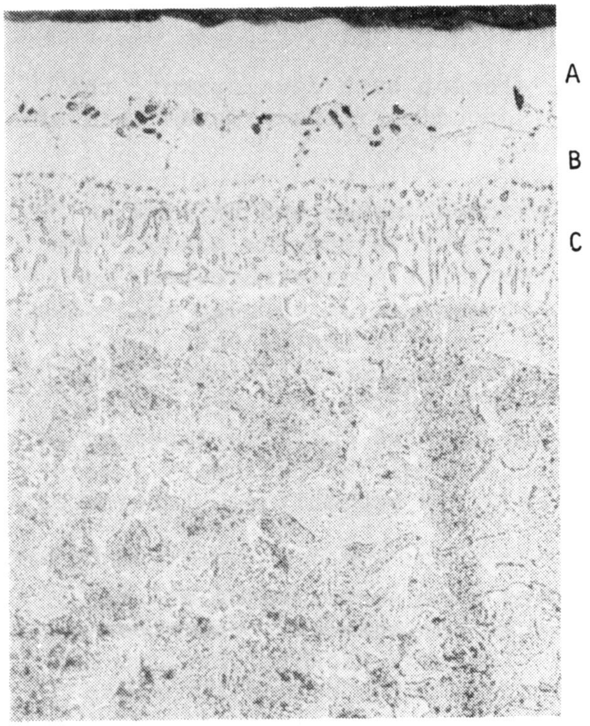

Figure 34.
Microstructure of Ni-15Al Coating

Magnification: 500X
Etchant: 2% Chromic

Electron microprobe analysis was performed on the Ni-20Al coating. The three zones were designated A, B and C, as seen in Figure 32. Using the substrate as the primary aluminum standard (4.95 weight percent aluminum), the coating thickness was probed to obtain an aluminum profile. The same technique was used for nickel using the 60.43 weight percent nickel in the substrate as the standard. The elemental profiles are shown in Figure 35. The aluminum level decreases with distance from coating surface. This structure and the corresponding elemental profiles are similar to those reported (Ref. 9) for aluminide coatings formed by inward diffusion of aluminum on Udimet 700 followed by a diffusional heat treatment. From their more complete analyses, the low level of nickel and aluminum found between regions B and C is very likely due to the presence of increased concentration of chromium and titanium. The chromium and titanium are probably present as carbide TiC and $Cr_{23}C_6$ in the C zone while the 'denuded' C zone contains some chromium and titanium in solution. The diffusion coating thus formed is composed of not only aluminum phases but also precipitates of insoluble phases derived from the substrate alloy. The overall coating composition was obtained by consideration of the microprobe data presented in Table 9, which were also normalized to the nickel and aluminum contents in the substrate alloy. (Normalization was done by considering only nickel and aluminum on a percent basis.) The averaged value over the three zones gave a nominal composition of Ni-20Al.

Further microprobe work on the other two aluminide coatings gave values of Ni-18Al and Ni-13Al, both of which were in agreement with the specified Ni-17Al and Ni-15Al within the ± 20 percent tolerance limits.

To summarize, the above discussion on single element pack development, the pack compositions of each system and the corresponding furnace parameters are listed in Table 10.

The next step in coating development was to process duplex and triplex coatings using the processes developed above to achieve program goals. The sequences used are explained in Table 1 and the final microstructures, as applied to MAR-M200+Hf(DS) coupons are shown in Figures 36 through 45. Also shown are structures after heat treatment. It was anticipated that these modified aluminide coatings would retain adequate hot corrosion/oxidation resistance together with good ductility and stability. Since both coating and alloy are non-equilibrium systems, the heat-treated coatings appeared to have undergone considerable interdiffusion and some of the secondary phases either redissolved or were less discernible at grain boundaries. Interfaces were also less sharply defined.

In the as-coated specimens, microprobe analyses were performed on all ten candidate systems and the results are summarized in Table 11. For these analyses, the MAR-M200 substrate contents of aluminum, nickel, chromium and columbium were utilized as the reference standards while pure silicon was used for silicon counts. In general, the measured compositions agreed well with program goals with the exception of silicon, which fell short of the 20 percent margin allowed.

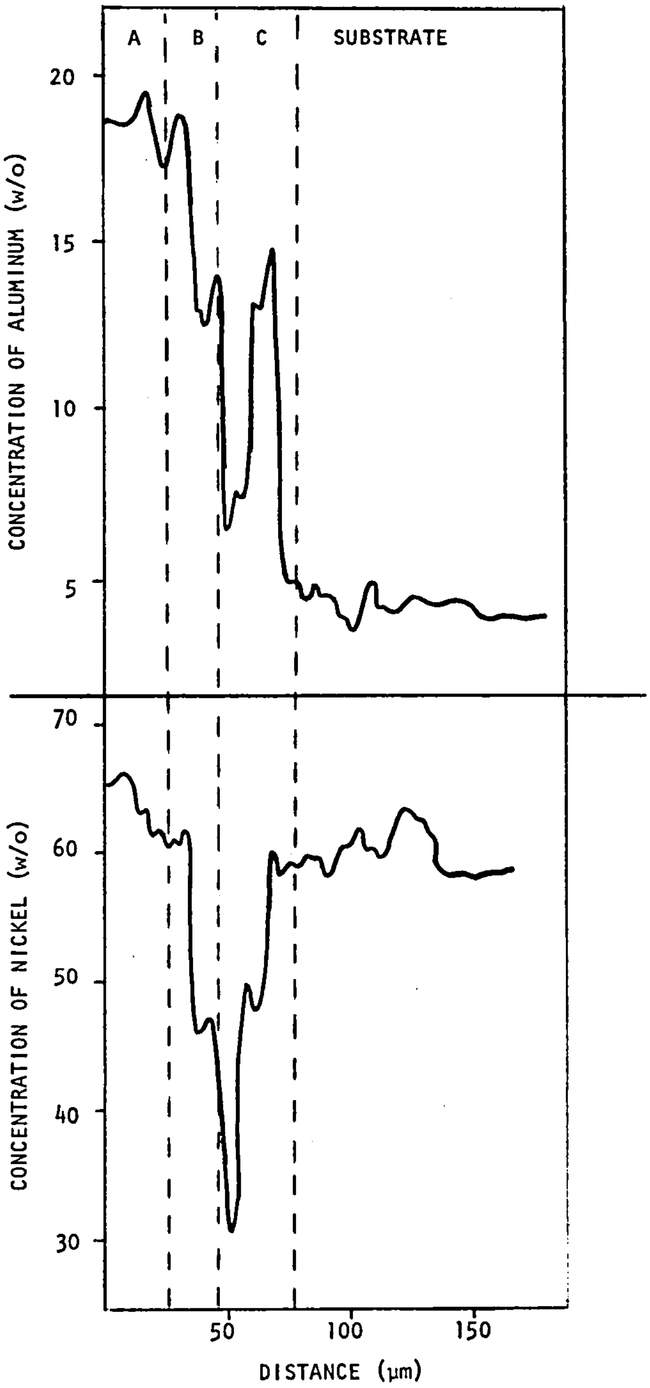

Figure 35. Nickel and Aluminum Concentration Profiles on Ni-20Al Coating on MAR-M421

Table 9

Microprobe Analysis of Three-Zone Nickel Aluminum Coating

Zone	Aluminum (w/o)	Nickel (w/o)
A	23	77
B	19	81
C	19	81
Substrate	5	60
Average = 80Ni-20Al		

Table 10

Coating Process Parameters

Pack Code	Element	Specimen Number	Pack Composition (w/o)	Activator (w/o)	Furnace Temp. (°C)	Furnace Time (hr)	Weight Gain (mg/cm^2)	Coating Thick. (μ)
A	Aluminum	A107	$60Al_2O_3$-24Ni-16Al	0.5 NH_4Cl	1079	16	8.3	75
B	Aluminum	A108	$60Al_2O_3$-25.6Ni-14.4Al	0.5 NH_4Cl	1079	16	7.4	75
C	Aluminum	A110	$60Al_2O_3$-26.8Ni-13.2Al	0.5 NH_4Cl	1079	16	6.6	75
D	Chromium	D400	$80Al_2O_3$-20Cr	0.5 NaCl	1100	4	4.0-9.0	51
E	Columbium	E101	75Cb-$25Al_2O_3$	0.5 NH_4Cl	1038	6	<0.5	~13
F	Silicon	F800	75Si-$25Al_2O_3$	None	871	4	3.0	33

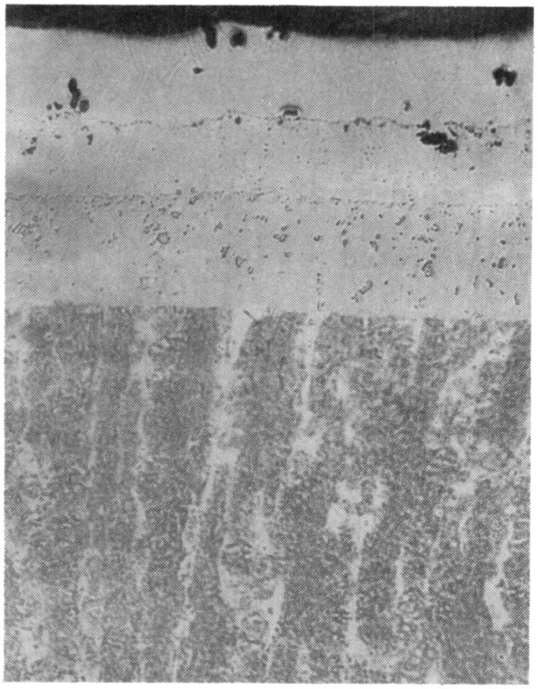

Magnification: 500X

Etchant: 2% Chromic

As Coated

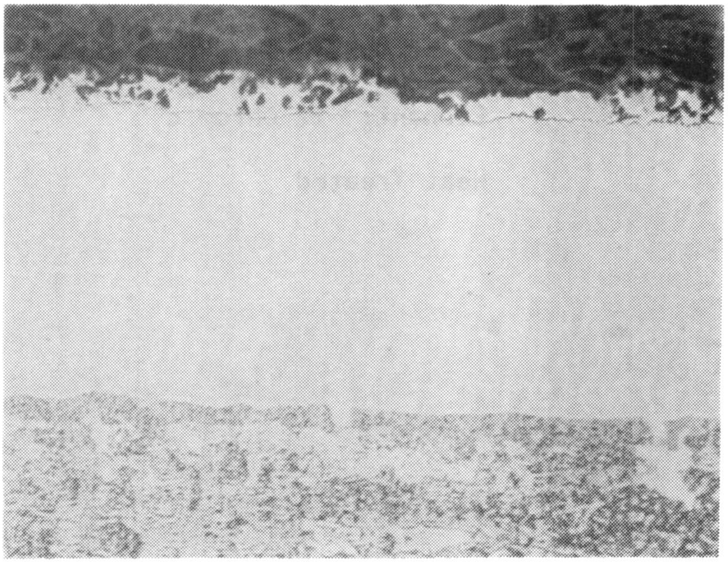

Magnification: 500X

Etchant: 2% Chromic

Heat Treated

Figure 36. Ni-20Al Coating (#1) on MAR-M200 + Hf (DS)

Use or disclosure of proposal data is subject to the restrictions on the Title page of this Proposal. (DEC. 1966)

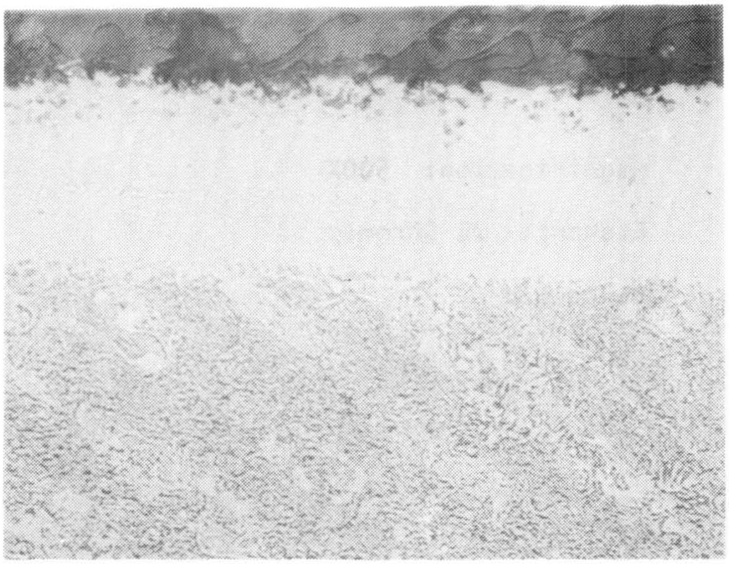

Magnification: 500X

Etchant: 2% Chromic

As Coated

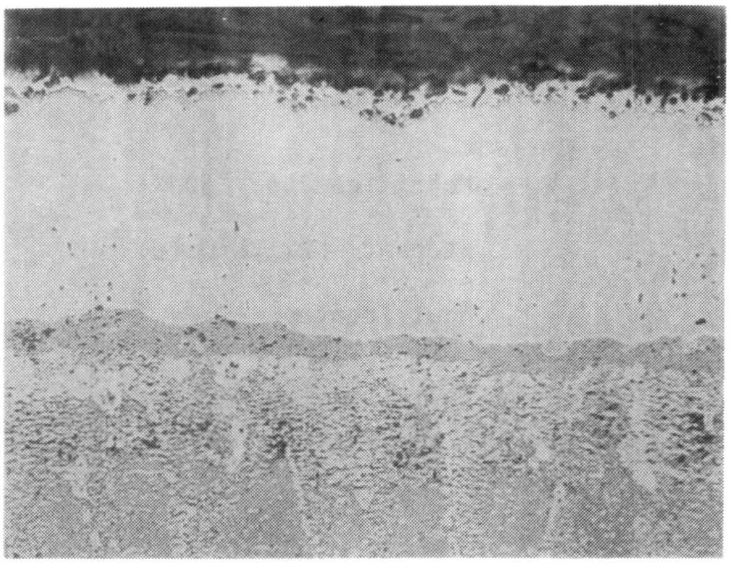

Magnification: 500X

Etchant: 2% Chromic

Heat Treated

Figure 37. Ni-19Al-1Cb Coating (#2) on MAR-M200 + Hf (DS)

Use or disclosure of proposal data is subject to the restrictions on the Title page of this Proposal. (DEC. 1966)

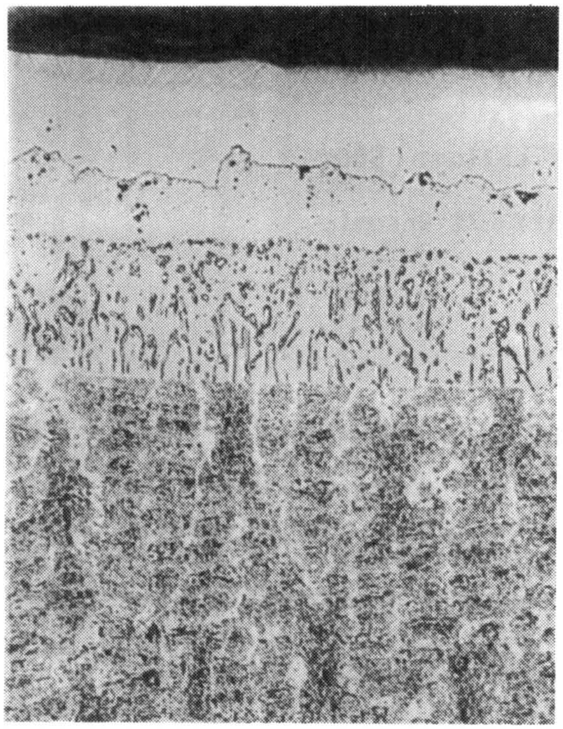

Magnification: 500X

Etchant: 2% Chromic

As Coated

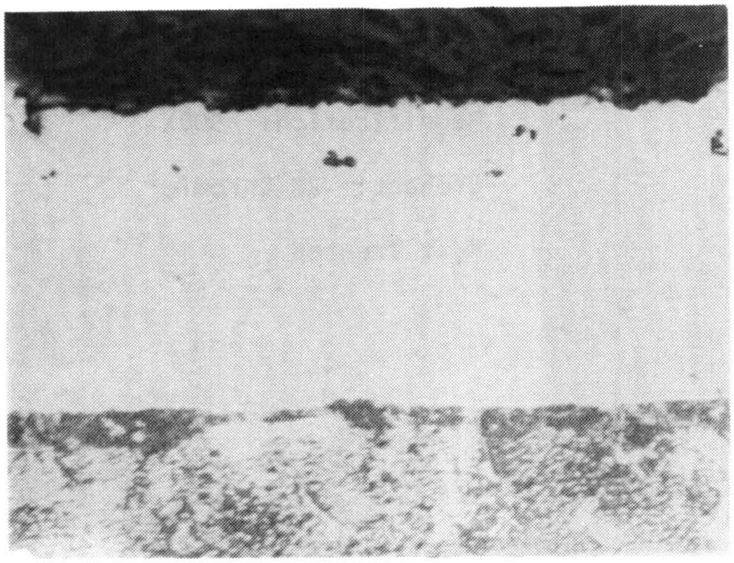

Magnification: 500X

Etchant: 2% Chromic

Heat Treated

Figure 38. Ni-17Al Coating (#2) on MAR-M200 + Hf (DS)

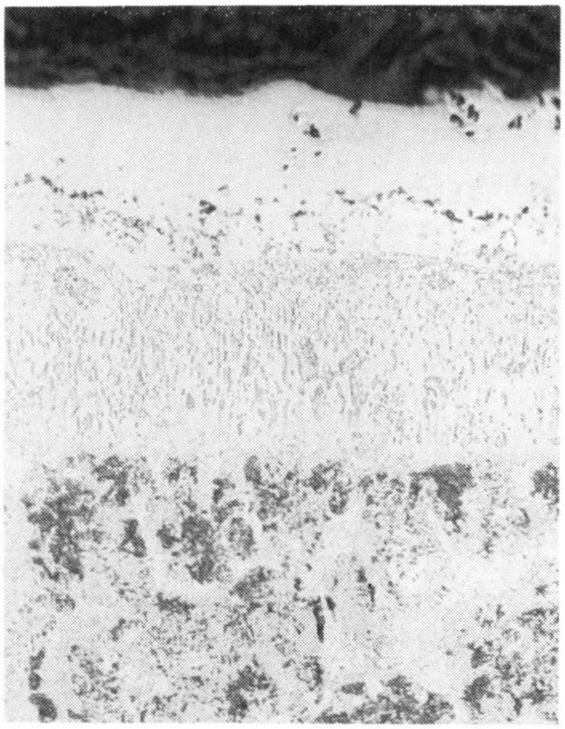

Magnification: 500X

Etchant: 2% Chromic

As Coated

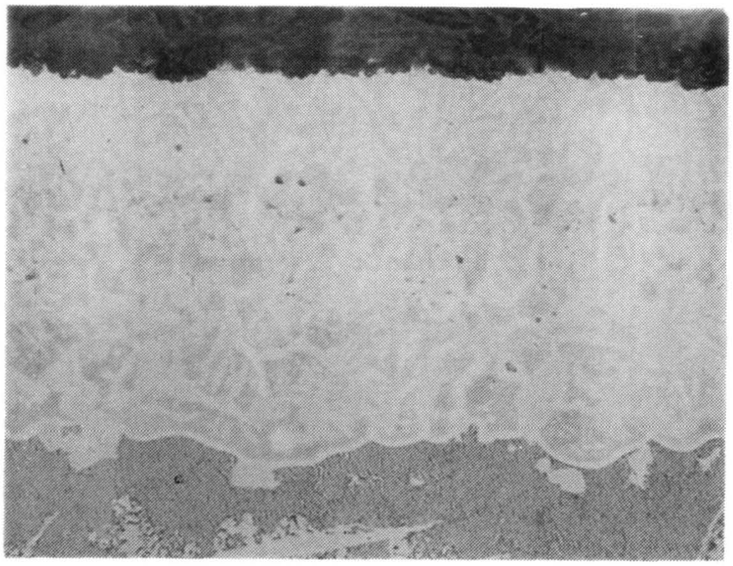

Magnification: 500X

Etchant: 2% Chromic

Heat Treated

Figure 39. Ni-16Al-5Si Coating (#4) on MAR-M200 + Hf (DS)

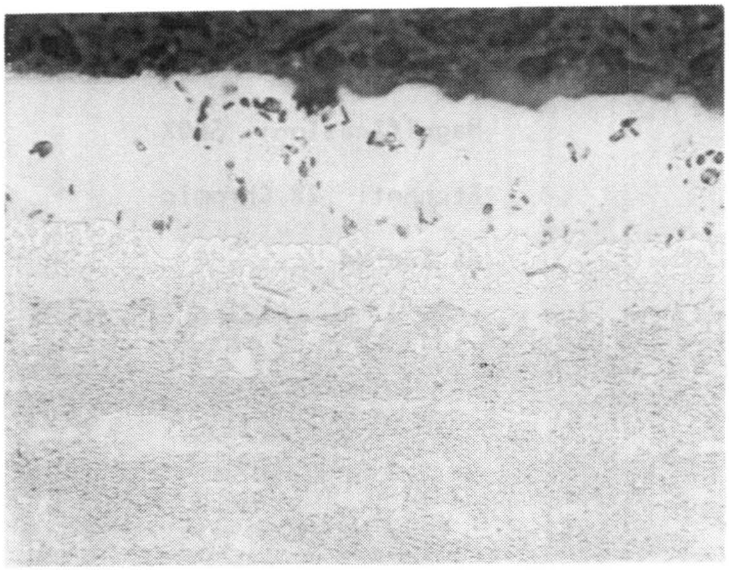

Magnification: 500X

Etchant: 2% Chromic

As Coated

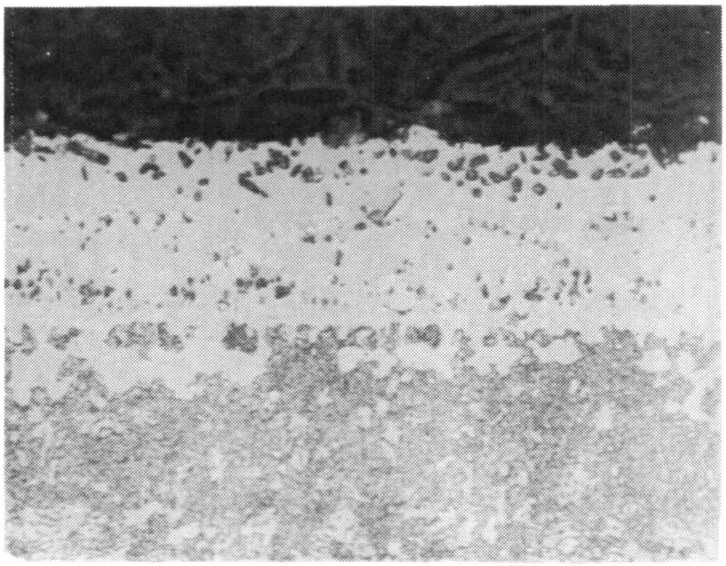

Magnification: 500X

Etchant: 2% Chromic

Heat Treated

Figure 40. Ni-14Al-20Cr Coating (#5) on MAR-M200 + Hf (DS)

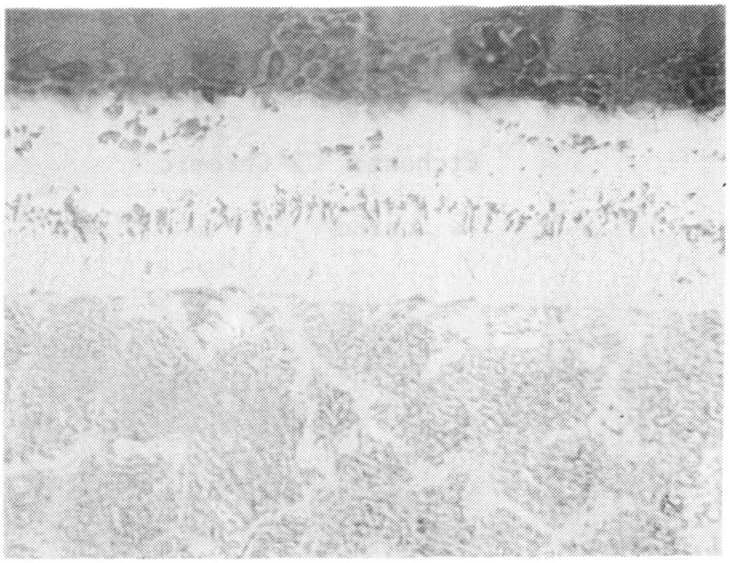

Magnification: 500X

Etchant: 2% Chromic

As Coated

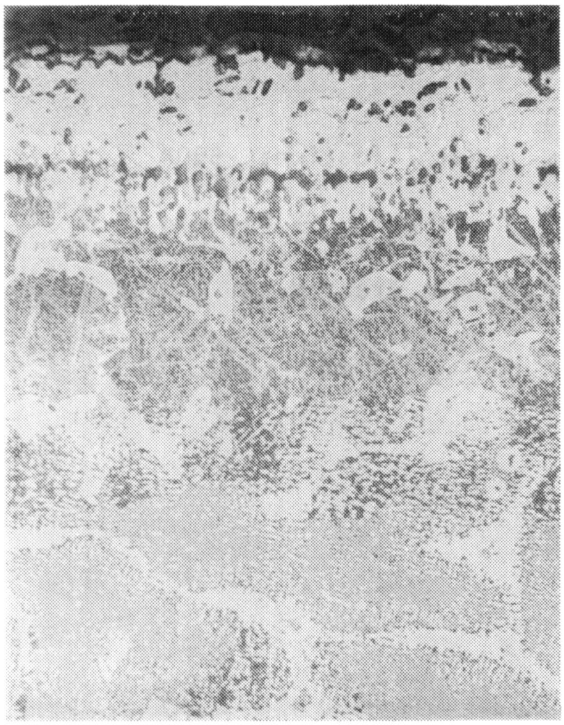

Magnification: 500X

Etchant: 2% Chromic

Heat Treated

Figure 41. Ni-13Al-20Cr-1Cb Coating (#6) on MAR-M200 + Hf (DS)

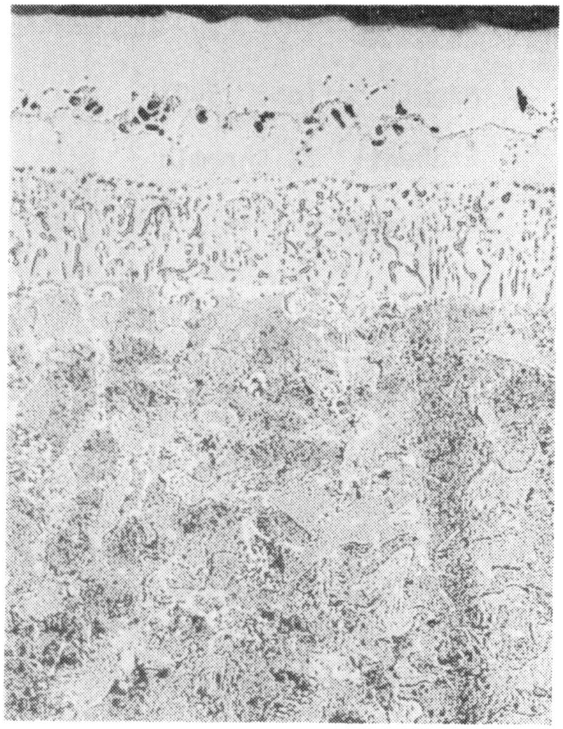

Magnification: 500X

Etchant: 2% Chromic

As Coated

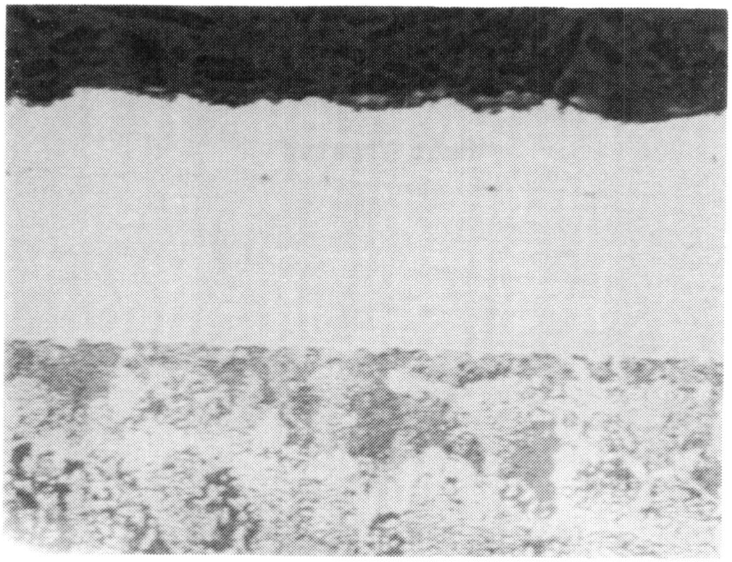

Magnification: 500X

Etchant: 2% Chromic

Heat Treated

Figure 42. Ni-15Al Coating (#7) on MAR-M200 + Hf (DS)

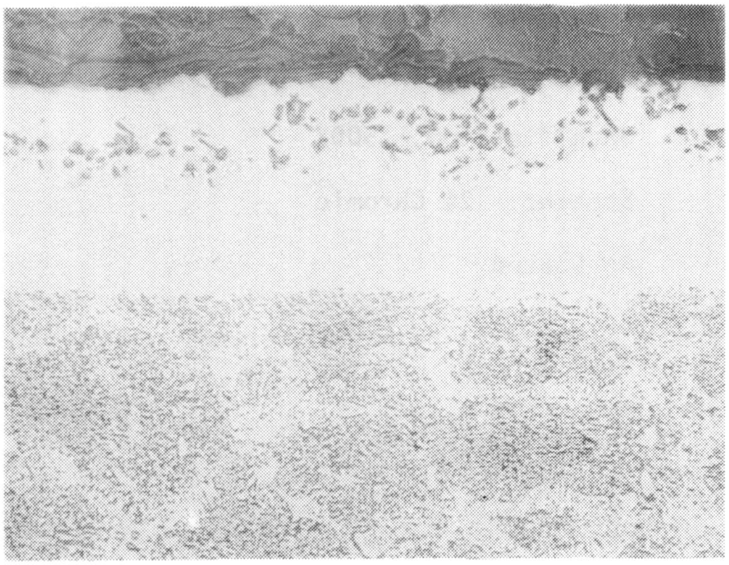

Magnification: 500X

Etchant: 2% Chromic

As Coated

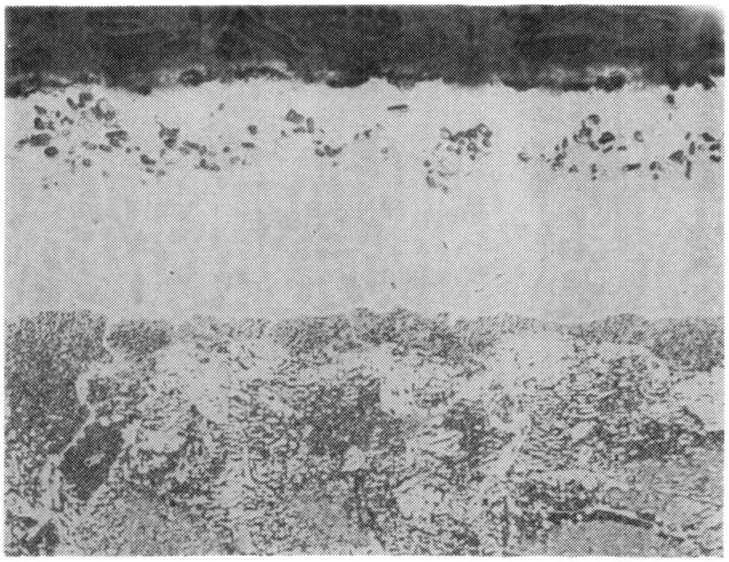

Magnification: 500X

Etchant: 2% Chromic

Heat Treated

Figure 43. Ni-14Al-1Cb Coating (#8) on MAR-M200 + Hf (DS)

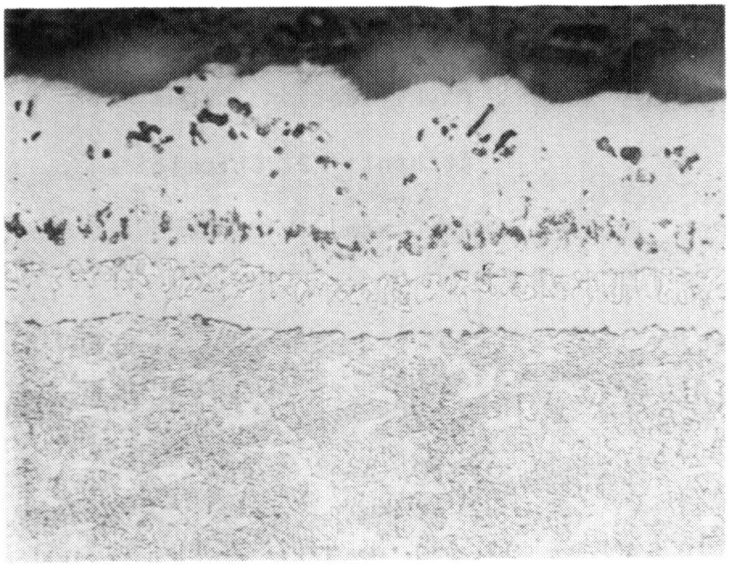

Magnification: 500X

Etchant: 2% Chromic

As Coated

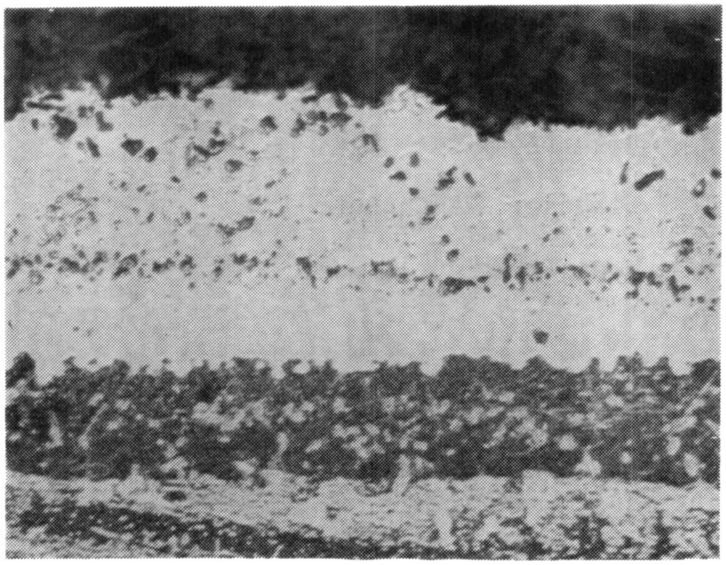

Magnification: 500X

Etchant: 2% Chromic

Heat Treated

Figure 44. Ni-12Al-20Cr Coating (#9) on MAR-M200 + Hf (DS)

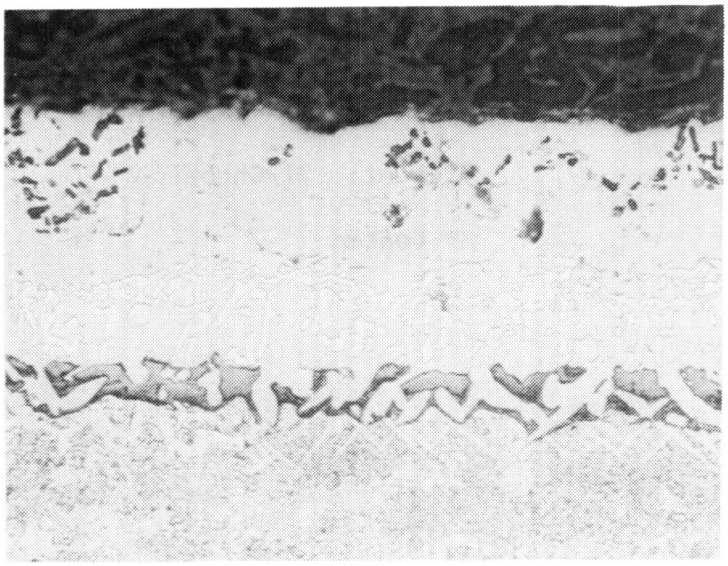

Magnification: 500X

Etchant: 2% Chromic

As Coated

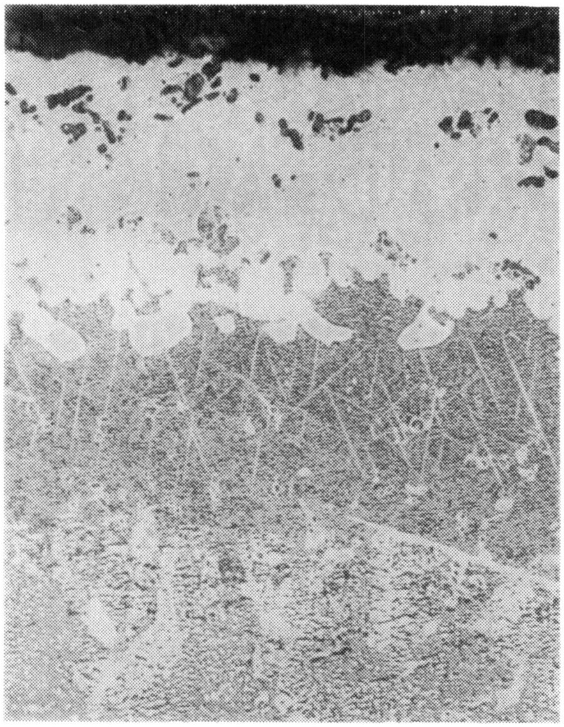

Magnification: 500X

Etchant: 2% Chromic

Heat Treated

Figure 45. Ni-12Al-20Cr-5Si Coating (#10) on MAR-M200 + Hf (DS)

Table 11

Microprobe Analysis of Coating Composition

Coating Number	Program Composition	Actual Composition
1	Ni-20Al	Ni-17Al
2	Ni-19Al-1Cb	Ni-22Al-1Cb
3	Ni-17Al	Ni-18Al
4	Ni-16Al-5Si	Ni-13Al-2Si
5	Ni-14Al-20Cr	Ni-14Al-24Cr
6	Ni-13Al-20Cr-1Cb	Ni-9Al-23Cr-1Cb
7	Ni-15Al	Ni-13Al
8	Ni-14Al-1Cb	Ni-14Al-2Cb
9	Ni-12Al-20Cr	Ni-13Al-23Cr
10	Ni-12Al-20Cr-5Si	Ni-12Al-21Cr-1Si

4

COATING EVALUATION

Turbine blades are typically subjected to extremely high mechanical and thermomechanical stresses, thus making material selection a critical and often difficult process. Therefore, the choice of a coating for protection from oxidation/hot corrosion must be critically evaluated and tested to minimize degradation of substrate properties and to ensure compatibility of the coating/substrate alloy system. One of the primary considerations is coating ductility as the blades are strained over a wide temperature range, typically from ambient to 1800°F. Most aluminide and chromium coatings are brittle in nature, being composed primarily of environmentally resistant phases such as beta aluminide and alpha chromium solid solution. In this program, by controlling the concentration of aluminum and chromium in the coatings and by forming secondary phases with additives such as columbium and silicon, it is anticipated that the ability of these coatings to accommodate thermomechanical stresses may be enhanced without compromising their resistance to oxidation and corrosion attack.

The screening tests for the candidate coatings include strain tolerance/ductile-brittle transition temperature (DBTT) testing followed by burner rig tests in both oxidizing and corrosive environments.

STRAIN TOLERANCE/DBTT TESTING

Ten round (6.3 mm) test bars were coated with each of the ten coatings and tensile tested in an incremental fashion as described in Section 2. The test results are reported in Table 12 and Figure 46. In Table 12, two strain values were reported, the first indicating the level at which cracking was first initiated at the coating surface and the second indicating the strain leading to specimen rupture.

The concentration of aluminum in these coatings ranged from about 9 to 22 weight percent and it is not surprising, therefore, to note large variations in coating ductility. Coating 9 (Ni-AlCr system) exhibited the best ductility; no detectable cracks were observed till rupture occurred at ambient temperature and 10.4 percent strain level. This remarkable strain tolerance far exceeds the reported ductility of cast MAR-M200 alloy, which is nine percent at ambient temperature (Ref. 10) and 6.1 percent for Hf-doped DS alloy (Ref. 2) in the longitudinal direction. Specimen No. 4, which is a Ni-Al-Si system, also exhibited high strain tolerance at room temperature.

Table 12

Strain Tolerance Test Results

Coating Number	Coating Composition	Temperature (°C)	Strain to Cracking (%)	Temperature (°C)	Strain to Rupture (%)
1	Ni-20Al	600	1.5	25	8.9
2	Ni-19Al-1Cb	350	5.7	350	5.7
3	Ni-17Al	500	2.1	25	7.7
4	Ni-16Al-5Si	25	7.1	25	7.1
5	Ni-1rAl-20Cr	350	3.0	350	3.0
6	Ni-13Al-20Cr-1Cb	216	6.0	216	6.0
7	Ni-15Al	500	2.03	25	16.1
8	Ni-14Al-1Cb	450	5.3	450	5.3
9	Ni-12Al-20Cr	25	10.4	25	10.4
10	Ni-12Al-20Cr-5Si	350	3.6	25	6.0

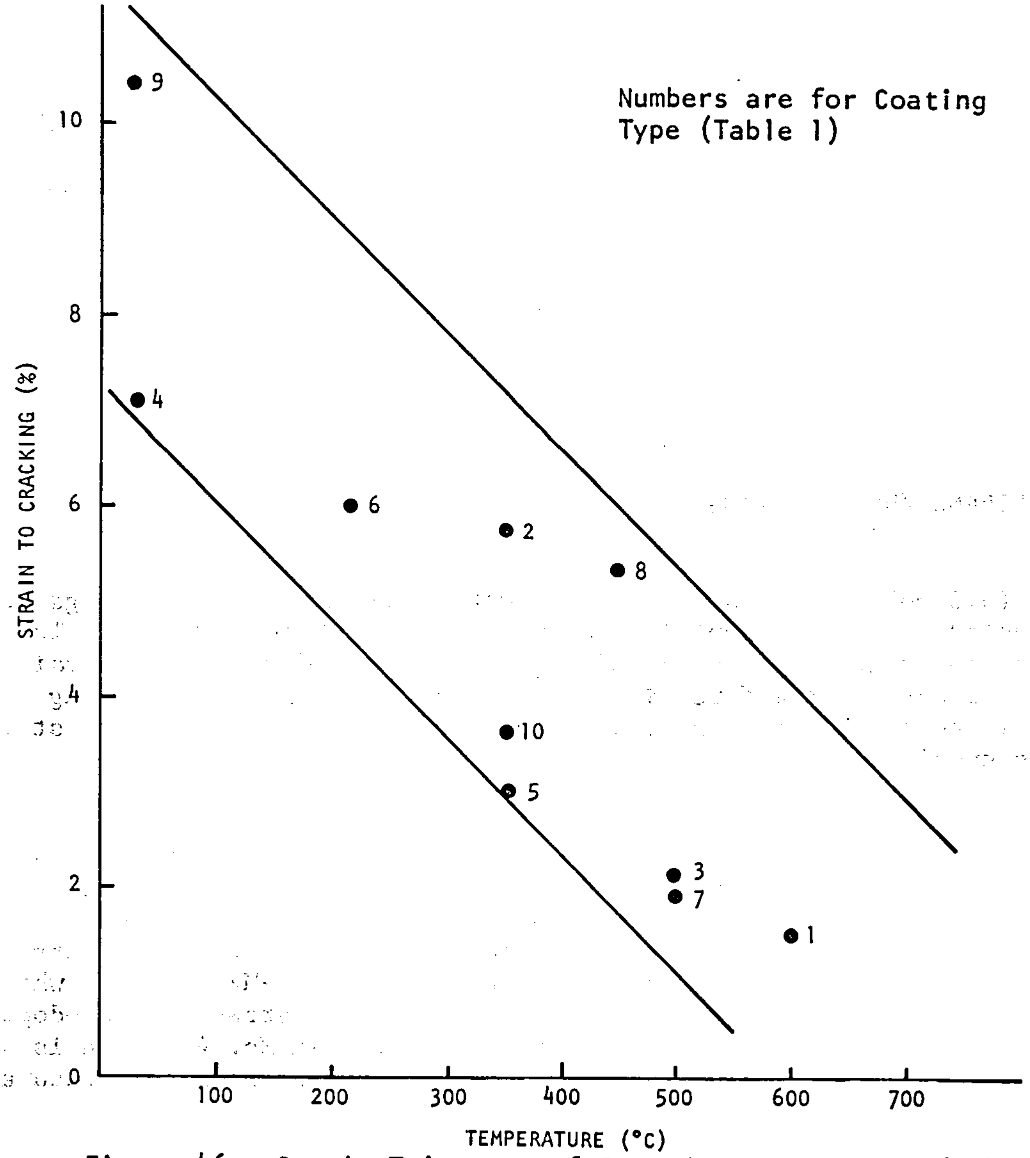

Figure 46. Strain Tolerance of Coated MAR-M200 + Hf (DS)

On the other extreme, the simple aluminide coatings (1, 3 and 7) were the least ductile, and failed at or above 500°C at fairly low strain levels. Microprobe analysis conducted earlier on coating 1 (Table 9) indicated the presence of a beta phase at the outermost layer of this coating. As ductility decreases with increasing aluminum, this layer would be much more brittle than the underlying zones and fracture could initiate and propagate from this beta zone.

The coatings with intermediate ductility include the remaining duplex and triplex systems. In the case of coating 2, which differs from coating 1 only in the addition of columbium, significant ductility enhancement was observed. The same observation can be made for coatings 5, 6 and coatings 7, 8; columbium is present in 6 and 8 and not in 5 and 7. Again, marked improvement in strain tolerance was observed. Therefore, it can be concluded from the above observation that the presence of columbium lowers DBTT in aluminide coating systems. A mechanism for ductility enhancement by columbium is not clear at this time; however, it has been established (Ref. 11) in alloy development that small additions of columbium plus tantalum can be beneficial to hot corrosion resistance and also for strengthening effects.

The strain-to-rupture values reported in Table 12 appear to vary considerably. In this type of incremental testing, after cracking is initiated, the test was continued in a similar manner until rupture occurred. However, due to the fact that the strain history of each specimen was quite different depending on the number of iterations required to determine the DBTT, rupture occured over a range of values and at different temperatures.

HOT CORROSION TESTING

Burner rig tests in a corrosive (sea water doped fuel) hot gas flame were performed with duplicate specimens of each candidate coating system. After 49 hours, one specimen of each composition was removed for evaluation while the remaining specimens were tested until failure. Air flow checks were made on the 40 test specimens, both before and after coating processing to determine the degree of internal restriction induced by the processing. Flow data obtained are reported in Table 13. The calculated percent flow reduction after coating application was less than 20 percent generally, except for a group of specimens (P13 to P16) which registered flow resistance over 20 percent. Table 14 summarizes the coating weight gains of each coating system, which also included the external CCRS CoNiCrAlY coating.

After the first 49 hours, the test was stopped and one half of the specimens removed and inspected. Specimen parameters were measured and are reported in Table 15. The mass flow values obtained after 49 hours of exposure appear to be comparable to pretest values with the exception of specimens P5, P13 and P22. However, it was later discovered that the P5 reading was incorrect as a small piece of foil had obstructed the airflow passage. Two of the specimens, P22 and P25, had to be cut from the holder and therefore, weight values were not available. The other specimens registered weight gains ranging from 1 to 20 mg. The specimen diameters were also recorded at a defined position and Table 15 shows diameter increases in all cases as oxide scales and salt deposits formed on the external CCRS coating.

Table 13
Cold Flow Check of Coated Burner Rig Test Specimens

Specimen Number	Pre-Coating	Post-Coating	% Reduction
P1	120	112	7
P2	131	121	8
P3	115	102	11
P4	129	116	10
P5	123	104	15
P6	123	106	14
P7	127	116	9
P8	121	108	11
P9	122	111	9
P10	117	109	7
P11	125	102	18
P12	117	104	11
P13	123	79	36
P14	125	99	21
P15	139	117	16
P16	123	93	24
P17	107	109	2
P18	121	113	7
P19	121	115	5
P20	119	111	7
P21	116	103	11
P22	122	104	15
P23	122	111	9
P24	120	110	8
P25	120	110	8
P26	127	106	17
P27	119	109	8
P28	117	104	11
P29	121	110	9
P30	131	110	16
P31	118	106	10
P32	125	100	20
P33	126	111	12
P34	137	116	6
P35	126	119	6
P37	120	115	4
P38	125	110	12
P39	120	110	8
P41	124	104	16

Figure 47 shows the cross section of one of the transverse holes of specimen P1 and is an excellent example of the overlay region between the internal and external coatings. Note the uniformity of the coatings and that the CCRS coating merged into the aluminide coating without creating a break in coverage.

The three basic aluminide coatings, Ni-20Al, Ni-17Al and Ni-15Al, are fundamentally similar in nature and differ only in the concentration of aluminum in the coating. The primary protective phase in the nickel aluminide system is the beta (NiAl) phase, followed by the gamma prime (Ni_3Al) with the solid solution, gamma, being the least resistant to environmental attack. It has been suggested (Ref. 6) that the oxidation of beta and beta plus gamma prime

Table 14

Coating Weight of Burner Rig Test Specimens

Coating Number	Coating Composition	Specimen Numbers	Average Weight Gain (g)
1	Ni-20Al	P1 - P4	0.129
2	Ni-19Al-1Cb	P5 - P8	0.148
3	Ni-17Al	P9 - P12	0.137
4	Ni-16Al-5Si	P13 - P16	0.146
5	Ni-14Al-20Cr	P17 - P20	0.154
6	Ni-13Al-20Cr-1Cb	P21 - P23	0.160
7	Ni-15Al	P24 - P27	0.127
8	Ni-14Al-1Cb	P28 - P31	0.144
9	Ni-12Al-20Cr	P32 - P35	0.146
10	Ni-12Al-20Cr-5Si	P37 - P41	0.140

Table 15

Specimen Parameters After 49 Hours Hot Corrosion Test at 899°C

Specimen		Mass Flow			Weight Gain (mg)	Diameter (mm)		
Coating Number	Specimen Number	Before	After	Change (%)		Before	After	Change (mm)
1	P1	112	109	-3	14.9	3.01	3.09	+.08
2	P5	104	12	-88*	19.6	3.15	3.20	+.05
3	P9	111	113	+2	7.0	3.05	3.10	+.05
4	P13	79	735	-	5.0	3.21	3.23	+.02
5	P18	113	109	-4	19.1	3.07	3.09	+.02
6	P22	104	84	-19	-	3.09	3.09	-
7	P25	110	108	-2	-	3.11	3.13	+.02
8	P29	110	104	-5	1.3	3.12	3.16	+.04
9	P33	111	114	+3	11.6	3.14	3.17	+.03
10	P37	115	114	-1	10.3	3.22	3.27	+.05

* Incorrect value due to blockage of passage

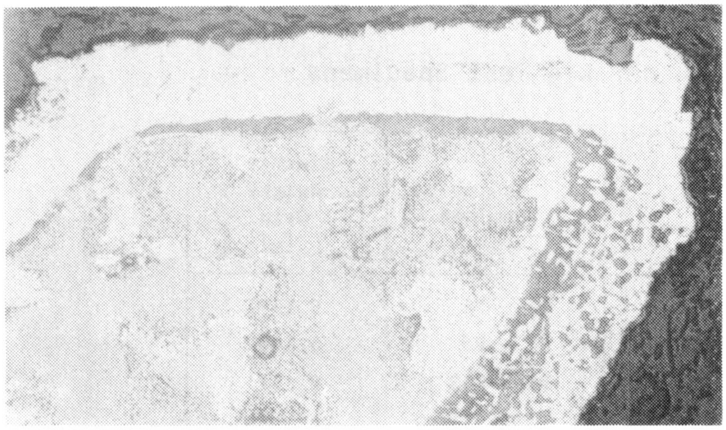

Figure 47.

Cross-Section of Transverse Hole in Specimen P1 After 49 Hours of Hot Corrosion Testing

Magnification: 250X

Etchant: 2% Electrolytic Chrome

phases proceed in a parabolic fashion in forming a protective Al_2O_3 scale at the coating surface. Coating degradation occurs when this scale spalls and more aluminum is consumed in order to replenish the oxide layer. As aluminum is depleted, the beta phase decreases and is converted to the gamma prime phase. With continued exposure to the oxidizing environment, formation of Al_2O_3 decreases and complex, less protective oxides such as the spinel $NiAl_2O_4$ and NiO are formed (Ref. 12).

Figures 48, 49 and 50 show the microstructure of the three nickel aluminide coatings after 49 and 219 hours of exposure. These coatings exhibited equivalent resistance to the hot corrosive environment with penetration into one-third of the coating. At the corrosion front, small Kirkendall voids were observed due to the selective outward diffusion of aluminum. The base material, MAR-M200+Hf, is solid solution strengthened by refractory elements (W and Cb) which are minimally soluble in the nickel aluminides. It is believed that these alloying metals decrease corrosion resistance (Ref. 13). The addition of small amounts of columbium to the Ni-20Al and Ni-15Al coatings (Nos. 2 and 8) resulted in significant loss of protection, especially in the latter case (see Figs. 51 and 52) which was a low aluminum coating and was fully consumed within 219 hours. The Ni-19Al-1Cb (No. 2) coating appeared to be adequate within the specification of this program. The triplex coating Ni-13Al-20Cr-1Cb (No. 6) failed catastrophically, as can be seen in Figure 53, exposing the substrate to intergranular attack.

The presence of silicon in the aluminide matrix (solubility is less than 10 atomic percent) is believed to improve corrosion and oxidation resistance (Ref. 15) by increasing scale adherence. However, in this investigation, the silicon containing coatings, Nos. 4 and 10, performed very poorly in hot corrosion testing (see Figs. 54 and 55). It should be noted that the silicon content was low in both coatings, about 1 to 2 weight percent. The Ni-16Al-5Si (No. 4) coating was 100 percent penetrated while the triplex coating, No. 10, retained a continuous coating layer. The latter effect was probably due to the presence of chromium solid solution which is a highly corrosion resistant phase. Available test data on silicon coatings are empirical in nature and extrapolation is precarious at best.

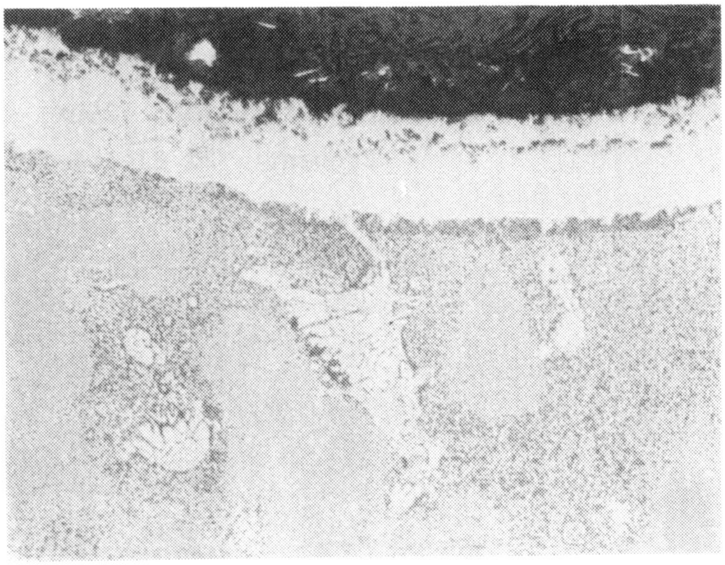

A. Specimen P1

Magnification: 250X

Etchant: 2% Electrolytic Chrome

After 49 Hours

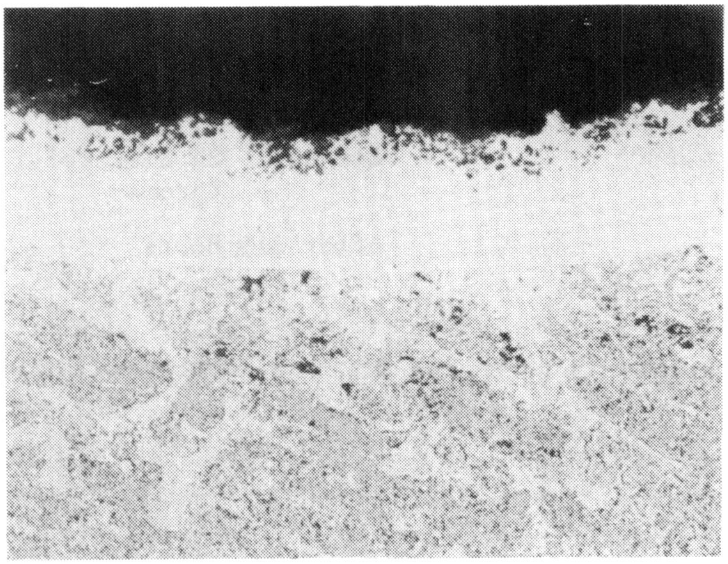

B. Specimen P2

Magnification: 250X

Etchant: 2% Electrolytic Chrome

After 219 Hours

Figure 48. Ni-20Al Coating (No. 1) After Hot Corrosion Testing at 899°C

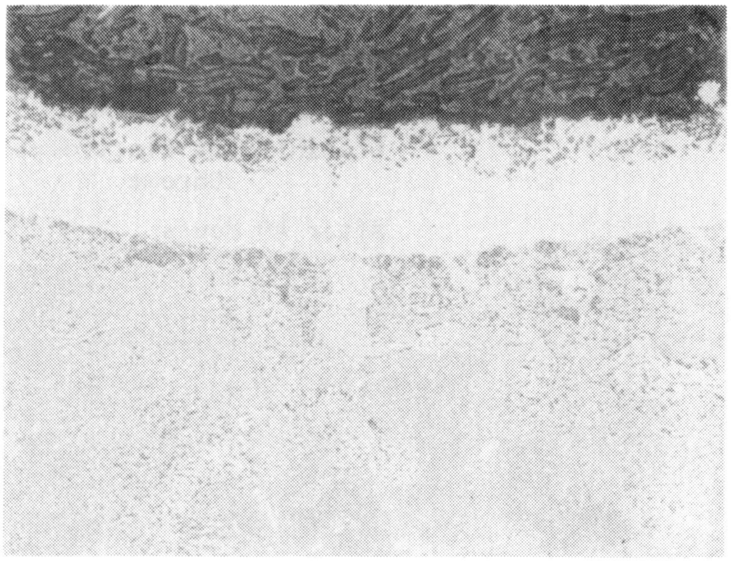

A. Specimen P9

Magnification: 250X

Etchant: 2% Electrolytic Chrome

After 49 Hours

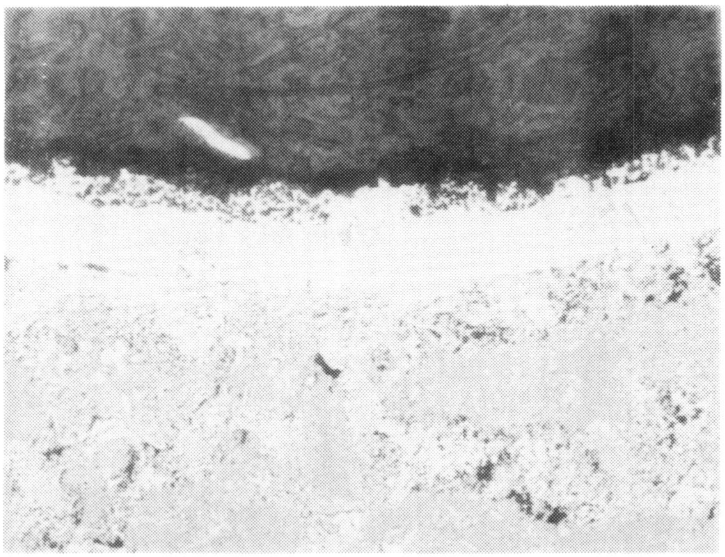

B. Specimen P10

Magnification: 250X

Etchant: 2% Electrolytic Chrome

After 219 Hours

Figure 49. Ni-17Al Coating (No. 3) After Hot Corrosion Testing at 899°C

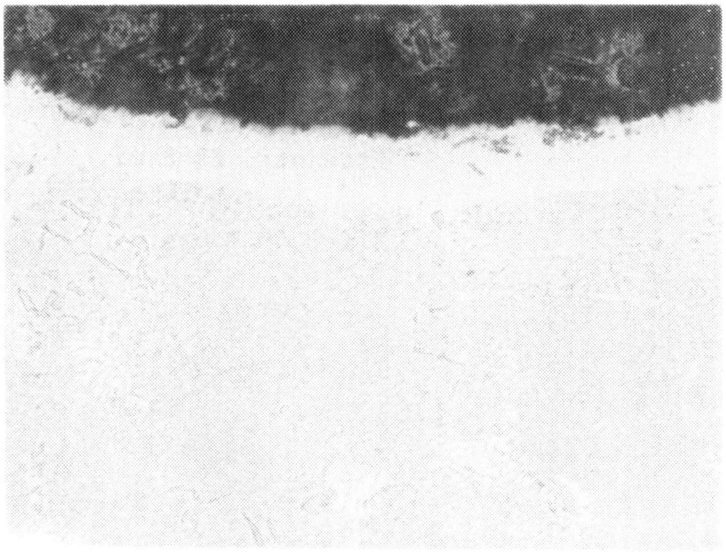

A. Specimen P25

Magnification: 250X

Etchant: 2% Electrolytic Chrome

After 49 Hours

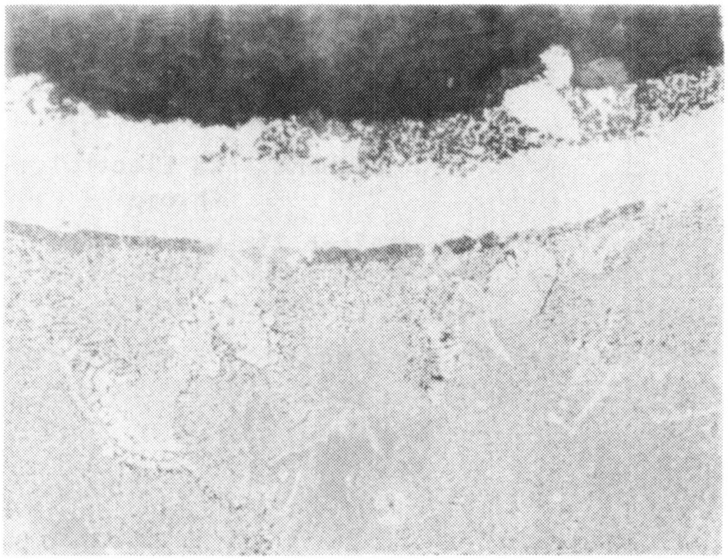

B. Specimen P26

Magnification: 250X

Etchant: 2% Electrolytic Chrome

After 219 Hours

Figure 50. Ni-15Al Coating (No. 7) After Hot Corrosion Testing at 899°C

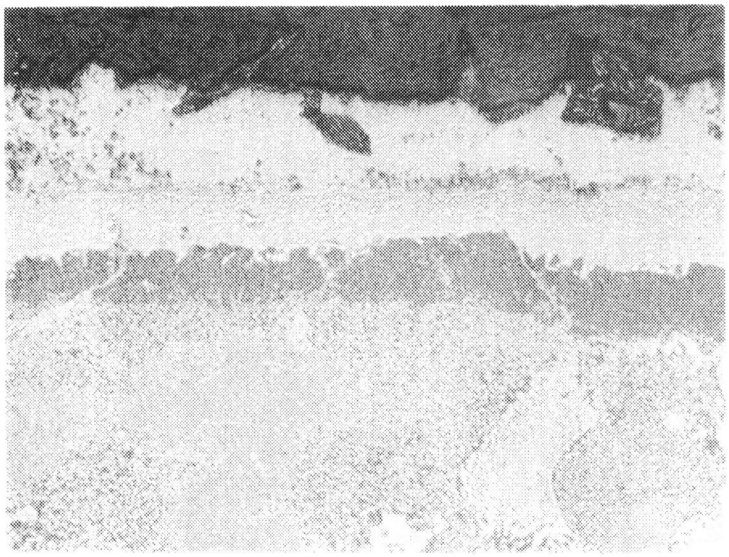

A. Specimen P5

Magnification: 250X

Etchant: 2% Electrolytic Chrome

After 49 Hours

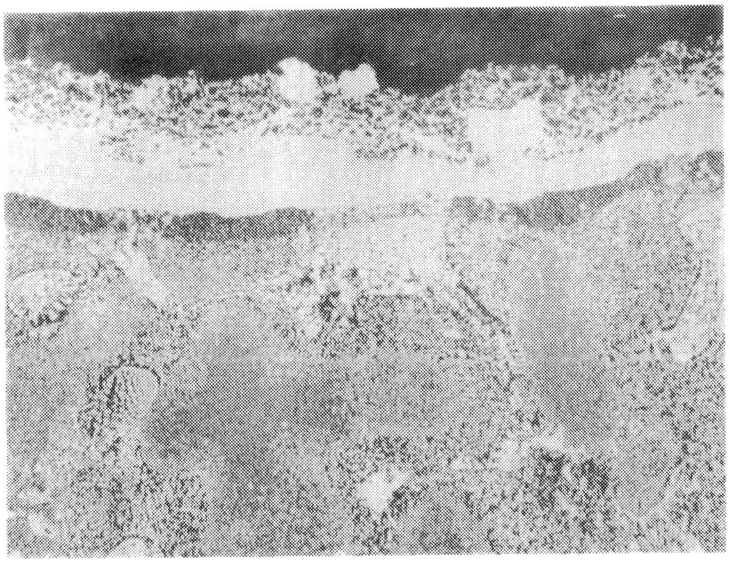

B. Specimen P6

Magnification: 250X

Etchant: 2% Electrolytic Chrome

After 219 Hours

Figure 51. Ni-19Al-1Cb Coating (No. 2) After Hot Corrosion Testing at 899°C

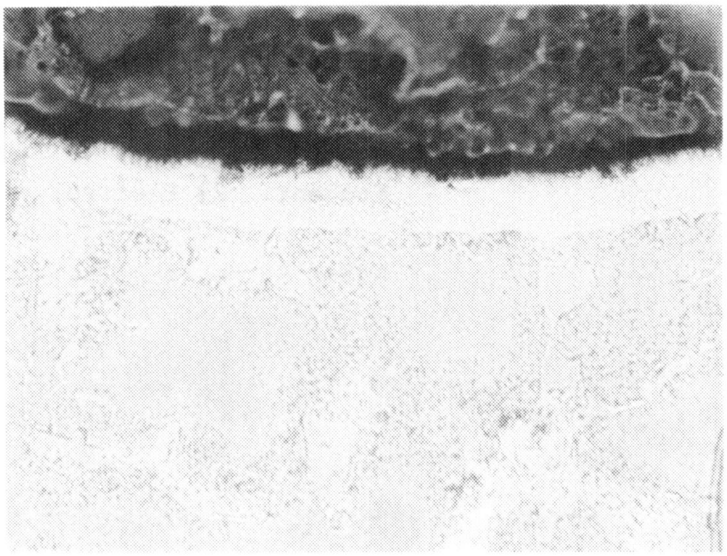

A. Specimen P29

Magnification: 250X

Etchant: 2% Electrolytic Chrome

After 49 Hours

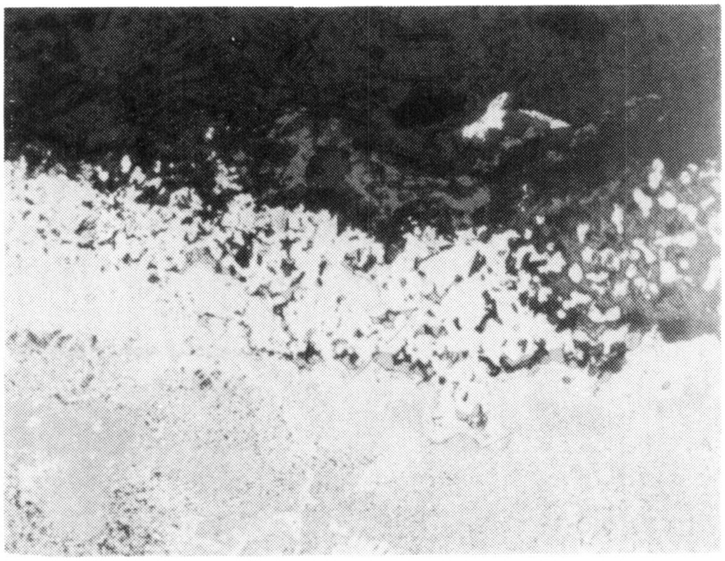

B. Specimen P30

Magnification: 250X

Etchant: 2% Electrolytic Chrome

After 219 Hours

Figure 52. Ni-14Al-1Cb Coating (No. 8) After Hot Corrosion Testing at 899°C

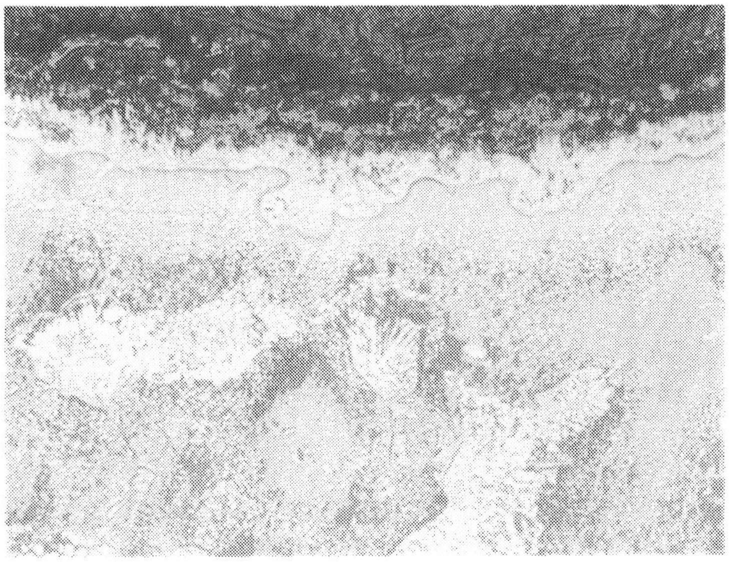

A. Specimen P22

Magnification: 250X

Etchant: 2% Electrolytic Chrome

After 49 Hours

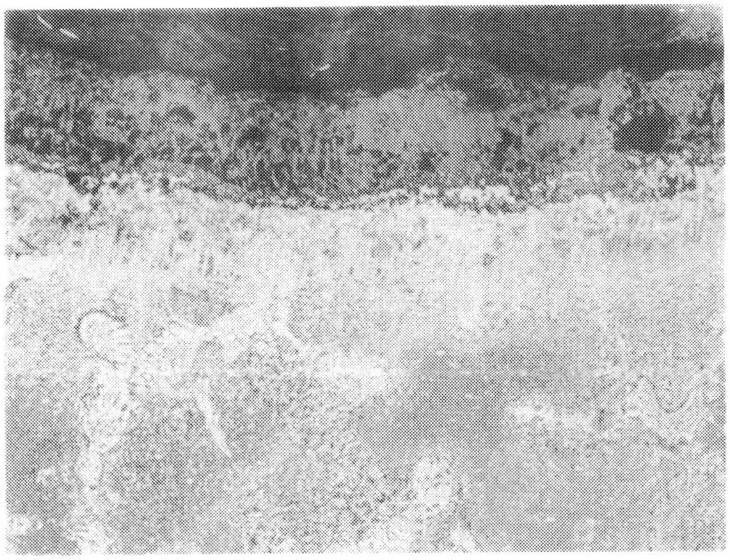

B. Specimen P21

Magnification: 250X

Etchant: 2% Electrolytic Chrome

After 219 Hours

Figure 53. Ni-13Al-20Cr-1Cb Coating (No. 6) After Hot Corrosion Testing at 899°C

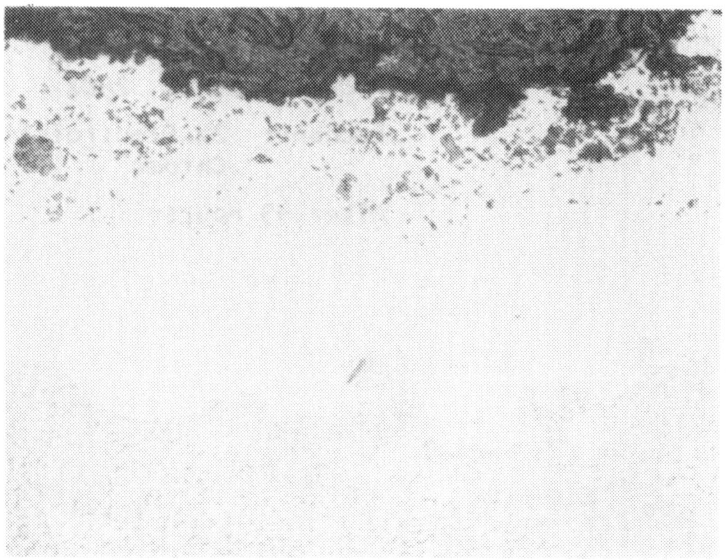

A. Specimen P13

Magnification: 250X

Etchant: 2% Electrolytic Chrome

After 49 Hours

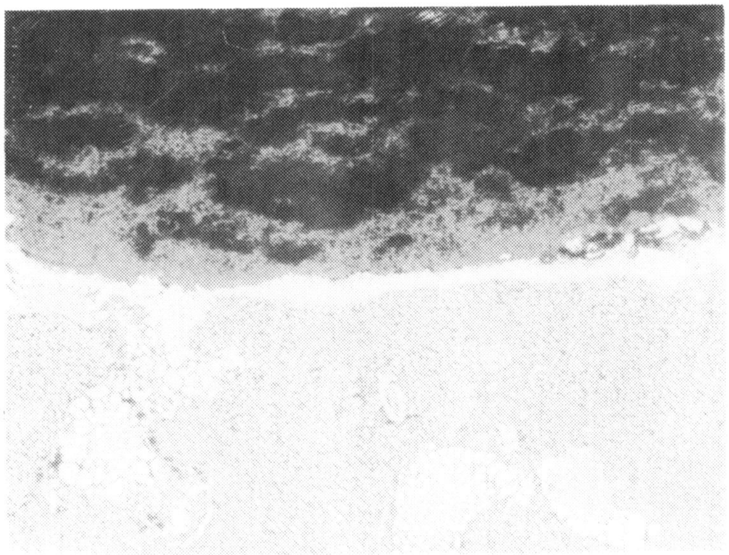

B. Specimen P14

Magnification: 250X

Etchant: 2% Electrolytic Chrome

After 219 Hours

Figure 54. Ni-16Al-5Si Coating (No. 4) After Hot Corrosion Testing at 899°C

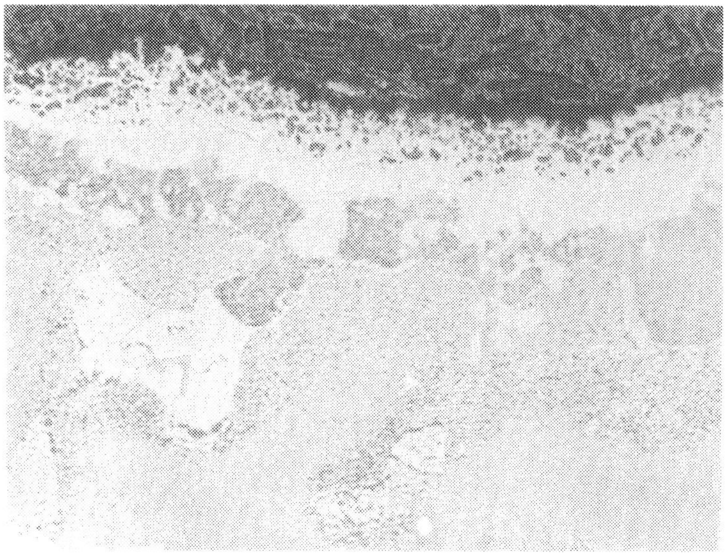

A. Specimen P37

Magnification: 250X

Etchant: 2% Electrolytic Chrome

After 49 Hours

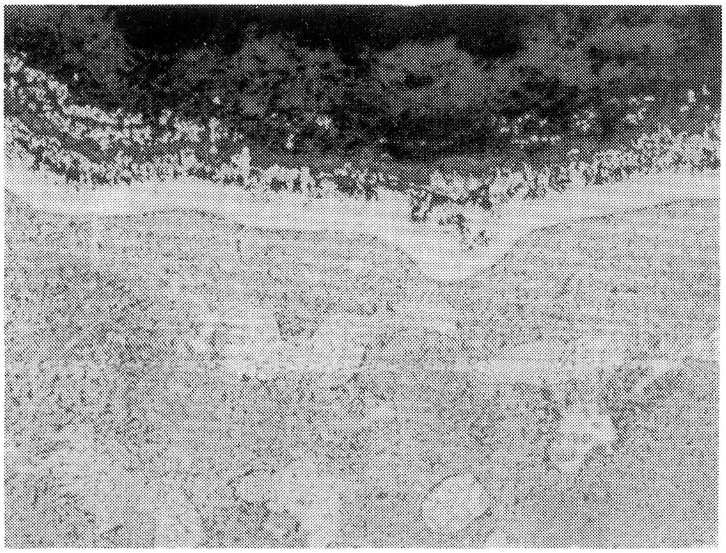

B. Specimen P38

Magnification: 250X

Etchant: 2% Electrolytic Chrome

After 219 Hours

Figure 55. Ni-12Al-20Cr-5Si Coating (No. 10) After Hot Corrosion Testing at 899°C

Figures 56 and 57 show the microstructures of the Ni-Cr-Al coatings (Nos. 5 and 9). It is difficult to rationalize the poor performance of the Ni-14Al-20Cr coating. One possibility is the incomplete removal of the halide activators used in vapor transport from the pack to the specimens. Even traces of the highly corrosive NaCl salt would induce accelerated attack and rapid deterioration of the coating.

The hot corrosion test results are summarized in Table 16 which reports the depth of penetration after 49 and 219 hours as both absolute values and as a percentage of the coating thickness at the spot measured.

DYNAMIC OXIDATION TESTING

The ten candidate coating systems were tested for dynamic oxidation resistance. One hour cycles were imposed on the specimens which were heated to 1050°C (1922°F). During dynamic oxidation testing, one of the test specimens came loose from the specimen holder and damaged two other test specimens. As a result, data on coatings Nos. 6, 7 and 10 were not available except after the first 72 hours when the first set of specimens were removed.

The 'simple' aluminides, Ni-20Al, Ni-17Al and Ni-15Al, were predominantly beta NiAl systems with Ni_3Al precipitated during heat treatment. After 72 hours of exposure at 1050°C, evidence of loss of aluminum can be observed, as shown in Figures 58, 59 and 60. As the aluminum near the coating surface was consumed to form Al_2O_3, inter-phase diffusion occurred, reducing the amount of NiAl phase present and developing the less resistant Ni_3Al and finally the gamma solid solution phases. Furthermore, the areas of high MC and $M_{23}C_6$ carbides (precipitated from the substrate matrix) are susceptible to oxidation attack. After prolonged exposure of 235 hours, much of the coating was deteriorated and the substrate immediately below the coating interface appeared to be adversely affected, as indicated by the different etched appearances. The cause of substrate deterioration is the relative instability of beta coating on the gamma-gamma prime substrate. With long-term exposure (as in this test), the gamma-gamma prime ratio in the substrate was decreased near the interface and at the same time the beta in the coating was reduced to the less protective gamma prime. In order to minimize this interdiffusion towards an equilibrium state, elements such as columbium, chromium, etc., which are not soluble in the coating matrix may be beneficial as diffusion inhibitors.

In superalloy development work, it was found (Ref. 10) that columbium interferes with selective oxidation of aluminum and promotes the formation of chromium-rich surface oxides. In oxidation testing, no improvement was noted by adding columbium to the No. 2 and No. 8 coatings (Ni-19Al-1Cb and Ni-14Al-1Cb) as seen in Figures 61 and 62. Coating No. 8 failed catastrophically while coating No. 2 exhibited some protection up to 235 hours.

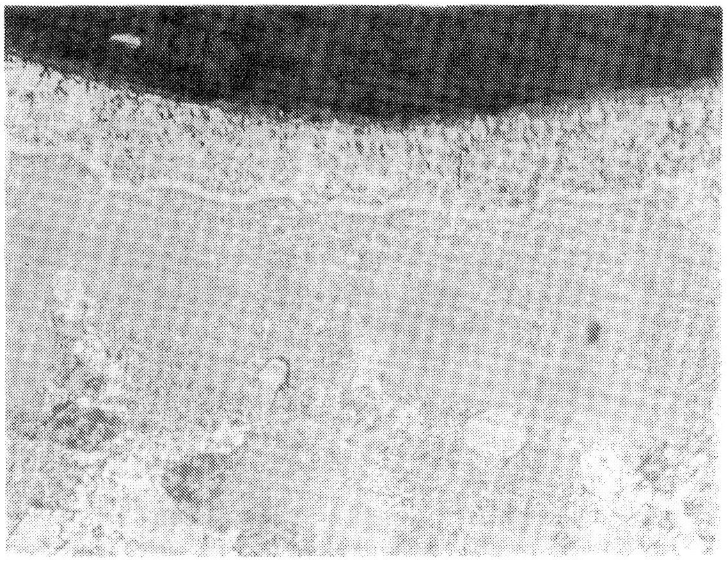

A. Specimen P18

Magnification: 250X

Etchant: 2% Electrolytic Chrome

After 49 Hours

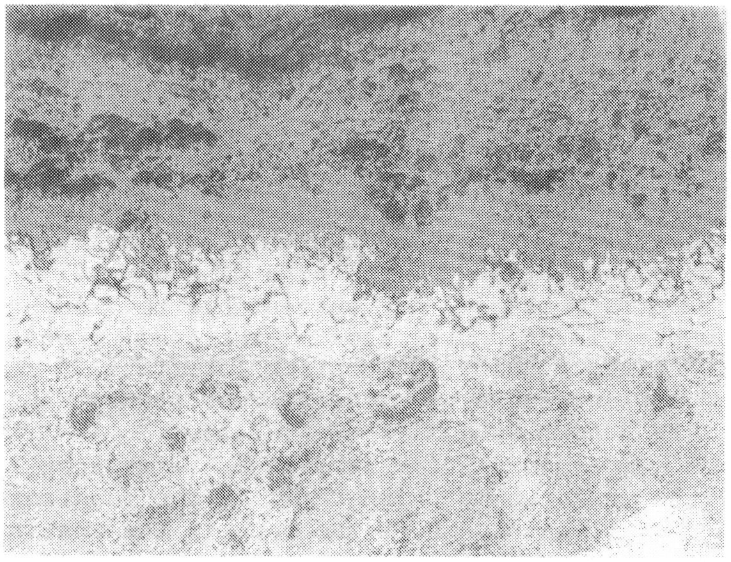

B. Specimen P17

Magnification: 250X

Etchant: 2% Electrolytic Chrome

After 219 Hours

Figure 56. Ni-14Al-20Cr Coating (No. 5) After Hot Corrosion Testing at 899°C

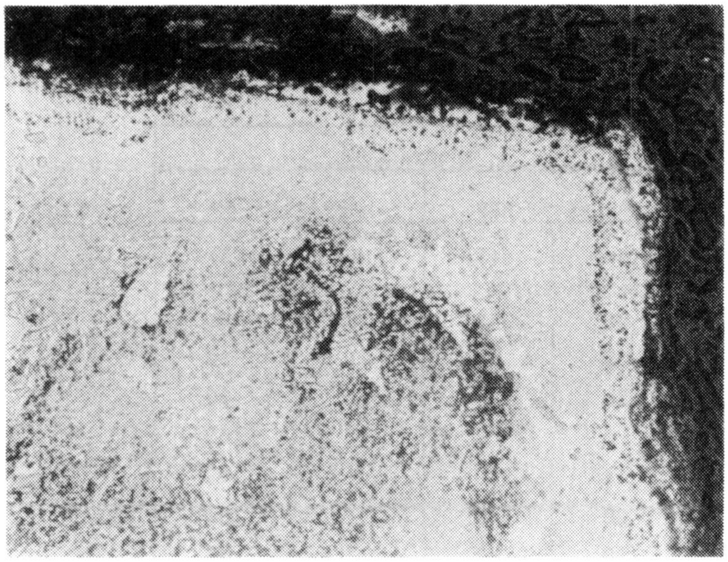

A. Specimen P33

Magnification: 250X

Etchant: 2% Electrolytic Chrome

After 49 Hours

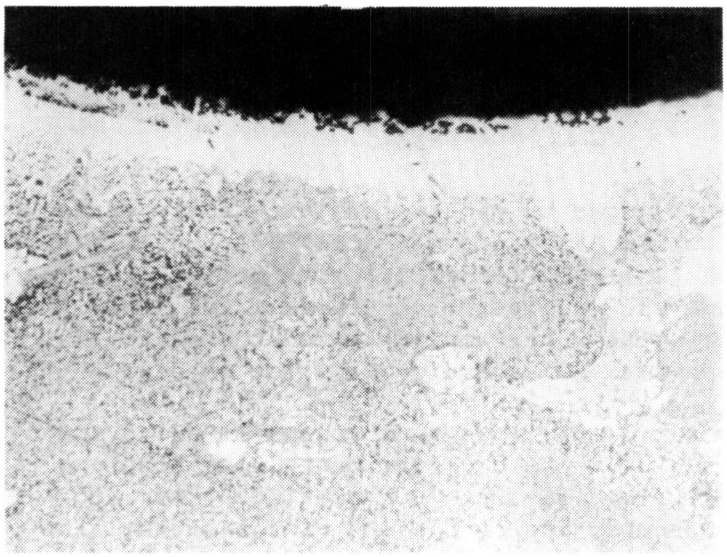

B. Specimen P34

Magnification: 250X

Etchant: 2% Electrolytic Chrome

After 219 Hours

Figure 57. Ni-19Al-1Cb Coating (No. 2) After Hot Corrosion Testing at 899°C

Table 16
Hot Corrosion Test Data

Coating	Composition	Penetration			
		After 49 Hrs		After 219 Hrs	
		(μm)	(%)	(μm)	(%)
1	Ni-20Al	20	33	20	31
2	Ni-19Al-1Cb	∿0	∿0*	41	50
3	Ni-17Al	20	33	15	30
4	Ni-16Al-5Si	70	50	-	100
5	Ni-14Al-20Cr	41	80	-	100
6	Ni-13Al-20Cr-1Cb	30	60	-	100
7	Ni-15Al	∿0	∿0	25	36
8	Ni-14Al-1Cb	5	14	-	100
9	Ni-12Al-20Cr	∿20	40	∿15	∿50
10	Ni-12Al-20Cr-5Si	30	50	25	63

* Localized oxidation only.

Coatings Nos. 4 and 10, as shown in Figures 63 and 64, exhibited fair oxidation resistance. Upon close examination of Figure 63, after 235 hours, there appeared to be isolated areas which resembles the gamma-gamma prime structure of the substrate, indicating considerable depletion of aluminum from the coating. Also, interdiffusion across the interface minimized the sharp demarkation at the interface between beta and gamma/gamma prime phases.

Due to the lack of final microstructural information on coatings Nos. 7 and 6 (Figs. 60 and 65), coating evaluation of these chromium containing coatings cannot be performed. The Ni-14Al-20Cr and Ni-12Al-20Cr coatings (Figs. 66 and 67) exhibited about 50 percent penetration at the end of 235 hours. The Ni-14Al-20Cr coating (No. 5) appeared to resist the onset of oxidation, as seen in the almost unaffected microstructure after 72 hours in Figure 66, but the oxidation front penetrated 50 percent into the coating by the end of the test.

The above observations are summarized in Table 17 which reports the depth of penetration observed after 72 and 235 hours.

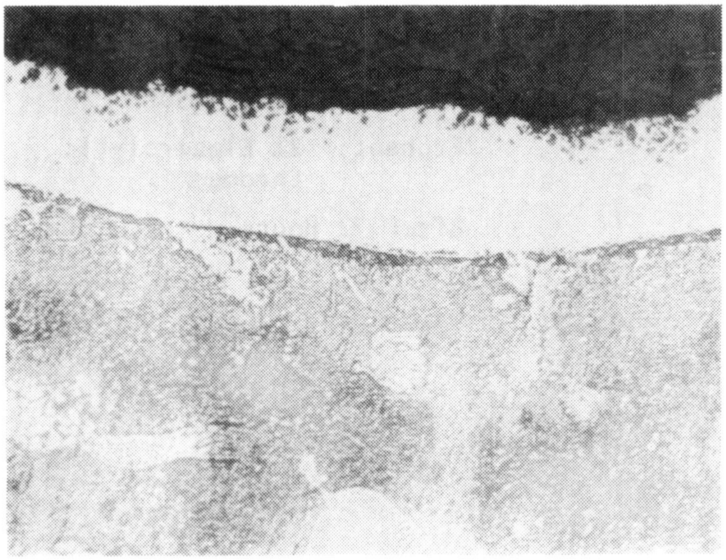

A. Specimen P3

Magnification: 250X

Etchant: 2% Electrolytic Chrome

After 72 Hours

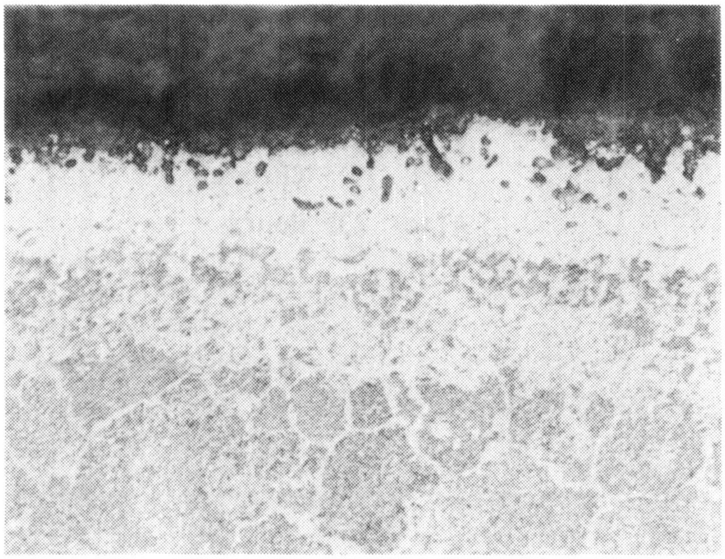

B. Specimen P4

Magnification: 250X

Etchant: 2% Electrolytic Chrome

After 235 Hours

Figure 58. Ni-20Al Coating (No. 1) After Dynamic Oxidation Testing at 1050°C

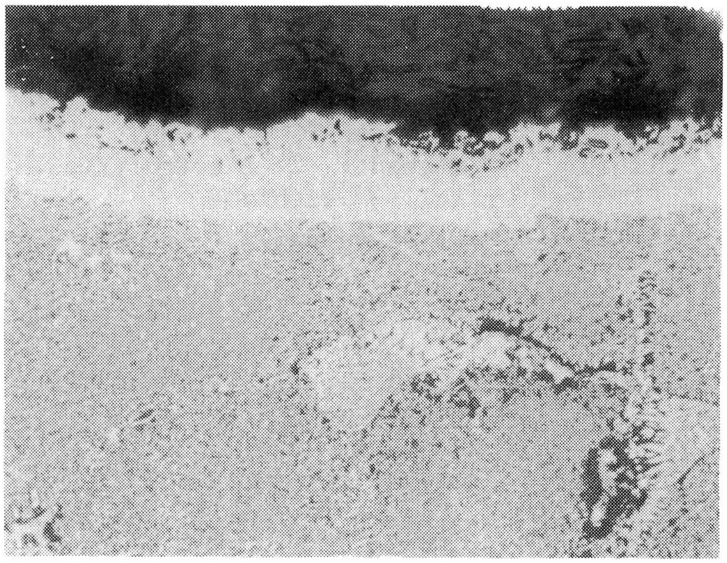

A. Specimen P12

Magnification: 250X

Etchant: 2% Electrolytic Chrome

After 72 Hours

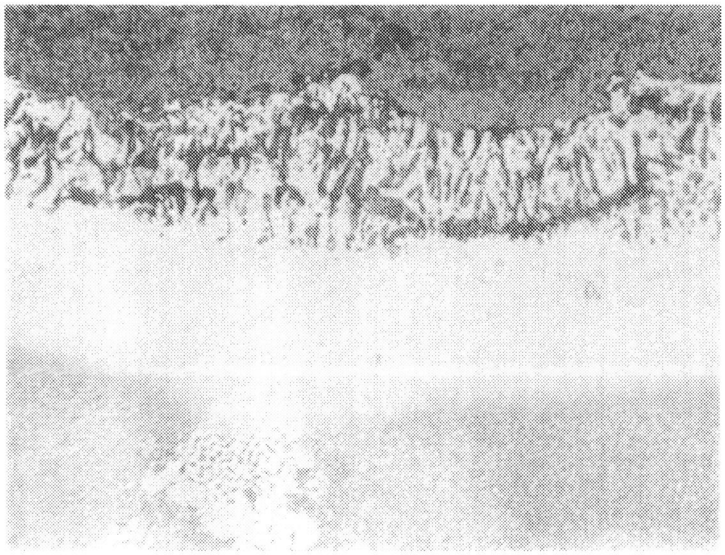

B. Specimen P11

Magnification: 250X

Etchant: 2% Electrolytic Chrome

After 235 Hours

Figure 59. Ni-17Al Coating (No. 3) After Dynamic Oxidation Testing at 1050°C

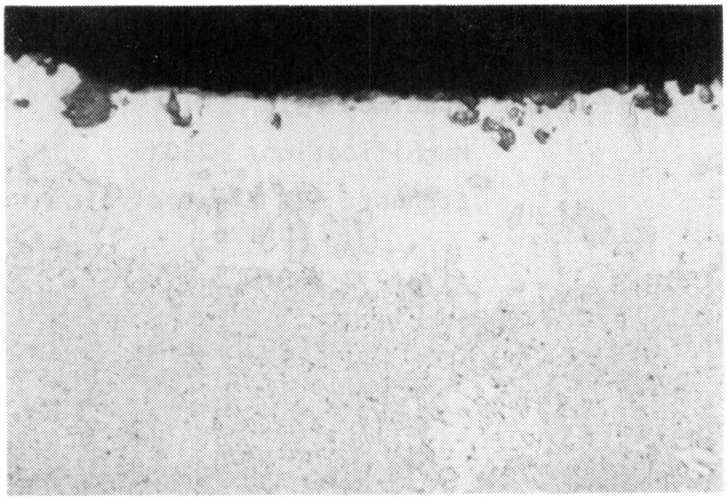

A. Specimen P28

Magnification: 250X

Etchant: 2% Electrolytic Chrome

After 72 Hours

Figure 60. Ni-15Al Coating (No. 7) After Dynamic Oxidation Testing at 1050°C

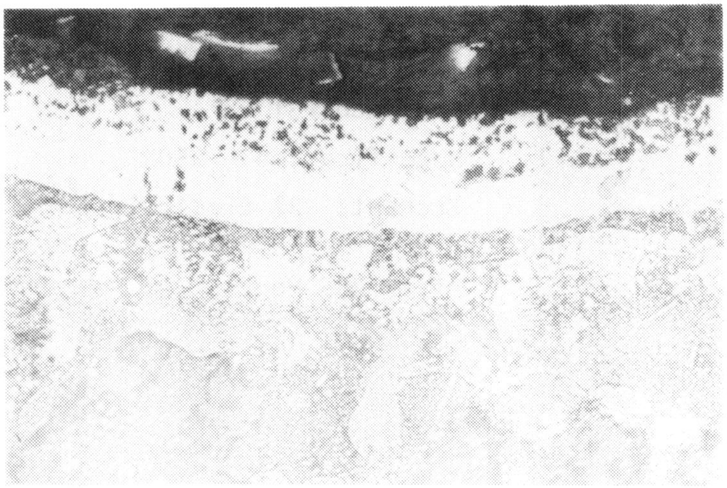

A. Specimen P7

Magnification: 250X

Etchant: 2% Electrolytic Chrome

After 72 Hours

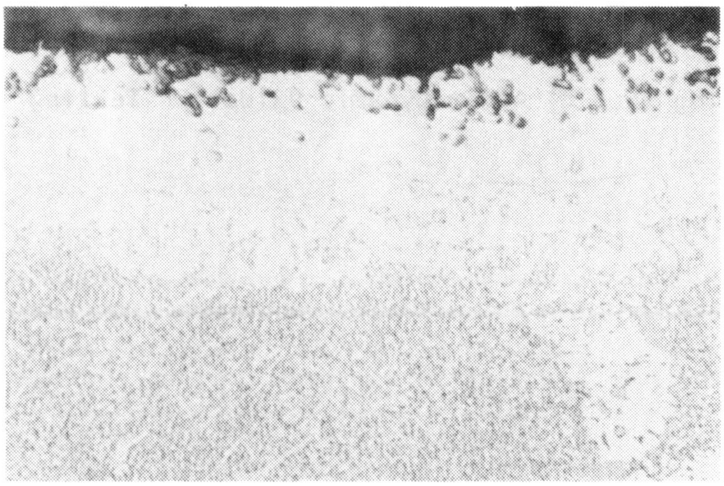

B. Specimen P8

Magnification: 250X

Etchant: 2% Electrolytic Chrome

After 235 Hours

Figure 61. Ni-19Al-1Cb Coating (No. 2) After Dynamic Oxidation Testing at 1050°C

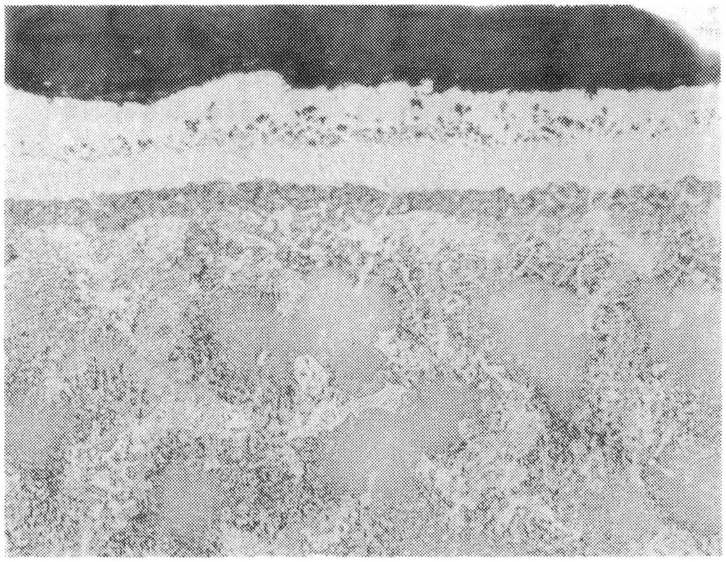

A. Specimen P32

Magnification: 250X

Etchant: 2% Electrolytic Chrome

After 72 Hours

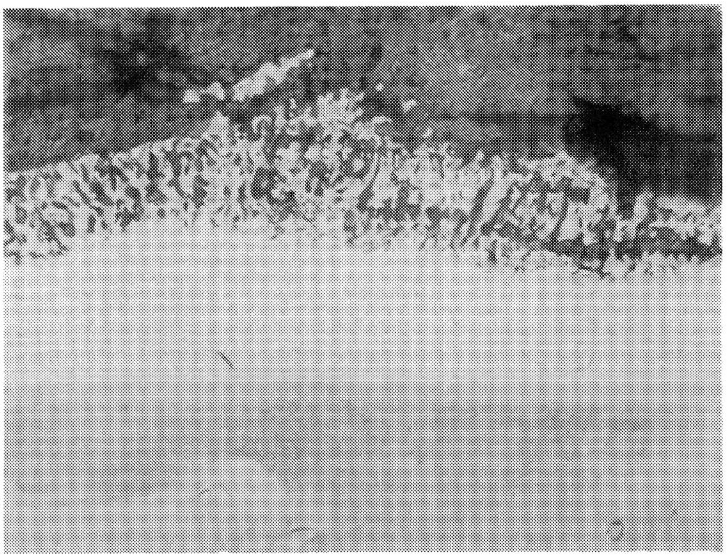

B. Specimen P31

Magnification: 250X

Etchant: 2% Electrolytic Chrome

After 235 Hours

Figure 62. Ni-14Al-1Cb Coating (No. 8) After Dynamic Oxidation Testing at 1050°C

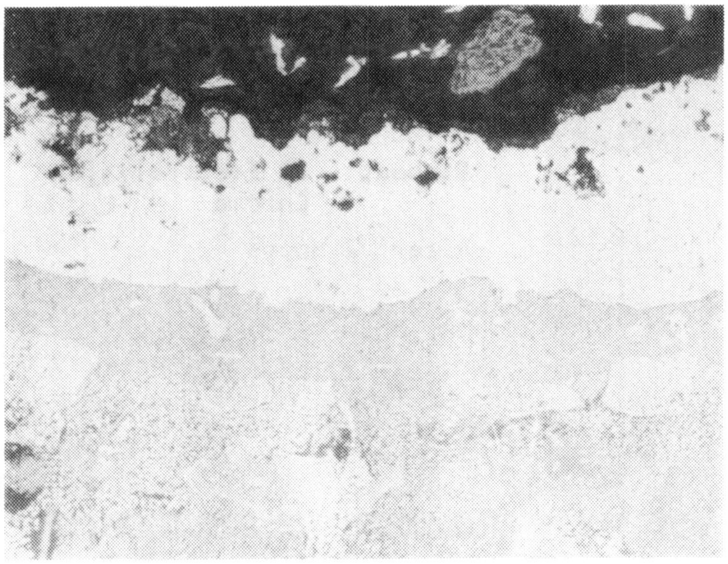

A. Specimen P15

Magnification: 250X

Etchant: 2% Electrolytic Chrome

After 72 Hours

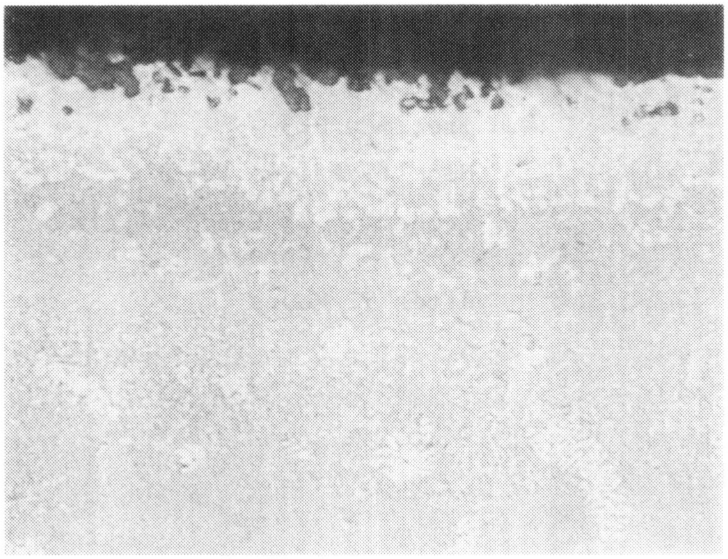

B. Specimen P16

Magnification: 250X

Etchant: 2% Electrolytic Chrome

After 235 Hours

Figure 63. Ni-16Al-5Si Coating (No. 4) After Dynamic Oxidation Testing at 1050°C

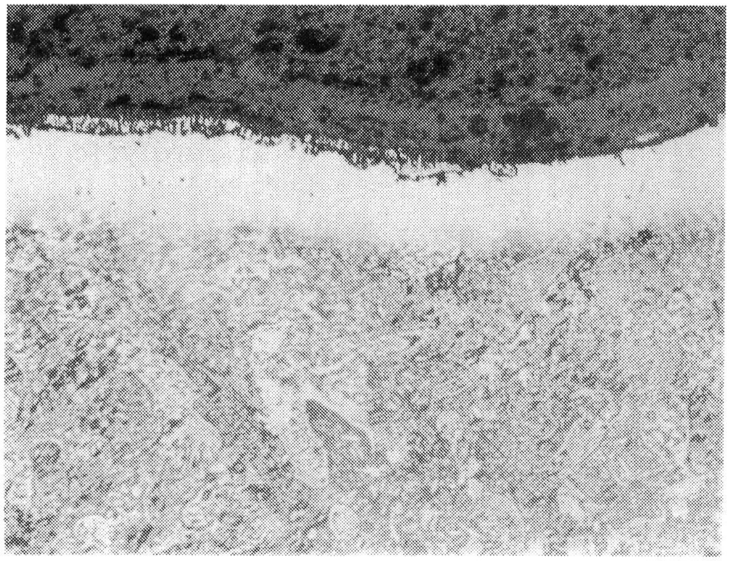

A. Specimen P39

Magnification: 250X

Etchant: 2% Electrolytic Chrome

After 72 Hours

Figure 64. Ni-12Al-20Cr-5Si Coating (No. 10) After Dynamic Oxidation Testing at 1050°C

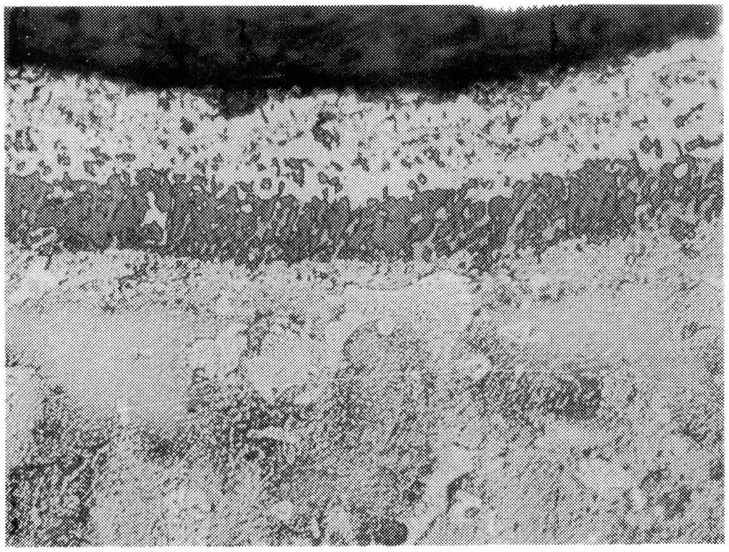

A. Specimen P23

Magnification: 250X

Etchant: 2% Electrolytic Chrome

After 72 Hours

Figure 65. Ni-13Al-20Cr-1Cb Coating (No. 6) After Dynamic Oxidation Testing at 1050°C

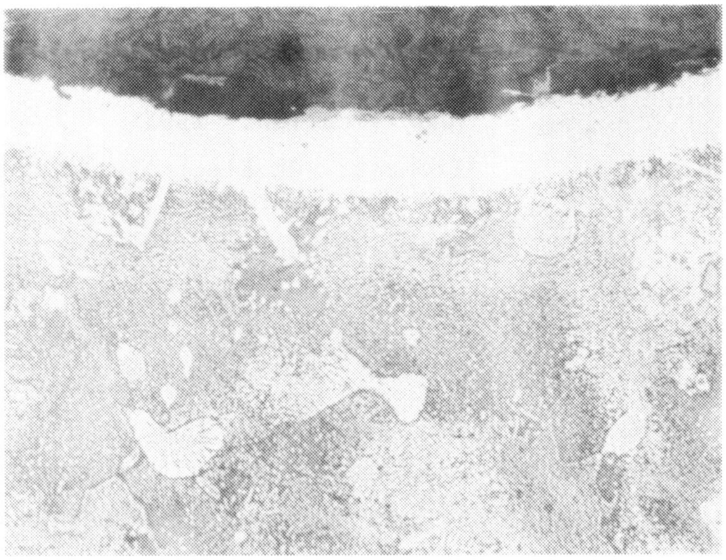

A. Specimen P20

Magnification: 250X

Etchant: 2% Electrolytic Chrome

After 72 Hours

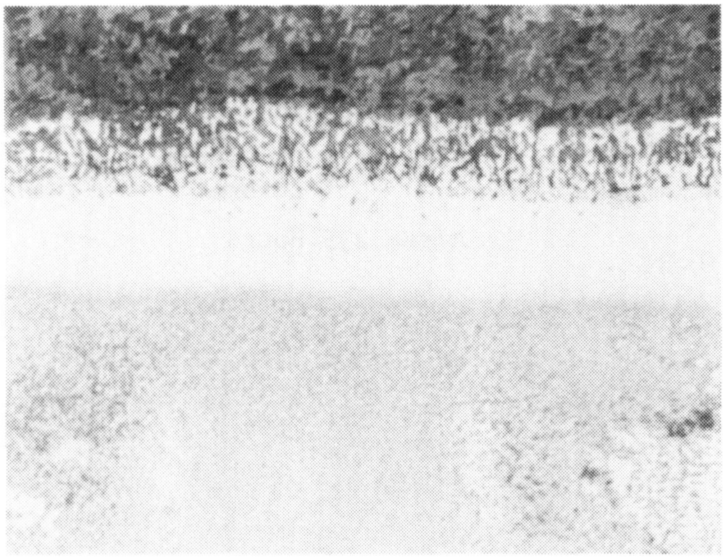

B. Specimen P19

Magnification: 250X

Etchant: 2% Electrolytic Chrome

After 235 Hours

Figure 66. Ni-14Al-20Cr Coating (No. 5) After Dynamic Oxidation Testing at 1050°C

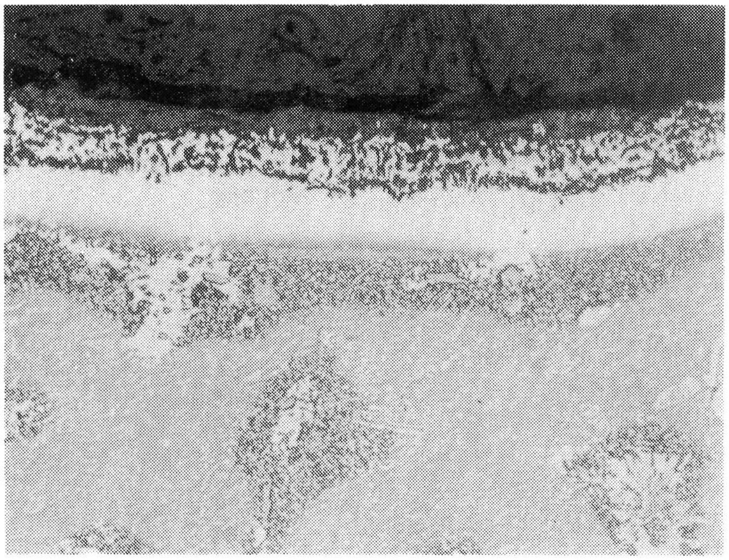

A. Specimen P41

Magnification: 250X

Etchant: 2% Electrolytic Chrome

After 72 Hours

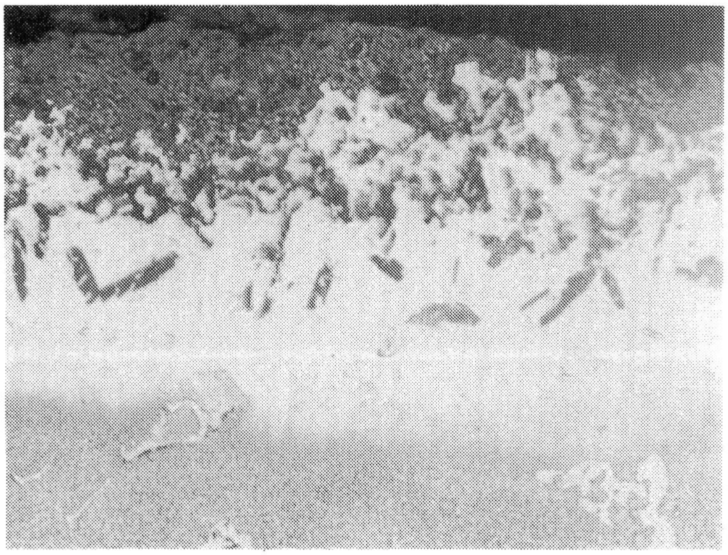

B. Specimen P35

Magnification: 250X

Etchant: 2% Electrolytic Chrome

After 235 Hours

Figure 67. Ni-12Al-20Cr Coating (No. 9) After Dynamic Oxidation Testing at 1050°C

Table 17
Dynamic Oxidation Test Results

Coating	Coating Composition	Penetration After 72 Hrs (μm)	Penetration After 72 Hrs (%)	Penetration After 235 Hrs (μm)	Penetration After 235 Hrs (%)
1	Ni-20Al	10	14	24	40
2	Ni-19Al-1Cb	34	50	34	50
3	Ni-17Al	15	33	59	100
4	Ni-16Al-5Si	30	40	25	40
5	Ni-14Al-20Cr	∿0	∿0	49	100
6	Ni-13Al-20Cr-1Cb	49	50	-	-
7	Ni-15Al	25	25	-	-
8	Ni-14Al-1Cb	25	50	69	100
9	Ni-12Al-20Cr	30	55	98	100
10	Ni-12Al-20Cr-5Si	10	20	-	-

5

COATING APPLICATION OF ENGINE HARDWARE

SELECTION OF COATING

The selection of MAR-M200+Hf(DS) as the substrate alloy for coating development was prompted by two reasons. Firstly, the gamma prime strengthened superalloy has excellent high-temperature creep strength. The second factor was the relatively poor environmental resistance of this superalloy. In Reference 12, this alloy was ranked slightly better than B1900 (a Pratt and Whitney blade alloy, poor in oxidation resistance) and considerably inferior to IN-713C, Rene' 80, etc.

Consequently, in order to adequately protect MAR-M200+Hf(DS), an optimized coating is needed which includes significant amounts of the chromia and/or alumina formers (Cr and NiAl), both of which are present at low concentrations in this alloy. At the same time, high mechanical and thermomechanical thermomechanical stress imposed on MAR-M200 components dictate the need for adequate ductility in the coating for strain accommodation, especially at medium to low temperatures (such as 400-800°C) experienced during transients and at startup or shutdown.

From the discussion in Section 4, it can be seen that the simple aluminides Ni-20Al, Ni-17Al and Ni-15Al (Nos. 1, 3 and 7) performed best in burner rig tests. These coatings were composed of beta and gamma prime, which are more oxidation/corrosion resistant than the gamma-gamma prime alloy. However, the inverse relationship between aluminum level and ductility means that these three coatings were the most brittle of all ten candidate coatings. For the applications of this program, these three low ductility coatings can only be viewed as providing baseline data for other duplex and triplex systems.

In order to review the performance of the remaining coatings and rate them relative to the three baseline aluminides, Table 18 was prepared using a simple grading scale of good, medium and poor to summarize the test results. The highly ductile coatings generally exhibited poor environmental resistance. Besides coatings Nos. 1, 3 and 7, the only system which exhibited adequate environmental resistance plus good ductility was No. 2, Ni-19Al-1Cb. It is easy to understand the protectivity of this coating as it had 19 weight percent aluminum, but it is much more difficult to account for ductility enhancement induced by the presence of columbium. In order to provide greater strain accommodation, the columbium in the coating must be able to facilitate dislocation movement in the crystal lattice or must produce minor fine cracks not observed in penetrant inspection in our strain accommodation test.

Table 18

Review of Test Results

Coating	Composition	Ductility	Corrosion*	Oxidation*
1	Ni-20Al	Poor	Good	Medium
2	Ni-19Al-1Cb	Medium	Medium	Medium
3	Ni-17Al	Poor	Good	Poor
4	Ni-16Al-5Si	Good	Poor	Medium
5	Ni-14Al-20Cr	Medium	Poor	Poor
6	Ni-13Al-20Cr-1Cb	Medium	Poor	-
7	Ni-15Al	Poor	Good to Medium	-
8	Ni-14Al-1Cb	Medium	Poor	Poor
9	Ni-12Al-20Cr	Good	Medium	Poor
10	Ni-12Al-20Cr-5Si	Medium	Medium	-

* Zero-33% = good; 33-67% = medium; 67-100% = poor.

Empirically, it was decided that under the test conditions described herewith in this report, the Ni-19Al-1Cb coating (No. 2) performed best and was selected for application to turbine blades.

COATING OF MARS BLADE

Prior to coating, the blade specimens were first cleaned and prepared. This included degreasing plus an acid etch in $HCl-H_2O_2$. Following this, the parts were cold flowed and vapor degreased as the final preparatory step. The first attempt to coat a Mars blade using the slip pack method resulted in considerable pack sintering and great difficulty in pack removal, especially from the small holes near the trailing edge. The coating process was repeated next in an identical fashion with one exception: no solvent was added to the powder pack. In other words, a dry pack was prepared in place of the wet slurry pack. The second experiment was successful with regard to ready removal of the spent pack. In the first case, the presence of a solution mixed with metal particles in a confined volume meant that upon drying (prior to firing), the vehicle (xylene) gradually evaporated from in between the particles and the bisque formed was compacted. Thus, when the pack was activated at temperature, the interparticle distances were small and readily bridged by the halide vapors and surface reactions resulted in significant interparticle and pack-to-substrate bonding. The second (dry pack) blade registered <2 percent flow reduction. Five blades were subsequently processed, as described in the next section.

Processing Steps for Coating Application of Mars 1st-Stage Blade

1. Degrease blades thoroughly in trichloroethylene, making sure the internal passages are also cleaned.
2. Cold flow part to determine degree of mass flow through blade.
3. Repeat degreasing (Step 1) to remove grease and oils from Step 2.
4. Acid etch.
5. Rinse in water for 5 minutes, allowing continuous flow of water through internal passages.
6. Acetone rinse, let dry and weigh.
7. Prepare 75Cb-25Al_2O_3-0.5NH_4Cl pack and fill the blade completely with pack material.
8. Place in Hastelloy X retort, weld seal and cycle purge three times with argon gas, and leaving a small positive pressure in the retort.
9. Place purged retort in 1038°C furnace for 6 hours.
10. Remove from furnace, cool and cut open retort.
11. Remove all spent pack particles.
12. Acetone rinse, dry and weigh.
13. Prepare CCRS CoNiCrY slurry and spray 30 to 40 mg/cm^2 on external surfaces, using an air mask fixture to keep gill holes open.
14. Air dry.
15. Holding the blade by the firtree only, carefully fill blade with 60Al_2O_3-24Ni-16Al-0.5NH_4Cl pack, taking care not to affect CCRS bisque.
16. Mask the firtree area by brushing on an undercoat of organoceram, followed by a heavy coating of Al_2O_3-ZrO_2 in xylene.
17. When dry, carefully place blade in CCRS pack in retort, keeping firtree section above pack level.
18. Weld seal retort, cycle purge three times with argon and place in a 1079°C furnace for 16 hours.
19. Remove from furnace, cut open and remove blade.
20. Break up masking on firtree, remove internal pack and brush off any remnants of the external pack.
21. Pressure wash thoroughly and acetine rinse.
22. Let dry and weigh.
23. Flow check again to determine internal flow restriction.

EVALUATION OF COATED MARS BLADE

Four 1st-stage blades cast in MAR-M200 + Hf (DS) were selected for coating application with Ni-19Al-1Cb coating, as described in the previous section. One of the blades (M1) was sectioned in several places for metallographic inspection of coating formation and Figure 68 shows schematically the location represented by photomicrographs A through H in Figure 69. Note that A and B, which are coating microstructures at the trailing and leading edges, respectively, exhibit markedly two layer structures with the layer nearer the substrate containing filigree like secondary phases. This is especially pronounced in A where space limitations would restrict the amount of pack material available for coating formation. The other photomicrographs taken from the central cavity (C to H) show precipitates which appear to form an almost continuous band in the middle of the coating.

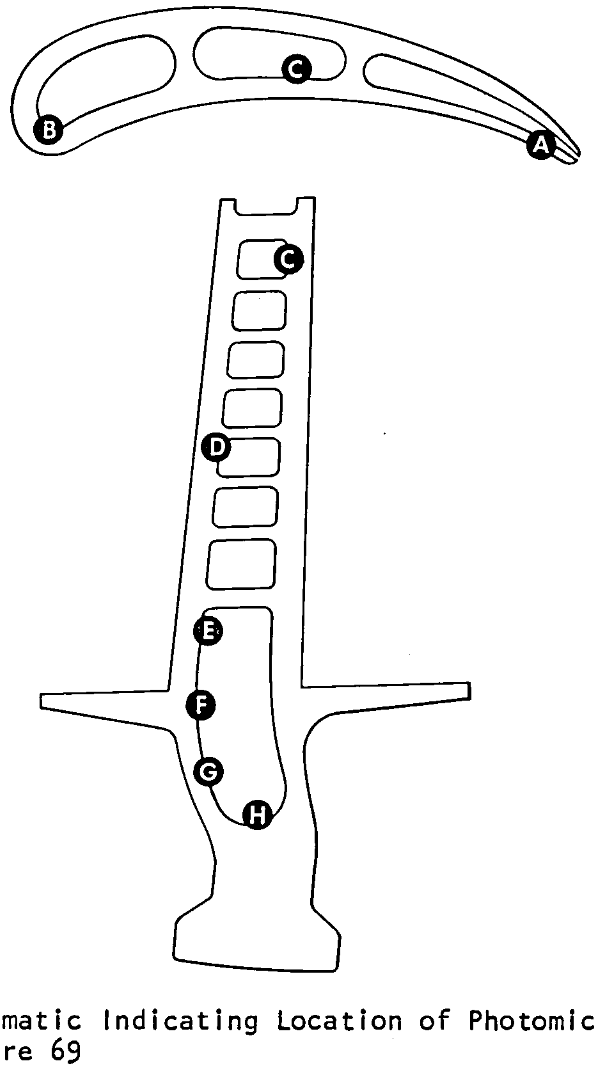

Figure 68. Schematic Indicating Location of Photomicrographs in Figure 69

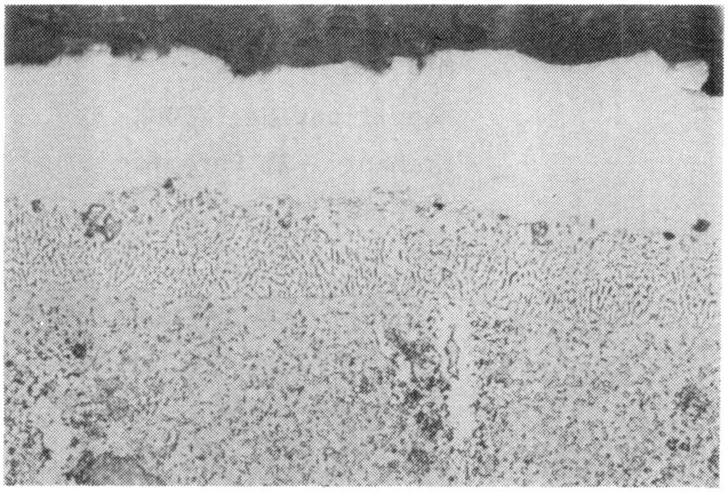

A. Trailing Edge
Magnification: 500X
Etchant: 2% Chromic

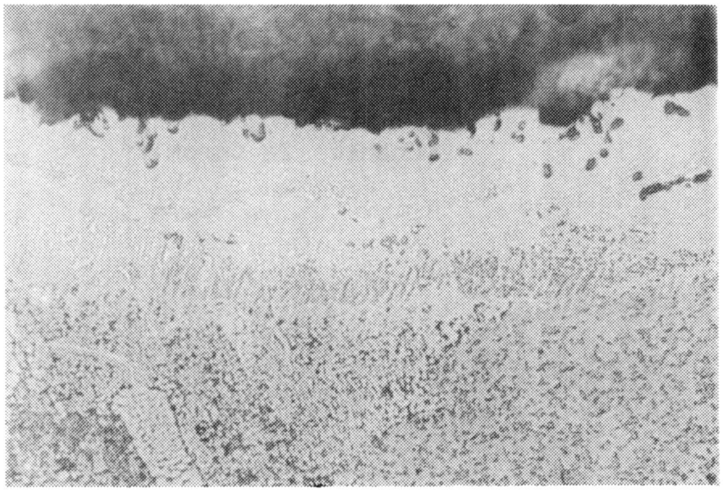

B. Leading Edge
Magnification: 500X
Etchant: 2% Chromic

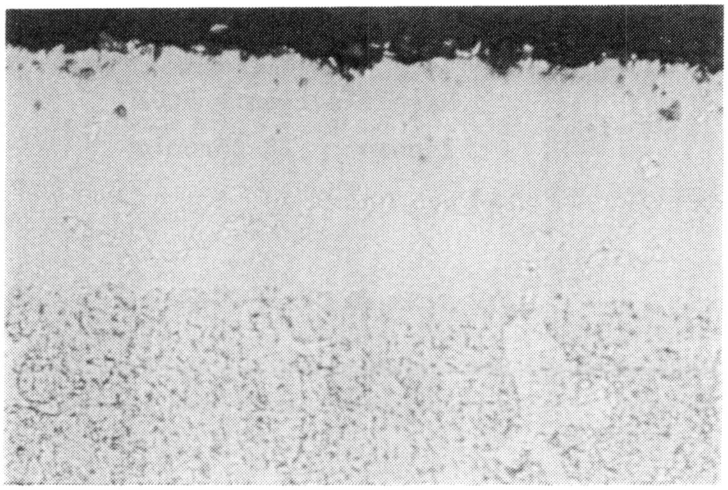

C. Mid Section
Magnification: 500X
Etchant: 2% Chromic

Figure 69. Internally Coated (Ni-19Al-1Cb) Air-Cooled Blade (Sheet 1 of 3)

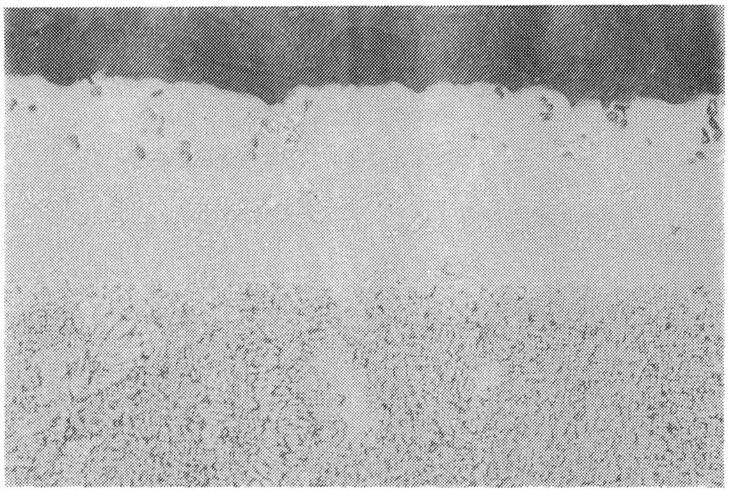

D. Mid Chord
Magnification: 500X
Etchant: 2% Chromic

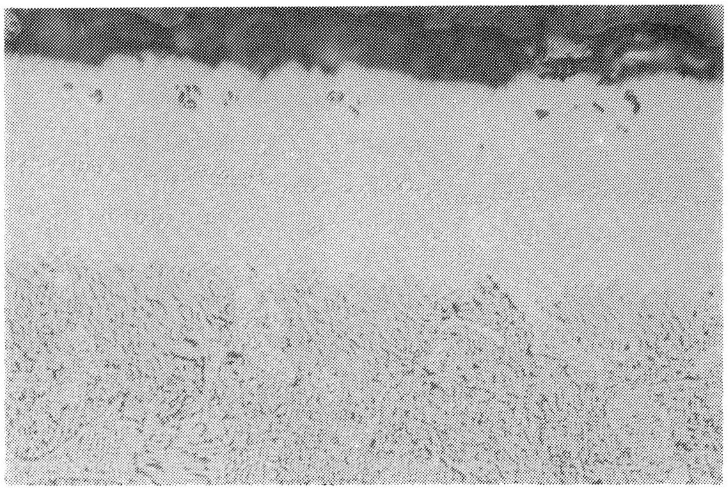

E. Lower Chord
Magnification: 500X
Etchant: 2% Chromic

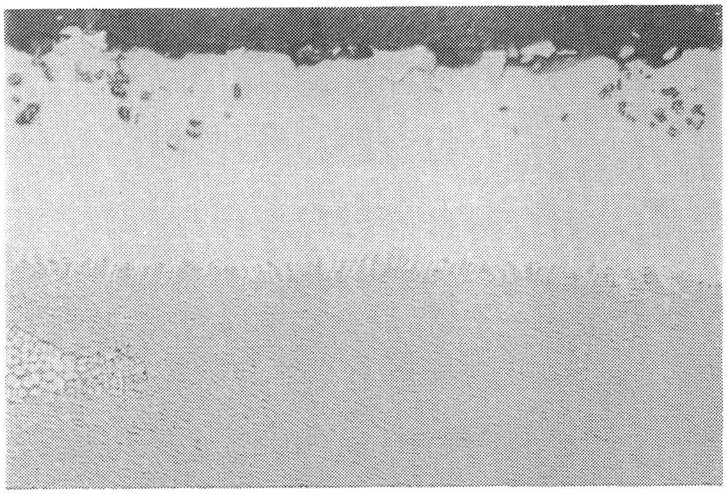

F. Platform Level
Magnification: 500X
Etchant: 2% Chromic

Figure 69. Internally Coated (Ni-19Al-1Cb) Air-Cooled Blade (Sheet 2 of 3)

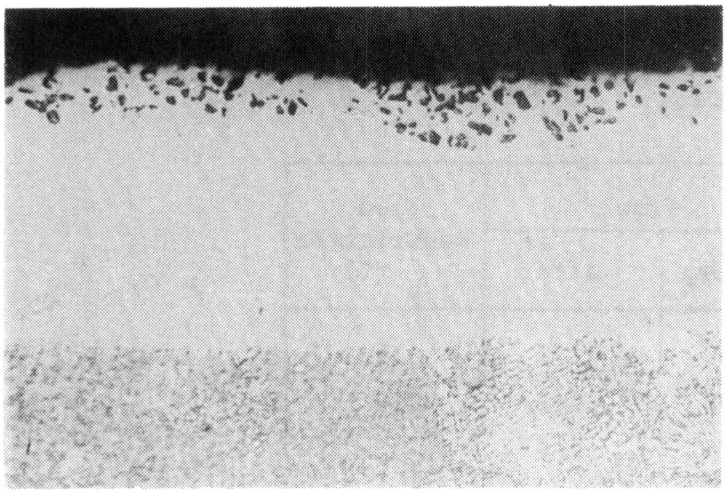

G. Below Platform
Magnification: 500X
Etchant: 2% Chromic

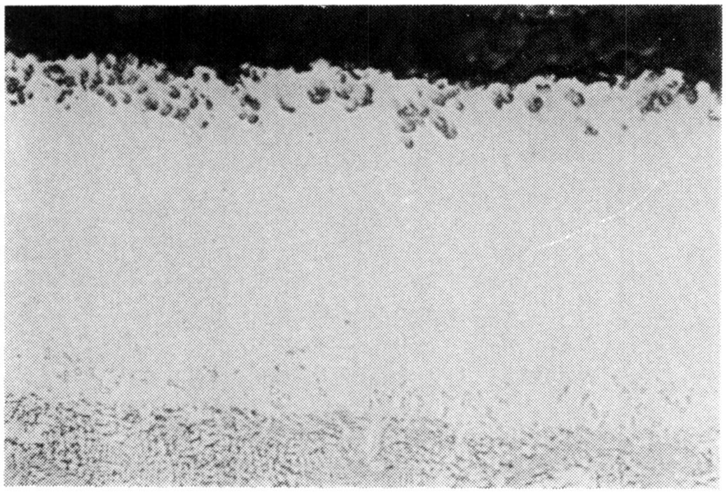

H. Firtree
Magnification: 500X
Etchant: 2% Chromic

Figure 69. Internally Coated (Ni-19Al-1Cb) Air-Cooled Blade (Sheet 3 of 3)

Coating thicknesses near the leading and trailing edges are 50 and 35 μm, respectively, with 62 μm at C. From D to H, the measured coating thickness ranged from 55 to 90 μm. The average coating thickness is 60 μm with a standard deviation of ±10 μm.

Mass flow readings taken before, during and after coating processing are reported in Table 19. All three blades registered 18 percent or less flow reduction. These parts will be returned to the sponsor for their evaluation.

Table 19

Mass Flow Data of Mars Blades

Blade Number	Flow		Flow Restriction (%)
	Before	After	
2	179	151	16
4	198	162	18
6	191	169	12

6

CONCLUSIONS

The goals of this program were to (1) develop ten aluminide type coatings for internal protection of air-cooled blades; (2) test these ten candidate systems and select one best coating based on ductility and corrosion/oxidation resistance; and (3) apply the selected coating on air-cooled blading with an external CCRS MCrAlY coating. All of the above mentioned goals have been met, and as a summary of this investigation, the following observations are made.

1. The duplex coatings, Ni-12Al-20Cr and Ni-16Al-5Si, exhibited excellent ductility, exceeding that of the substrate alloy (DS) MAR-M200 + Hf. At room temperature, strain-to-cracking was 10.4 and 7.1 percent, respectively, while the substrate was reported to fail at 6.1 percent (Ref. 2).

2. In general, the modified nickel-aluminide coatings of Ni-Al-Si, Ni-Al-Cr, Ni-Al-Cb, Ni-Al-Cr-Cb and Ni-Al-Cr-Si had low ductile-brittle transition temperatures with cracking occurring at less than 500°C and greater than 3 percent strain.

3. The 'simple' aluminides (Ni-20Al, Ni-17Al and Ni-15Al) were the most brittle of the ten candidate coatings with failure occurring at 500° and 600°C and at low strain levels of <2 percent.

4. Addition of columbium to the nickel-aluminide matrix improved coating ductility without comprising oxidation/corrosion resistance.

5. Al_2O_3 was a satisfacrory diluent for coating packs because of its relative inertness, especially to water, and also its availability in a wide range of particle sizes.

6. Process parameters such as pack composition, activator, furnace time and temperature, were empirically selected to deposit the desired amount of aluminum, chromium, silicon and columbium to form the Ni-Al, Ni-Al-Cr, Ni-Al-Si, Ni-Al-Cb, Ni-Al-Cr-Cb and Ni-Al-Cr-Si coatings.

7. The internal surfaces of the air-cooled Mars first-stage blade were successfully coated by the dry pack process with minimal sintering and pack removal problems.

8. The coating process resulted in less than 18 percent drop in air flow through the internal passageway of air-cooled blades.

9. Coating surfaces, as observed on the internal surfaces of the coated airfoil, appear to be uniform in general, except near the trailing edge where volume limitations may have restricted the amount of pack material available for vapor transport and diffusion. The average coating thickness was 60μm with a standard deviation of ±10μm.

RECOMMENDATIONS

In order to take maximum advantage of the efforts made in this program, the results obtained should be used in a follow-on program to optimize the development of internally coated MAR-M200 + Hf (DS) blades. Based on the present program, the following items are recommended for further investigation.

1. Select two best coating compositions for optimization in a parametric study of process parameters.
2. Investigate coatings applied by both dry and wet pack methods.
3. Utilize analytical methods to monitor rinse water to ensure complete removal of activator from internal cavities.
4. Design rig test specimen configuration that will fulfull several functions: close simulation of air-cooled blade configuration, ready availability, economical and suitable for dry pack processing.
5. Advanced coating development studies should utilize scrapped air-cooled blades for coating uniformity control in order to avoid problems of technology transfer from coupons or standard test specimens to complex engine components.
6. Upon completion of coating optimization, a set of blades should be prepared for engine testing.
7. Further testing of candidate systems should incorporate commercially available coatings to establish baseline data.
8. Based on the recommended internal coating as applied to the Mars first-stage blade, an estimate of material, labor and equipment costs should be done. Cost figures can be estimated from batch processing of hardware, as determined from current and projected sales of the Mars engine. At the same time, two to three coatings from commercial sources should be similarily priced to provide comparison from the viewpoint of economics.

APPENDIX A

DETERMINATION OF RIG OPERATING CONDITIONS

APPENDIX A

DETERMINATION OF RIG OPERATING CONDITIONS

In order to determine the characteristics of the burner rig test, the key elements of flow, pressure and temperature must be carefully regulated. The major items used to ensure reproducible rig operation are:

- Fuel flow and pressure regulators
- Combustor pressure regulator
- Airflow on five Δp manometers
- Airflow reducing regulator controls
- Temperature controller and recorders.

Flow

Fuel flow was measured by means of a Brooks type (250 mm) Rotometer Direct Reading Flow Meter, with a maximum capacity of 20 kg/hr (44 lbs/hr) of JP-5 fuel. Calibration was performed prior to testing and the fuel flow required to attain temperature and velocity requirements was recorded.

The air flow was determined by calculating the incoming air across a 304 stainless steel orifice plate (radius tap) with 1-inch diameter orifice and 1.5-inch pipe diameter. The equation for compressible fluid flow through a orifice is:

$$W_a = Y\, C_d M A \sqrt{2g\rho_a (P_1 - P_2)}$$

where W_a = air flow rate

Y = expansion factor of stainless steel plate

C_d = coefficient of discharge

M = velocity of approach factor

A = area of orifice

g = gravitational constant

ρ_a = air density

P_1 = upstream air pressure

P_2 = downstream air pressure

A computer program was set up to perform the above calculations over a range of pressure values across the orifice plate and at several inlet air temperature readings. By inserting the appropriate values of air temperature, and the upstream, downstream air pressures, the air flow rate was determined.

Temperature

The gas stream temperature was determined in two ways. Initially, a platinum-rhodium thermocouple was placed in the hot gas stream one inch above the nozzle plate and the temperature was read directly. A second method was to calculate the gas temperature (assuming complete combustion) based on the fuel-to-air ratio together with the incoming air temperature. (The incoming shop air goes through a heat exchanger in the exhaust stack and was preheated by the exhaust gas before entering the combustor.) The calculated flame temperature was found to be in fairly good agreement (±56°C) with measured values.

Pressure

Since the specimens are located one inch downstream of the combustor nozzle, the static pressure (P_s) may be safely assumed to be equal to the static pressure in the test cell and very nearly equal to the atmospheric pressure. The total pressure of the gas stream (P_T) is the combustor pressure, which was set at 8.5 psig or 23.2 psia. The pressure ratio P_T/P_S was calculated to be 1.58.

Velocity

From calibrations conducted on Solar's rigs, gas charts are available that relate the function $V/\sqrt{T}$ for specified values of gamma (ratio of specific heats) to the pressure ratio P_T/P_S. Figure 70 shows the chart used to calculate air velocity for gamma = 1.31.

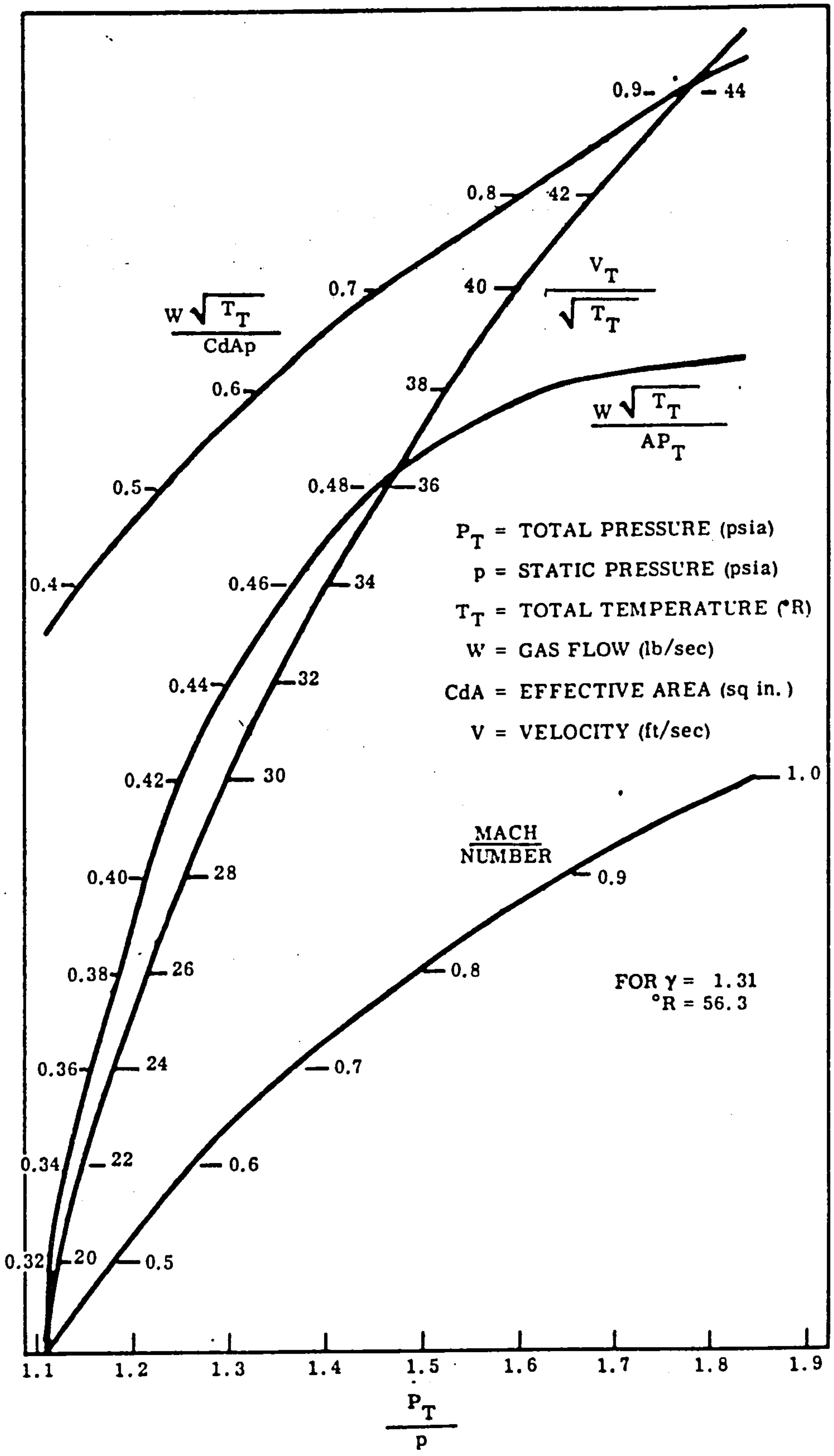

Figure 70. Erosion Rig Chart For Calculation of Hot Gas Stream Velocity

REFERENCES

1. Stevens, W.G. and Stetson, A.R., "Controlled Composition Reaction Sintering Process for Production of MCrAlY Caotings", Air Force Materials Laboratory Report AFML-TR-76-91, Contract F3361575-C-5268 (August 1976); Solar Turbines International Report No. RDR 1802-6.

2. Duhl, D.N. and Sullivan, C.P., "Some Effects of Hafnium Additions on the Mechanical Properties of a Columnar Grained Ni-Base Superalloy", J. of Metals, July 1971 (p. 38).

3. Doherty, J.G., Kean, B.H. and Giamei, A.I., "On the Origin of the Ductility Enhancement in Hf-Dopes MAR-M200", J. of Metals, Nov. 1971 (p. 59).

4. Dunn, R.G., Sponseller, D.L. and Dohl, J.M., "Ductility Improvements in Superalloys", Proceedings of Symposium on Toward Improved Ductility and Toughness, Kyoto, Japan, 1971.

5. Moore, V.S., Brentnall, W.D. and Stetson, A.R., "Evaluation of Coatings for Cobalt and Nickel Base Superalloys", NASA-Lewis Contract NAS3-940,

6. Levine, S.R. and Caves, R.M., "The Mechanisms and Kinetics of Pack Aluminide Coating Formation on IN-100", J. of Electrochemical Soc., Vol. 121, No. 8, p. 1051.

7. Powell, C.F., Oxley, J.H. and Blocker, Jr., J.M., "Vapor Deposition", John Wiley & Sons, Inc., New York, 1966.

8. Grale, G.M., "Investitation of NiAl-Ni_3Al Mechanical Properties of Intermetallic Compounds", Chap. 17, p. 358, Ed. by j. H. Westbrook, May 1959.

9. Goward, G.W. and Boone, D.H., "Mechanisms of Formation of Diffusion Aluminide Coatings, a Nickel Based Superalloy", Oxidation of Metals, Vol. 3, No. 5, 1971 (p. 475).

10. "Nickel Base Alloys", International Nickel Company, 1954.

11. Aldred, P., "Rene' 125, Development and Application:, Soc. of Automotive Engineers, National Aerospace Engineering and Manufacturing Meeting, Los Angeles, 1975.

12. Sevine, S.R. and Canos, R.M., "Thermodynamics and Kinetics of Pack Aluminide Coating Formation in IN-100", J. Electrochemical Society, Vol. 121, No. 8, 1974, p. 1051.

13. Goward, G.W., Boone, D.H. and Giggin, C.S., "Formation and Degradation Mechanisms of Aluminide Coatings on Nickel Base Superalloys", Trans. ASM, Vol. 60, 1967, p. 228.

14. Beltram, A.M. and Shores, D.A., "The Superalloys", Ed. C.T. Sims and W.C. Hagel, Wiley Interscience, p. 317.

15. Sowendel, H.W., "Corrosion Resistant Aluminide Coatings for Fe and Ni Base Alloys", J. of Metals, July 1975, p. 4.